

Fabrication of 3D Microwave and Millimetre-Wave Components in LTCC Technology

Razak Mohd Ali Lee

Submitted in accordance with the requirements for the degree of
Doctor of Philosophy

The University of Leeds
Faculty of Engineering
School of Electronic and Electrical Engineering

January, 2014

The candidate confirms that the work submitted is his own and that appropriate credit has been given where reference has been made to the work of others.

The candidate confirms that the work submitted is his/her own, except where work which has formed part of jointly-authored publications has been included

This copy has been supplied on the understanding that it is copyright material and that no quotation from the thesis may be published without proper acknowledgement.

©2014 The University of Leeds

and

Razak Mohd Ali Lee

Acknowledgements

In the name of Allah, The Most Gracious and The Most Merciful.

This research project would not have been possible without the support of many people as I mentioned in the following.

My sincere gratitude goes to my supervisor, Professor Ian Robertson for his patience, guidance and supervision throughout my time as his research student at the University of Leeds. I would not be able to complete this work without his inspiration and encouragement.

I would like to thank the Ministry of Education of Malaysia for the financial support. Without the support this study would not have been possible. My sincere acknowledgement also goes to the Universiti Malaysia Sabah (UMS) for giving me the opportunity to study abroad. I really appreciate all the encouragement and support throughout my study leave, and in a few occasions for visiting us in the UK.

I also want to thank all the staff at the School of Electronic and Electrical Engineering and members of the Institute of Microwaves and Photonics, especially Clair Atkinson, Louise Redmond for helping with ordering materials for my research, and Geoffrey for helping to set-up the laminator in our fabrication lab. Special appreciation also goes to John Sheard for helping me in more than one occasions to recover the harddisk from our laser machine and assist me to setup network connection that allowed the machine to receive remote assistance from Germany.

Special thanks to my friend and research partner, Lukui Jin for helping with the HFSS modelling works while at the same time keep motivating me to complete my fabrications part of hollow SIW especially during the hardest time when the laser machine was out of order for multiple times.

Not to forget Dilshani Rathnayake from the University of Loughborough for sharing the knowledge on the RF MEMS project, and Mario D'Auria from Imperial College London for the friendship.

It is my pleasure to thank all my colleague in the office in particular M. F Shafique, A. Laister, Osama Hatem, Divyang, Raed, Ni, A. Sunday, C. Russel, Noni, Fazlina, Zahril, Hizamel, Wilson and Nicholas.

I would also like to take this opportunity to thank those people who have not been mentioned above, but have spent their time and share the knowledge for helping me throughout my study at the University of Leeds.

My special acknowledgement goes to my family members for their prayers, encouragement and understanding during my studies. I dedicated this thesis to Mohd Ali Lee, Dalmatasiah Nul, Jamaluddin Mohd Ali, Faridah Mohd Ali, Mohd Roslee Mohd Ali, Marita Mohd Ali and the entire family. It is my honor to have a great family such you are. Lastly, to my beloved wife and my best friend Newati Wid for the supports and cheering me up during the hardest time and throughout period of my study. Being a PhD student, you have taught me the true meaning of patience. Thank you for loving me.

Abstract

Rapid prototyping through infra-red laser machining is adopted. The process does not involve chemicals and a single plain screen is sufficient for printing and via filling of any number of layers. The process does not require special masks and is performed in the ordinary laboratory environment. Optimisation of laser power, pulse rate, and scanning speed produce high repeatability and selective thinning, cutting and drilling of any positions and layers made possible with optical camera assisted alignment. The laser ablation of low loss LTCC 9K7 green state tape produces minimum damage with surface roughness below 1 μm which is acceptable for microwave fabrication requirements.

To fabricate hollow waveguide in LTCC, the standard LTCC process has been considered, and it was found unable to produce suitable channels/cavities. The hurdle was the lamination step. Experiments on lamination pressure, temperature, time duration and number of layers have been conducted to find the most influential parameters. 3D structures were successfully fabricated using a novel multi-stage/progressive lamination technique. With this technique, deformation-free 3D hollow structures laminated at pressure as low as 2 MPa have been realised. Three types of sacrificial inserts have also been prepared and examined to enhance the process variability. While organic-based and water-based sacrificial paste are more suitable for preparing trenches and channels in the micrometre scale, wax-graphite based sacrificial insert is better for large volume of channel and cavity application.

A WR28-like Hollow SIW (HSIW) is fabricated and measured using WR28 waveguide flanges. A multimode calibration technique was used to calibrate the complex propagation constant. The HSIW has been successfully demonstrated working in the millimetre-wave region with measurements on 26.5 to 40 GHz test samples. This is believed to be a significant milestone.

A HSIW-based antenna and filter as an integrated component was fabricated. The measurement of the radiation pattern of the waveguide antenna and cavity filter is performed using a 67 GHz PNA and a standard gain horn antenna placed inside an anechoic box. The measured radiation pattern shows both *E*- and *H*-plane pattern closely fit with the modelled performance.

Table of Contents

Acknowledgements	iii
Abstract	v
Table of Contents	vi
List of Figures	ix
List of Tables	xiii
Chapter 1 Introduction	1
1.1 Multi-chip modules	2
1.2 Low loss dielectric ceramic.....	4
1.3 Applications of LTCC.....	8
1.3.1 System-in-Package (SiP).....	8
1.3.2 Sensors and actuators	9
1.3.3 Microfluidics	10
1.3.4 Microelectromechanical systems (MEMS)	11
1.3.5 RF MEMS switches.....	12
1.4 Motivation and objectives	12
1.5 Review of thesis	13
Chapter 2 Standard LTCC process	14
2.1 Standard fabrication methods	16
2.1.1 Laser machining	16
2.1.2 Laser pulse rate and writing speed	19
2.1.3 Optimisation of laser parameters	20
2.1.4 Laser drilling and cutting.....	24
2.2 Screen printing	25
2.2.1 Conductive paste	26
2.2.2 Metallisation of vias.....	27
2.3 Alignment and stacking	28
2.4 Lamination.....	29
2.5 Sintering	30
2.6 Surface roughness	31
2.7 Laser scribing	32
2.8 Conclusion.....	33
Chapter 3 Enhanced LTCC process	34
3.1 Lamination techniques	34
3.1.1 Selection and influence of parameters	36

3.1.2 Experiments (lamination without insert)	38
3.1.3 Result and observation	39
3.1.4 Progressive lamination	40
3.2 Lamination with sacrificial inserts	42
3.2.1 Preparation of the sacrificial inserts.....	45
3.2.1.1 Organic-based paste	45
3.2.1.2 Water-based paste	46
3.2.1.3 Wax-graphite paste	47
3.2.2 Insertion of sacrificial paste.....	48
3.2.3 Lamination with sacrificial paste	49
3.2.4 Results and observation	49
3.3 Conclusion.....	54
Chapter 4 Hollow substrate integrated waveguide	55
4.1 Rectangular waveguides	55
4.2 Integrated waveguides/cavities	57
4.3 Hollow substrate integrated waveguide (HSIW)	59
4.3.1 HSIW structure and design	61
4.3.2 Fabrication of HSIW structure	63
4.3.3 Multimode calibration method	67
4.3.4 Measurement and results.....	68
4.4 Conclusion	71
Chapter 5 Hollow waveguide components in LTCC technology.....	72
5.1 Antenna.....	73
5.1.1 Waveguide slot antenna.....	73
5.1.2 HSIW antenna.....	77
5.2 Filter	79
5.2.1 Waveguide filter	79
5.2.2 Cavity waveguide filter design.....	79
5.3 Integrated waveguide antenna and filter	83
5.4 Conclusion	86
Chapter 6 Conclusions and suggestions for future work.....	87
6.1 Conclusions.....	87
6.2 Issue with research with LTCC.....	89
6.3 Potential improvements.....	89
6.3.1 Material development.....	90

6.3.2 Process development.....	90
6.4 Suggestions for future work.....	91
6.4.1 LTCC based RF MEMS.....	91
6.4.2 Waveguide at sub-THz region.....	92
6.4.3 Other 3D fabrication techniques.....	93
6.5 Publications.....	93
Coference posters and proceedings.....	93
Publications	94
List of References	95
List of Abbreviations.....	101
Appendix A	103
Appendix B	105

List of Figures

Figure 1.1	MCM and PCB cost per substrate connection pad	3
Figure 1.2	Directions for research and development of dielectric components. Q-f are shown as a function of relative permittivity	5
Figure 1.3	Integration development of electronic packaging.....	8
Figure 1.4	SiP application of LTCC.....	9
Figure 1.5	LTCC based gas flow sensor and optical fluid detector	10
Figure 1.6	A microfluidic reactor and biosensor with integrated fluidic and lid from LTCC.....	10
Figure 1.7	Silicon microphone packaging and spectrometer in LTCC	11
Figure 2.1	Laser ablation mechanism where only the absorbed energy is effectively used in the material processing, while other transmitted or reflected	18
Figure 2.2	The three axis positioning system fo Protolaser 200	19
Figure 2.3	Laser pump current with respect to optical output power	20
Figure 2.4	Laser pulse rate with respect to optical output power	20
Figure 2.5	The etch rate of LTCC determined from etch depth of the varying laser repetition	21
Figure 2.6	A linear laser etch rate under condition of power/pulse/speed: 5.2 W/40 kHz/500 mm ⁻¹	22
Figure 2.7	Flow of laser etching process optimization.....	23
Figure 2.8	Laser machining follows the tracks of contour line and hatch lines	24
Figure 2.9	The composition dependence of resistance values Ag-based pastes	26
Figure 2.10	Resistance measurement scheme of conductor strip to check the improvement in the conducting layer.....	27
Figure 2.11	Green state LTCC sample is laser drilled and cut before being metallised with conductive paste. In these pictures, the vias are filled with DuPont LL601 silver paste.	28
Figure 2.12	Alignment jig	29
Figure 2.13	Uniaxial and isostatic laminator	30
Figure 2.14	LTCC sintering type	31

Figure 2.15	To achieve the desired dielectric constant and low loss performance properties the green tape undergoes 26.5 hours co-fire profile control points [51]. Organic burnout phase occurs between 200 °C and 550 °C. The sintering phase of composite ceramics is completed at the peak temperature for 17-23 minutes.	31
Figure 2.16	The sintered LTCC surface measured by surface profiler. By changing the repetition of laser etching, the etch depth with a sufficient flat surface is achievable as observed on the sintered LTCC.....	32
Figure 3.1	(a) uni-axial laminator with upper and bottom platen controlled by temperature controller system. (b) The mechanism of uni-axial laminator.	37
Figure 3.2	Progressive lamination for hollow waveguide	40
Figure 3.3	The cross section of 3D hollow structure produced after green tapes were laminated at 2 MPa and sintered. An excellent bonding between layers and free of crack and deformation. Bottom is with single supporting layer. (b) The hollow structures fabricated in the LTCC substrate with the broadwalls and sidewalls need to be metallised to replicate rectangular waveguide in LTCC.....	41
Figure 3.4	Chart of sacrificial volume materials classified by its functionalities	43
Figure 3.5	Mechanism of air intake and buried paste oxidation. Note that air and/or degassing gas transport through LTCC occurs only at temperature below the LTCC open porosity elimination temperature.....	44
Figure 3.6	Screen-printing of sacrificial paste	48
Figure 3.7	(a) Heavy and (b) light screen-printed graphite paste	48
Figure 3.8	(a) organic-based sacrificial paste inserted underneath the bridge structures. (b) deformation of free-standing structures happened when sacrificial inserts dried in the oven at 70 °C for 30 min.....	50
Figure 3.9	Photo of sample with channel without paste with organic-based paste and water-based paste.....	51
Figure 3.10	The flow of large channel: (a) wax-graphite paste filling, (b) flattening, (c) laminating and (d) sintering and inspecting. The crack observed on the sintered sample may due to excessive pressure induced by sacrificial materials degassing during the oxidation process.	53
Figure 4.1	Rectangular waveguide	56
Figure 4.2	TE modes	57

Figure 4.3	cross-section of two example HSIW configuration: (a) with metallization outside: (b) with metallization inside the cavity	60
Figure 4.4	HSIW configuration: (a) cross section with metallization inside, (b) 3D view with metallization inside	62
Figure 4.5	Preparation of HSIW's middle part in the green state, where the metallic posts act as sidewalls.....	63
Figure 4.6	The metallization of vias with conductor paste.....	64
Figure 4.7	Flat broadwalls observed after lamination of top and bottom layers (b) holes for fixing the sample to waveguide flanges laser drilled around the back-to-back waveguides.....	66
Figure 4.8	Cross-section of HSIW after being cut and polished using whetstone. The sample was fired under unconstrained sintering. Metallic posts are clearly connected between layers to perform as a sidewalls to the waveguides	67
Figure 4.9	(a) photograph of sintered substrate incorporating three WR28-like HSIWs with lengths of 30, 40 and 50 mm respectively, (b) a back-to-back transversal slot-pair is used to couple the energy in and out. The WR28-like HSIW measured by 67 GHz PNA using 2.4 mm coax-to-WR28 adapter that is mounted and screwed to the HSIW.....	69
Figure 4.10	The modeling and measurement of HSIW with length of 30 mm	70
Figure 4.11	Extracted attenuation constant and phase constant of the WR28-like HSIW	70
Figure 4.12	The attenuation of HSIW with respect to WR28 RWG and WR28-like SIW.....	71
Figure 5.1	Surface current distribution for rectangular waveguide TE ₁₀ mode: (a) cross-section view shows <i>E</i> - and <i>H</i> -fields. (b) side view shows polarity of <i>E</i> -field along the waveguide. (c) surface view shows broadwall and sidewall current and <i>H</i> -field.	74
Figure 5.2	Radiating slots cut in the walls of RWG.....	75
Figure 5.3	Standing-wave arrays with longitudinal slot elements is fed from the waveguide end.....	76
Figure 5.4	Dimensional parameters of HSIW-based antenna arrays extracted from HFSS modeling	77
Figure 5.5	Simulated <i>H</i> -plane of slotted antenna arrays	78
Figure 5.6	The "In-house" fabricated HSIW-based slot antenna arrays	78

Figure 5.7	A waveguide cavity and its equivalent circuit	80
Figure 5.8	The impedance inverter	81
Figure 5.9	General illustration of direct-coupled waveguide cavity filter	81
Figure 5.10	The dimensional parameter of second order cavity filters	82
Figure 5.11	The simulation result of the second order direct-coupled cavity filter	81
Figure 5.12	Illustration of cavity filter with a slot antenna fabricated using the same technique as HSIW.....	82
Figure 5.13	(a) Photograph of the waveguide cavity filter showing the three irises of the cavity filter before the top broadwall is laminated, and (b) complete integrated slot antenna and waveguide filter after firing.....	84
Figure 5.14	Measured return loss of the cavity filter. The measurement has hugely shifted from the simulated one due to shrinkage in the filter.....	85
Figure 5.15	Simulated and measured radiation pattern of the integrated antenna with filter. Linear polarization was observed with both <i>E</i>- and <i>H</i>-plane matching well.....	85
Figure 6.1	Suspended bridges made from LTCC has been sucessfully realised	92
Figure 6.2	System-in-Package vision	92

List of Tables

Table 2.1 Comparison between LTCC with other technologies	15
Table 2.2 Machining and structuring techniques in multilayer ceramic technology.....	17
Table 2.3 LPKF Protolaser 200 specifications	18
Table 3.1 Lamination techniques for fabricating 3D structures	35
Table 3.2 List of parameters and operations that can possibly influence the LTCC finishing.....	38
Table 3.3 Experimental parameters bt considering achievable precision of our equipment	39
Table 3.4 Organic-based sacrificial paste composition	45
Table 3.5 Water-based sacrificial pastes	46
Table 3.6 Wax-graphite-based sacrificial paste composition	47
Table 4.1 The parameters of WR28-like HSIW	63
Table 5.1 Dimensional parameters of second order direct coupled cavity filter	82

Chapter 1

Introduction

In microelectronic products, packaging plays important roles such as supplying power to integrated circuits (ICs) and distributing signals among microelectronic devices. As IC fabrication advances rapidly, microelectronic packaging and precision processing of silicon, ceramic, and polymer substrates also play a more important role.

The traditional approach of single chip packages on a PCB have intrinsic limitations in terms of silicon density, system size, and the contribution to the propagation delay. Considering the IC packaging efficiency, an ordinary PCB would only have at most a 6% efficiency of holding silicon which means 94% of the board area would be wasted, unavailable for active silicon and contributing to increased propagation delays [1].

With the introduction of very large scale integrated (VLSI) chips, even surface mount technologies (SMTs) became inefficient for high performance system design. Chip packaging becomes the bottle neck to further improvement in system performance. A reduction in packaging levels is necessary to meet the increasing demand in IC technology.

From a packaging point of view, fabrication of an entire system on a single wafer should be ideal. The idea of integrating a complete system on a wafer is referred to as wafer scale integration (WSI). However, it is plagued by several limitations such as lower yield for large wafers and is an expensive or impractical solution for a mix of technology types.

The packaging technology that is required for high performance systems should also fulfil certain basic requirements for the selection of packaging techniques such as high conductivity, low loss, and compatible thermal coefficient of expansion and, good heat conductivity for high power applications. These requirements can be met by Multi-Chip Modules (MCM) as will be described in the next section.

To develop a lower cost system, the selection of suitable materials together with simplified and inexpensive designs, processes, and manufacturing tools are the key to the future needs of packaging requirements.

1.1 Multi-Chip Modules (MCM)

As the demand for further miniaturization of consumer products grew, the MCM was designed for multiple integrated circuit (IC) to be use facilitate their use as a single package. In other words, MCM packaging is crucial for modern electronic miniaturization and microelectronic systems.

MCM approaches differ depending on the complexity and development philosophies of the designers, and the needs of the end user. For example, one customer may require pre-packaged ICs on a small printed circuit board, meant to replicate the package footprint of an existing chip package. Another user may need a fully custom package that integrates many chips on a substrate. For the both cases, MCM still could support the requirements due to the following features:

- Lower power supply because of shorter interconnect lengths,
- Smaller overall packages which enable greater miniaturization,
- Greater reliability with decreased number of interconnects between components,
- Flexibility through integration of various semiconductor technologies,
- Faster time-to-market i.e. ideal for products with short life cycles,
- Reduction in complexity by putting several devices into a single package,
- Lower cost.

Modern MCM substrates consist not only the interconnection lines but also of many integral (embedded) passives. There are three types of MCM technologies:

- i. MCM-D: interconnects are formed in a simple manner to those used to fabricate thin-film circuits, i.e. by depositing layers of conductors and dielectrics onto an underlying substrate,
- ii. MCM-L: multilayer structures are formed by lamination of printed circuit board materials with etched patterns on copper foils and metallised vias,
- iii. MCM-C: multilayer structures are often made by co-firing ceramic or glass/ceramic tapes, similar to a thick-film process. In LTCC technology, vias are punched in green tapes and filled with conductive paste, then the individual layers are printed on green ceramic tapes, laminated and co-fired at proper temperature to form a monolithic structure.

Figure 1.1 Illustrates a comparison of interconnection costs per substrate pad between PCBs (PWBs) and MCMs. This illustration shows that PCB with via holes and SMT are cost-effective below densities of 200 pads per in². MCMs are the more cost-effective for higher interconnect densities [2].

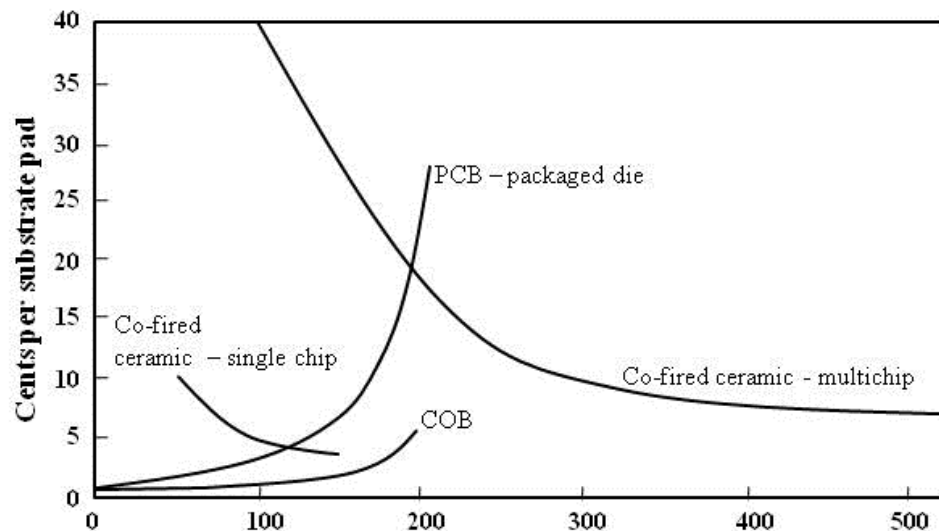


Figure 1.1 MCM and PCB costs per substrate connection pad [2].

Recently, the development of millimetre-wave wireless communication has been driven tremendously by commercial application, such as short-range

high-data rate wireless communication, passive imaging, and automotive radar. The requirements for these systems are usually high performance, compact size, high level of integration and most importantly, low manufacturing cost. To achieve extremely high levels of integration and miniaturize the overall device size, a lot of effort has been devoted into the development of system-on-chip (SoC), a concept to integrate the entire system, including RF front-end, analog and digital circuits, onto a single chip. However, the system performance might be degraded by the influence among different functional blocks through the common substrate and by the poor Q factor of the on-chip passives [3]. As an alternative, large area passive components, such as inductors, capacitors filters, and antennas, are usually built on a package platform instead of on the expensive active chips. Hence, the total cost will be significantly reduced [4, 5].

When the operating frequency goes into millimetre-wave region, packaging becomes particularly challenging. Historically, most of the mm-wave interconnects and passive components are in the waveguide configuration, which has very low loss. However, the waveguide structure is bulky, expensive, and very difficult to integrate with monolithic microwave integrated circuits (MMICs). Later on, LTCC with its advantage of stable permittivity and low loss at microwave and mm-wave frequencies has dominated packaging solutions for decades [5-7].

1.2 Low loss ceramic dielectric

The dielectric properties of a dielectric material determine its functionality. These properties are dielectric constant ϵ_r , quality factor Q which is the inverse of the dielectric loss $\tan \delta$, and the temperature coefficient of resonant frequency τ_f .

It is well known that low relative permittivity materials in the range of 4-12 are used for millimetre-wave communications and also as substrate for microwave integrated circuits [5-7]. High permittivity materials on the other hand are used as mainly for capacitors or resonators in mobile phones. Signal propagation with minimum attenuation is one of the most important aspects in electronic packaging. This is directly related to the relative

permittivity and metal conductivity. In the case of ceramic packages, the relative permittivity of the ceramic over and within the metal lines is deposited or embedded dictates the propagation delay t_d , which is given by [8],

$$t_d = \frac{l\sqrt{\epsilon_r}}{c} \quad (1-1)$$

where, l is the line length, ϵ_r is the relative permittivity of the substrate and c is the speed of light. Thus, substrates with low ϵ_r are required to increase the speed of the signal [9].

Large value in the product of quality factor and frequency $Q \cdot f (>1000 \text{ GHz})$ is normally required for the dielectric material. The value is determined by the ratio of resonant frequency to the bandwidth measured at 3 dB below the maximum height resonant frequency [10]. The theoretical relationship between Q and resonant frequency should be constant and this value is often quoted when comparing dielectric materials [5, 10]. The categories of microwave dielectric materials are shown in Figure 1.2 in which $Q \cdot f$ is plotted with respect to the dielectric constant [11]. Curve in the figure shows an out-

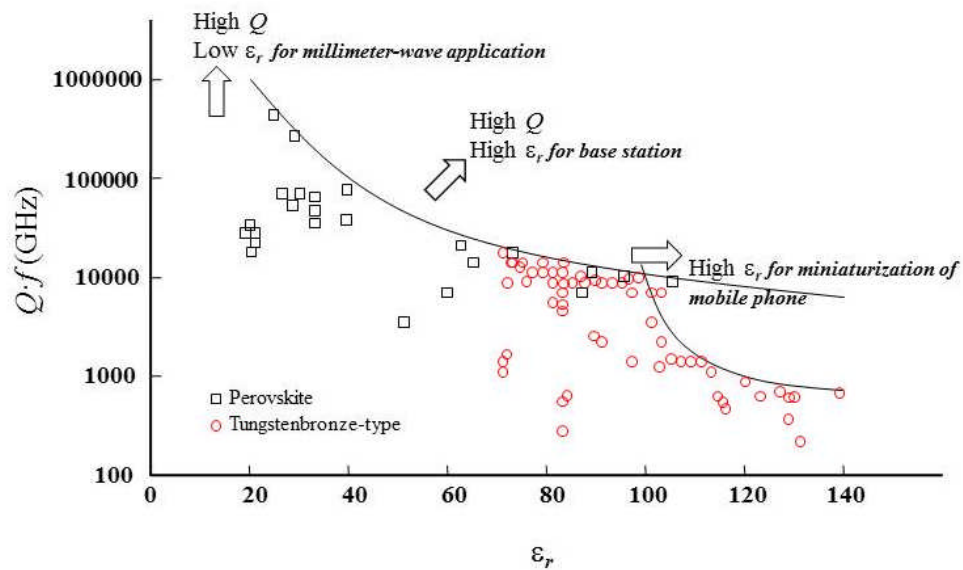


Figure 1.2 Directions for research and development of dielectric components. $Q \cdot f$ are shown as a function of relative permittivity, ϵ_r [11].

line of the upper limit of $Q \cdot f$. The first direction with the high ϵ_r is mainly on demand for miniaturization of mobile phone parts. The high Q and high ϵ_r is intended for increasing signal/noise ratio for application in mobile phone base station. The third direction with high Q and low ϵ_r is for devices working in millimetre-wave region. While crystal structure of perovskite refer to compounds such as BaTiO_3 , the tungstenbronze-type $\text{BaOLn}_2\text{O}_3\text{TiO}_2$ ceramics are well known microwave compositions having moderately high relative permittivity (70-100), high $Q \cdot f$ (>7000 GHz). $\text{BaO-Ln}_2\text{O}_3\text{-TiO}_2$ in 1:1:4 or 1:1:5 compositions are especially suitable for dielectric resonator in mobile phone [12, 13].

To meet the increasing demand to high-density packages, a technology that fulfils the criteria of high performance, simple processing, and cost effective in high volume production, mainly in the microwave packaging industry needs to be found. LTCC, for instance, offers high quality printable elements and passive components that could be embedded in the substrate, which leads to an increase in yield, reduction in cost and better lead time.

LTCC technology has great potential if applied to the integration of passive elements into monolithic, highly reliable, and robust LTCC modules, which consists of multilayer substrate material with 3D strip-line circuitry [3, 14]. The ability to co-fire many layers simultaneously has the advantage of reducing both the process cost and process variability [15]. LTCC has excellent properties for packaging applications, supported by low temperature conductor paste, simple process, and multi-layered structure. It has been used for high reliability applications in military, avionics, and automotive areas, and in MCMs for communication and mobile device application [16].

High-temperature co-fired ceramic (HTCC) technology was also developed to increase packaging density by building individual conductor/dielectric layers and then laminating them by firing at a high temperature with pressure applied.

New demands on the performance of miniaturization efforts utilizing traditional packaging techniques are necessitated by the demand for higher circuit density, fine line resolution, mixed signal circuitry, low EMI emission and susceptibility, higher temperature, and diverse severe mechanical and environment requirements. Therefore, a thorough understanding of the

materials and how they respond to the fabrication processes must be established to arrive at a cost-effective high performance assembly [17].

Multilayer LTCC substrates offer the opportunity to fabricate compact, low cost, high volume modules for a wide range of microwave applications since they combine well established screen printing techniques with multilayer ceramic lamination and low firing temperatures. This enables the integration of various materials to achieve passive components such as resistors, capacitors and inductors to provide increased functionality within a specified volume [18].

The continuously growing demand for increased packaging density in electronic devices cannot be met by just decreasing line widths and clearances on one conducting layer but also requires an extension into the third dimension. This leads to multilayer structures in the various fields of electronic packaging.

As the requirements for high performance systems continually increase, even MCM technology cannot cope. Hence, investigations have been conducted into more advanced technologies that would allow stringent requirements to be fulfilled. As a result, 3D packaging technology has evolved as a natural progression from 2D packaging technology as shown in Figure 1.3. It is a trend that 3D packaging including interconnection provides increased electrical performance and packaging density compared to two-dimensional 2D packaging which has been used for a long time. Packaging development comes with an increasing component I/O densities. Currently, among available solutions are 3D design and System-in-Package (SiP). The characteristic feature of these packaging developments is the use of the third dimension (z axis) to build a complex 3D electronic circuit, block or system.

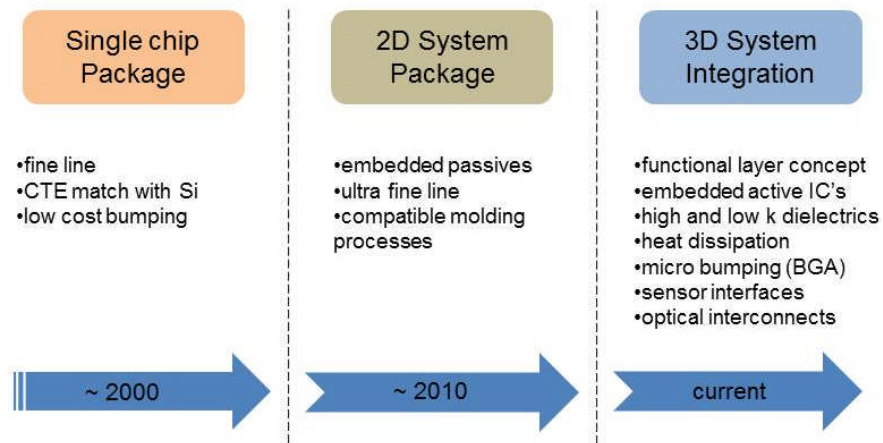


Figure 1.3 Integration development of electronic packaging [19].

This thesis presents a range of methods employed in manufacturing the 3D structures such as channels and cavities where the process may not be limited to the typical processing steps such as cutting, printing, laminating as well as sintering.

1.3 Applications of LTCC

The wealth of inter-disciplinary research opportunities motivated researchers to start cross-disciplinary research and have created concepts such as system-in-package (SiP), microelectromechanical systems (MEMS) and microfluidics. These systems involve electrical, mechanical, chemical and optical modules in a single package. In this chapter, the applications based on LTCC technology are described briefly. Special interest is put on RF MEMS.

1.3.1 System-in-Package (SiP)

LTCC is used mainly in the electronic packaging industry. LTCC provides stability, reliability and hermeticity to the device. Microwave filters, couplers, antennas and other components can be made in LTCC with very fine dimensions [20]. Broadside coupling and complex waveguide transitions are additional benefits of LTCC technology [21]. The dielectric sheets are processed in parallel so a large number of layers can be used, making the device more compact. Personal digital assistants, mobile phones, GPS devices, RF front-end modules, are few examples using LTCC SiP. Another

advantage of LTCC is the precise control of material properties. The permittivity and permeability of the dielectric can be tailored according to requirement during tape casting of LTCC tapes by appropriate composition. An example of an LTCC module is shown in Figure 1.4.

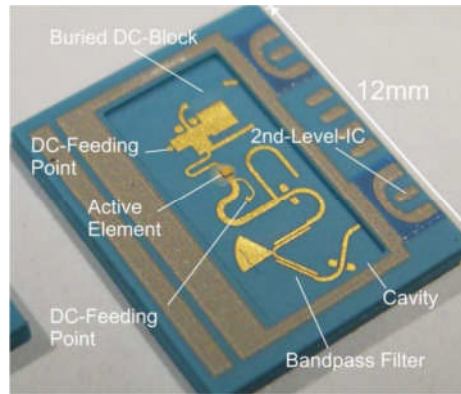


Figure 1.4 SiP application of LTCC [22].

1.3.2 Sensors and actuators

Ceramics are popular for their rigidity and their resistant nature to most chemicals, making them a popular solution for sensor and actuator applications in harsh environments. Other ceramics technologies, including HTCC, are not feasible for sensors that required unusual shapes whereas, LTCC has the intrinsic property of softness in the unfired state that allows it to be formed into shapes for various non-trivial actuator applications [23]. Moreover, LTCC retains its properties in various conditions thus providing a stable response. Examples of LTCC based sensors and actuators are pressure sensors, temperature sensors, proximity sensors, gas flow sensors, gas detection sensors, electrochemical sensors and hybrid micro-valve actuators [24].

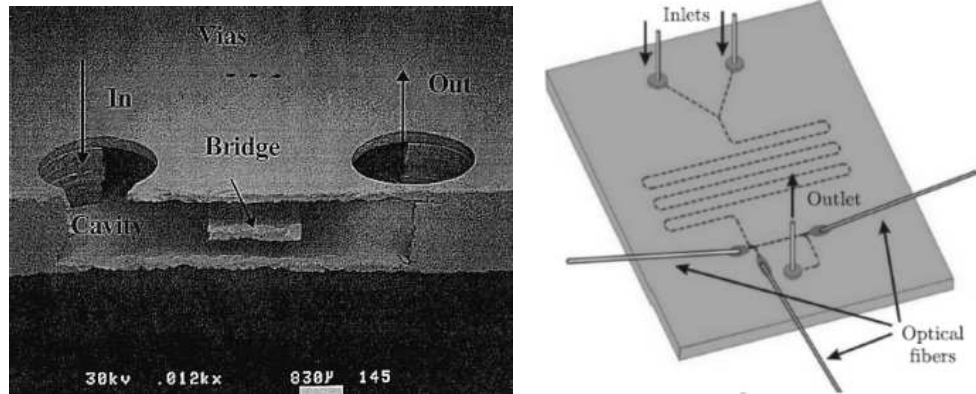


Figure 1.5 LTCC based gas flow sensor and optical fluid detector [25].

1.3.3 Microfluidics

Recent studies on microfluidic applications have shown LTCC to be a very desirable platform [26]. It allows the use of microfluidic components along with different sensors on a single substrate. From the analysis of hazardous chemicals to many biological applications, LTCC offers a variety of desirable features. The realisation of microchannels, micromixers, hotplates, microheaters and micropumps using a single technology is an advantage that cannot be overlooked lightly [27]. Easy processing of green state ceramic sheets, using mechanical or laser tools, is not only cost effective, but it is very reliable after firing and turning into a hard ceramic block with integrated tunnels and cavities that is not possible otherwise.

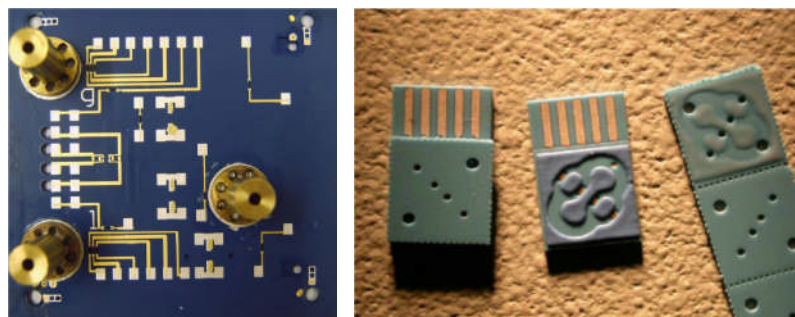


Figure 1.6 A microfluidic reactor and biosensor with integrated fluidic and lid from LTCC [28].

1.3.4 Micro-electromechanical systems (MEMS)

MEMS refers to miniaturized devices fabricated through fabrication techniques called “micromachining.” Since MEMS is based on the phrase “micro,” a suitable definition for a MEMS device could include any device possessing at least one feature size in the micrometre range, for example, between 0.1 and 100 μm [29]. MEMS devices are typically designed to operate in one or more energy domains, such as mechanical, electrical, fluidic, optical, RF, etc., and usually include a designed mechanical structure, which differentiates an integrated circuit from a micromechanical device with integrated electronics.

When it comes to MEMS, it has been claimed that up to 85% of the total cost is directly related to the packaging issues [30]. Until now, there are no generic MEMS packaging solutions. Silicon based MEMS structures required different operating conditions compared to ordinary chips. They are more sensitive to mechanical stress due to moving parts and for high frequency applications they demand an optimum signal propagation route. LTCC fulfils all the requirements of MEMS structures. It provides good hermiticity and closely matched thermal coefficient of expansion (TCE). Embedded cavities are possible with LTCC and the high conductivity gold tracks assist in signal propagation with low loss. The cost factor of LTCC packaging for MEMS applications is very low and the turn-out time is short [31, 32].

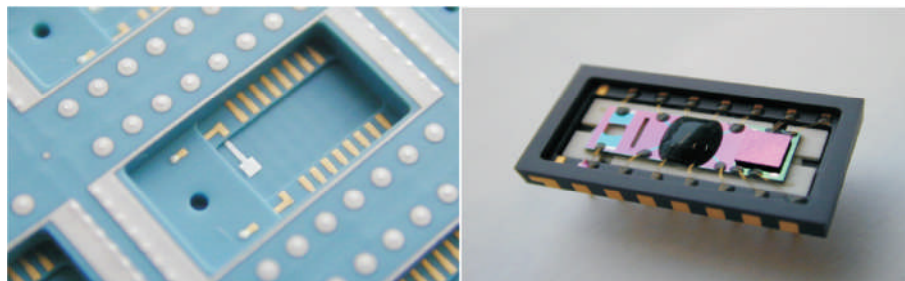


Figure 1.7 Silicon microphone packaging and spectrometer in LTCC [33].

1.3.5 RF MEMS switches

MEMS switches are intended to switch the propagation path of an analogue signal with high signal linearity. This function might be used to connect or disconnect an electrical potential, or to select signals, for instance the incoming and the outgoing signal of an antenna, or to reconfigure a sub-system. Typical applications of the latter type are switching of filter banks, tuning of filters by switching capacitors or inductors, switching of delay lines in phase-shifters, impedance matching by switching stub-lines or capacitors, and configuration of antenna patterns or frequencies by switching antennas or parts of an antenna. To switch DC to RF signals, the most important properties are an extremely large bandwidth from DC to a few tens of GHz with very good signal properties over the whole bandwidth. The switching speed and the power consumption are less important. Metal contact switches are good candidates for these applications.

Although further improvement in the reliability is needed, military and space applications favour MEMS components, because of their robustness against external influences such as radiation, temperatures and strong electromagnetic fields, and their high shock resistance.

1.4 Motivation & Objectives

The continuously growing demand on packaging density in electronic devices cannot be realized by just decreasing line widths and clearances on one conducting layer but also requires an extension into the third dimension. This leads to multilayer structures in the various fields of electron packaging.

In particular, the multilayer LTCC substrates offer the opportunity to fabricate compact, low cost, high volume modules for a wide range of microwave applications since they combine well established screen printing techniques with multilayer ceramic lamination and low firing temperatures. These enable the integration of various passive elements and components to provide increased functionality within a specified volume.

This study presents the methods employed in manufacturing the three dimensional structures such as channels and cavities where the process is not limited to the standard LTCC processes, with the following objectives:

1. To allow 3D fabrication on LTCC that is not normally sustained standard lamination,
2. To demonstrate low cost and low loss hollow waveguides which will be the basis to realise microwave and millimetre-wave components.

1.5 Review of thesis

Chapter 1 has mentioned the importance of electronics packaging.

Chapter 2 describe about standard process of LTCC.

Chapter 3 describe enhanced LTCC process where multi-stage/progressive lamination and sacrificial insert are introduced.

Chapter 4 describe the concept of hollow substrate integrated waveguide and how it is design and fabricated.

Chapter 5 describe about hollow waveguide components. Slot antenna and cavity filter has been briefly studied to find the possibility of integration of both components under the same platform.

Chapter 6 concludes the work by summarising the achievements, suggestion for further improvements and future work.

Chapter 2

Standard LTCC Process

LTCC technology has demonstrated great potential to meet the increasing demands for higher density and performance packages, especially in the high-end RF packaging [34]. The ability to co-fire many layers simultaneously has the advantage of reducing the process cost and time [15]. Although other materials are also often used as the substrate material for flip chip packages, ceramic, especially LTCC substrates, result in the best reliability of microelectronic packages because the coefficients of thermal expansion of such substrates are close to that of silicon chips. For these reasons, LTCC has the flexibility in the fabrication of electronic devices, and has a potential to replace conventional tin-lead (Sn-Pb) solders in printed circuit boards (PCBs), integrated circuits (ICs), and chip packaging for environmental reasons [35].

LTCC also has an advantages due to its low surface roughness, good thermal performance, high print resolution of conductors, good dielectric thickness control, passive integration, high frequency performance, and excellent stability [36]. Applications of LTCC among others include microwave modules, opto-electronics modules, meta-material antennas, automotive, military, medical, sensor packaging, integration for silicon micro-fluidics, capacitance sensing, and cavity resonators.

Sintered LTCC material usually has very good temperature stability up to 650°C, and some compositions also exhibit a high degree of chemical resistance, making them suitable for fabrication of chemical micro-reactor and harsh environment [37].

Apart from LTCC, the high temperature co-fired ceramic (HTCC) technology was also developed to increase packaging density by building individual conductor/dielectric layers but, fired at a higher temperature above 1000°C and applied pressure [2]. While inheriting the advantages of both thick film and HTCC technologies, LTCC has other advantages as described in Table

2.1. LTCC also is a technology with excellent properties for packaging and MCM applications, featuring good conductors, low associated capacitances, simpler processes and high layer count as being described by M. R. Gongora-Rubio *et al.* [16].

Table 2.1 Comparison between LTCC with other technologies [38].

Technical Characteristic	PCB μ via	Silicon	HTCC	LTCC
Insulation resistivity	-	-	+	+
High temperature resistivity	-	-	++	+
Thermal conductivity	-	+++	++	+
Electrical conductivity	+	-	-	+-
Integration density	+-	+++	+-	+-
Integration of passive components	-	+-	-	+
Integration of fluidic components	-	+-	-	+

+ and – were used as a comparison of the four materials with respect to each technical characteristic.

A typical LTCC circuit has surface conductors for connecting components, and has internal and via-fill conductors for making up the internal components of the circuit. The multilayer ceramic packaging process consists of green tape preparation, metallization layout, lamination, and co-firing. Electrical interconnections in LTCC are provided by networks of conductive lines (usually Ag, Au, or Ag-Pd), which are usually deposited

onto green or fired LTCC material using a screen-printing method. A bonding between LTCC green state tapes is formed during the lamination and co-firing processes.

The other important point is the ability to support 3D system configuration for the next generation communication technologies. LTCC due to its flexibility, provides the potential to fabricate 3D structures through its multi-layered green tapes.

2.1 Standard fabrication methods

The processing parameters considered to have a direct effect on the final device properties are discussed in the following section. The main fabrication processes for LTCC here are laser etching, screen-printing, lamination and sintering.

2.1.1 Laser machining

Applying LTCC green tapes as a platform for the construction of 3D structures requires the micromachining of via holes, channels and cavities with defined geometries and structures. Mechanical processing for structuring these unfired tapes are cutting, drilling and thinning. To perform these tasks suitable parameters such as precision and processing speed are essential.

A laser is a powerful tool for surface patterning and micromachining because of its non-contact nature of processing. Also, structures with high aspect ratios, which are challenging to achieve with traditional microfabrication techniques such as chemical or plasma etching can be conveniently fabricated with laser processing [39]. Laser machining, or specifically the direct laser etching process, has a potential to offer a rapid and very cost effective solution to the prototyping of LTCC-based components [40]. Comparison between structuring and machining techniques is given in Table 2.2.

Table 2.2 Machining and structuring techniques in multilayer ceramic technology [41].

<i>Technique</i>	<i>Advantage</i>	<i>Disadvantage</i>
Punching	<ul style="list-style-type: none"> -Micro-vias with diameters of 30-100 μm possible -Moderate via density, volume, and throughput 	<ul style="list-style-type: none"> -Deformation, cracks for via pitch less than 1 mm -Micro punches with diameter below 100 μm could easily damaged
Mechanical milling/CNC	<ul style="list-style-type: none"> -Complex geometries with dimensions of 100-125 μm 	<ul style="list-style-type: none"> -Chip formation -Wear and tear of tools -Micro-tools with diameter less than 100 μm could easily damaged
Hot Embossing	<ul style="list-style-type: none"> -Complex geometries with dimensions of 25-100 μm -High throughput through roller embossing 	<ul style="list-style-type: none"> -Wear and tear of molds -Structures depth limited by thickness of the green tape -Sticking of green tape on mold -Stress, cracks problem
Chemical etching	<ul style="list-style-type: none"> -Structure with dimensions of 25-30 μm 	<ul style="list-style-type: none"> -Chemical etchant required -Masking process needed -Control of etching rate is difficult -Dissolve of ceramic materials
Laser machining	<ul style="list-style-type: none"> -Complex geometries with dimensions of 20-120 μm -Non-contact technique -High accuracy, high via density, high volume possible 	<ul style="list-style-type: none"> -Tapered vias and channels -Low to moderate volume throughput compared to other methods

In this study all samples are micromachined using a Nd:YAG laser (Proto Laser 200 by LPKFTM). A test pattern for laser machining has been used to evaluate parameters such as optical power output, P [W], pulse frequency, f [kHz], beam scanning speed, v [mm/sec.], and number of repetition cycles, n .

Table 2.3 LPKF Protolaser 200 specifications.

<i>Specification</i>	<i>Value</i>
Pulse duration	0.5 -7.5 nsec.
Maximum optical power	13 W
Focal diameter	25 μm
Laser beam source	Nd:YAG
Laser beam wavelength	1064 nm
Pulse repetition range rate	20 – 100 kHz
Laser write speed range	1 – 1000 $\text{mm}\cdot\text{s}^{-1}$
Maximum working area	115 x 115 mm^2

Among them, it has been reported that Nd:YAG laser initiates the process of sublimation in LTCC substrates, which is considered as a suitable candidate for conductor etching and LTCC micromachining [40, 42]. The direct laser etching process has been investigated in this work. The laser prototyping machine LPKF Protolaser 200 features an Nd:YAG (Neodymium-doped Yttrium Aluminium Garnet) solid-state laser source capable of producing up to 13 W of optical power at wavelength of 1064 nm [43]. The attributes of this system are shown in Table 2.3. Figure 2.1 shows the illustration of how the direct laser etch is performed.

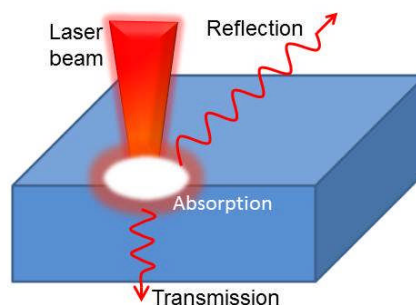


Figure 2.1 Laser ablation mechanism where only the absorbed energy is effectively used in the material processing, while others transmitted or reflected.

The process developed in this work is believed to be applicable to all forms of laser pulses. Figure 2.2 shows the laser positioning system.

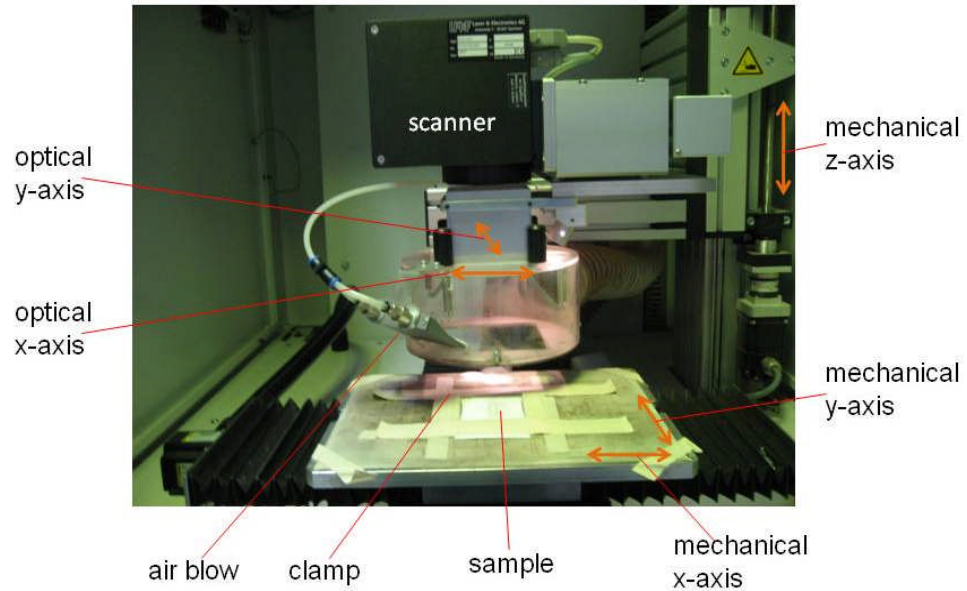


Figure 2.2 The three axis positioning system of Protolaser 200.

The laser beam is deflected into the desired direction via deflecting mirrors. The mechanical z-axis allows material of a wide range of thicknesses to be machined. The mechanical z-axis is driven by a 3-phase stepping motor via a gear, thus achieving positioning accuracy of $\pm 1 \mu\text{m}$. Combined with an optical calibration system, the z-axis adjust the laser beam for the optimal focus point.

2.1.2 Laser pulse rate and writing speed

The pulse frequency and writing speed are two closely related parameters which play an important role in the throughput of the process. The writing speed is the laser etching speed when laser is in ON state. The writing speed can be set to any value between 1 mms^{-1} to 1000 mms^{-1} ; a higher scanning speed requires a high pulse rate to compensate local laser ablation that decreased due to increased writing speed.

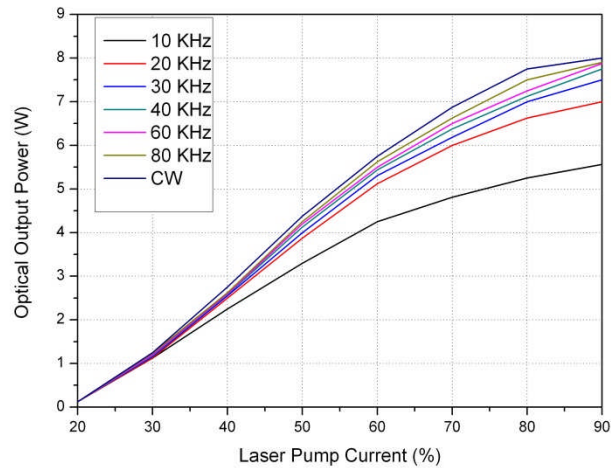


Figure 2.3 Laser pump current with respect to optical output power.

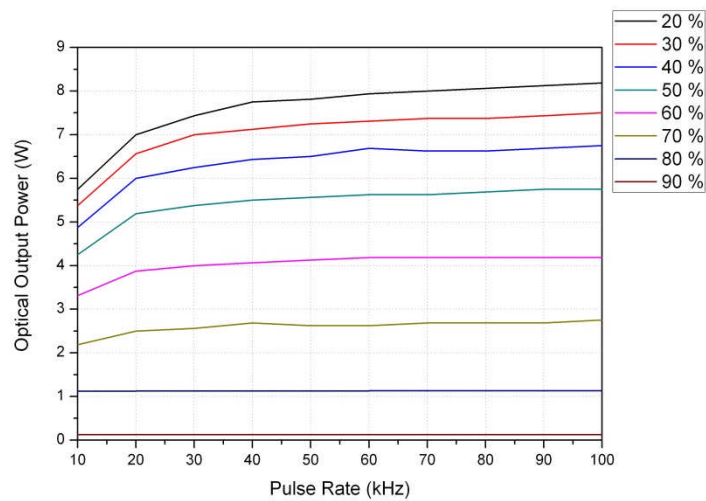


Figure 2.4 Laser pulse rate with respect to optical output power.

The optical output power to laser pump current (fluence) and to pulse rate is given in Figure 2.3 and Figure 2.4 respectively. It was found that power of 5.8 W (60%), pulse rate of 40 kHz, and scanning speed of 500 mm⁻¹ produced less damage with moderate etch speed.

2.1.3 Optimisation of laser parameters

Once the effects of varying laser power, pulse rate and scanning speed were individually analysed, it was found that all the parameters are mutually dependent and they cannot be optimised separately. Thus, the optimisation goals for the parameters are:

- i. to achieve the clean design features at a high etching speed
- ii. to reduce the substrate damage.

To attain (i) and (ii), this part will briefly discuss the etch rate and the laser thinning process that both important in micromachining process.

- **Etch rate and laser thinning**

As the commercial LTCC green tapes came at dimensions specified by the supplier, there is a need to tailor made the dimension according to the desired one. For particular purposes, the control of thickness is very important to meet a certain design dimensions such as in cavities and channels.

To achieve a more precise etch depth, the green state 9K7X LTCC needs to be sintered according to the temperature profile shown in the sintering section. Figure. 2.5 shows laser paths that has been done on the fired LTCC sample. The etch depth was then measured using surface profiler from KLA Tencor™.

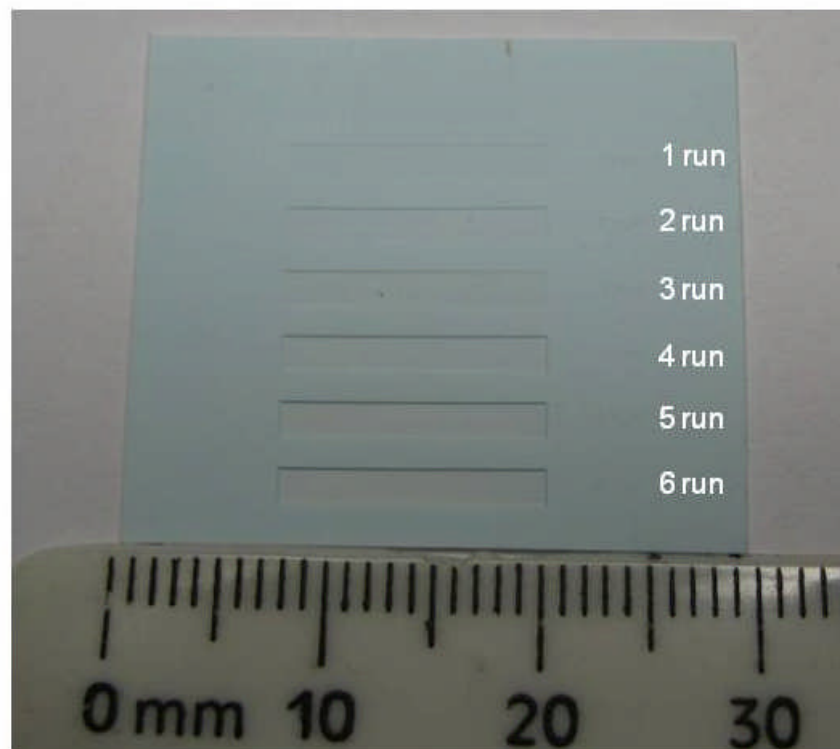


Figure 2.5 The etch rate of LTCC determined from etch depth of the varying the laser repetition.

The speed of laser etch can be determined by dividing the etch depth to the number of laser repetition. By plotting the etch depth to laser repetition, a linear relation could be suggested for the etching speed as shown in Figure 2.6. The laser centre condition was set as power: 60%, pulse frequency: 40 kHz, scanning speed: 500 mms^{-1} for having a relatively high etching rate and from the observations that carbon particles were not produced on the laser paths.

Considering 60% of laser power, which is approximately 5.2 W, the etch speed of $36 \mu\text{m}/\text{repetition}$ is deduced, which is with 7 repetitions a single layer thickness of green state 9K7X tape could etched through as could be explained from Figure. 2.6. In the figure, the first laser etch exhibits lower etch speed due to low power absorption of green state tape's surface, which is composed mainly of organic binder. The etch proceeds in a linear fashion after the first repetition.

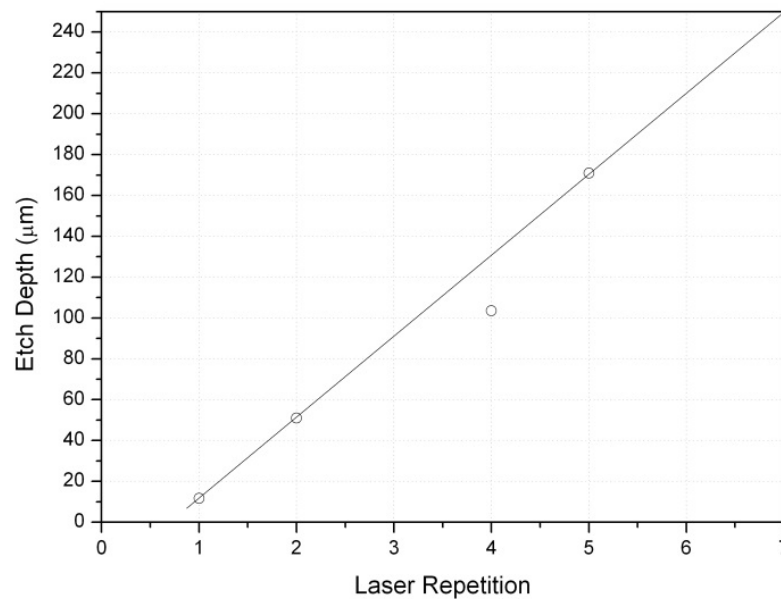


Figure 2.6 A linear laser etch rate under condition of power/pulse/speed: 5.2 W/40 kHz/500 mms^{-1} .

To minimise the damage on the surface, the working sequence adopted in the etching process was to machine the contour line before thinning or removal of unwanted bulk areas. If these bulk areas are etched before

machining the contour lines then cracks may appear in the design features. Once machined, the contour lines isolate the design from the bulk area to be ablated, the heat produced during laser etching of the bulk area could be isolated from the design features. Figure 2.7 shows the optimization flow of the laser etching process in order to gain desirable thickness, roughness and minimum damage to the green state LTCC with and without metallic layer.

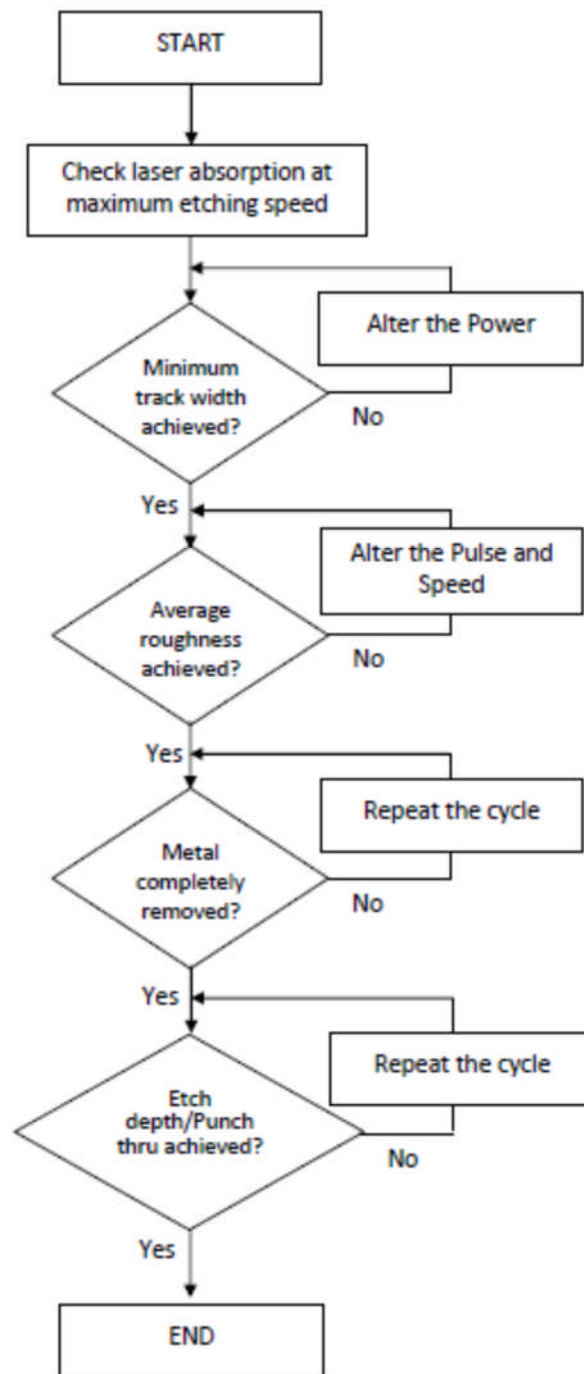


Figure 2.7 Flow diagram of laser etching process optimization.

The CAD drawing is uploaded into the operational panel that control the laser machine. The design features as shown in Figure 2.8 are comprising of the paths called contour line and hatch lines which the laser beam follows during the etching process. Apart from isolation, the contour lines play a significant role in defining the edge resolution.

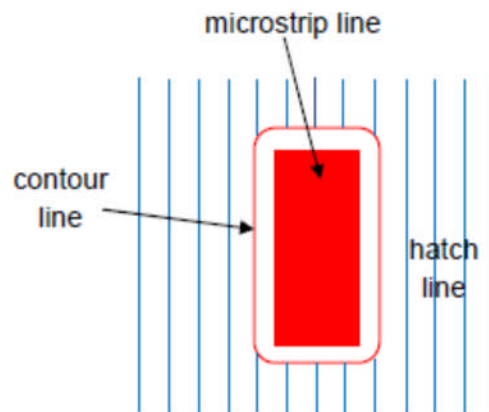


Figure 2.8 Laser machining follow the tracks of contour line and hatch lines.

The first thing that requires attention is the absorption of laser pulses into the substrate. The 25 μm laser beam may not result in etching 25 μm wide tracks in the conductor. The major obstacle in achieving narrow gaps in LTCC conductor machining is the composition of the printed conductive paste. Since metal particles are mixed with organic vehicles, these metal particles are not physically bonded, therefore thermal ablation results in rough edges and the gap formed is wider than the beam diameter.

It was realised that by optimising the laser parameters, the minimum gap of 50 μm achievable with diameter of 25 μm laser beam. During the optimisation process, the writing speed for rapid prototyping, power and pulse frequency was set to 500 mms^{-1} , 60% and 80 kHz respectively to produce suitable surface roughness. The process was repeated to ensure the complete isolation of patterns with various lines and spaces width.

2.1.4 Laser drilling and cutting

Laser machining of microvias in LTCC has been reported in various studies [44]. In one study, the use of laser machining on LTCC substrates of various

thicknesses using different type of lasers to achieve via diameter of 75 μm was demonstrated in a 254 μm thick substrate using Nd:YVO₄ laser, while in another study, 85 μm vias were realised with an Nd:YAG laser [34]. The laser and material interaction produces evaporation or sublimation of the material in the substrate which creating microvias and grooves. This interaction relates to laser wavelength and the type of material. In the drilling and cutting works a Nd:YAG laser beam with wavelength of 1064 nm was used. 254 μm thick 9K7X LTCC tape was used for the experiments.

Microvias can be created by pulsing a focused laser beam on the desired spot. However, these vias are not cylindrical and they do not open completely on the bottom side in the thick substrate due to insufficient absorption and penetration of the laser beam to the material [39, 45, 46]. As a solution, the diameter of the vias is fixed to certain sizes which is should be larger than the laser beam diameter. An alternative technique is to ablate with the focused laser surrounding the microvias which we call contour routing. This technique is promising in drilling microvias with a diameter of 100 μm and above onto 500 μm thick substrate. To perform these tasks a higher laser power of 6.2 W is required as compared to the thinning and conductor etching.

The cutting and machining of grooves is similar to via machining. Considering the width of the laser path of 30 μm , the layout of the design should consider laser cutting by setting 30 μm extra width of the original design dimension such as pad or microstrip line or 30 μm less for their desired groove width.

2.2 Screen printing

Various thick-film metal deposition techniques can be used in LTCC fabrication, but the most commonly used are screen printing and photoimageable material processing.

Screen printing is a conductor printing process in which the screen is held above the green tape and the conductor paste is pushed through the stencil onto the green tapes. The screen is produce according to the required print resolution and thickness of the conductive layer. The mesh type, mesh wire

diameter, and mesh count are selected on the basis of the desired thickness and resolution of the print.

2.2.1 Conductive paste

Conductive paste is obtained by dispersing conductive metal powder in an organic vehicle as a binder or plasticiser using a roll mill, and kneading it in a mixer. Metal powder is used as the conductive ingredient and for inorganic additives, normally low melting point glass and reactive oxides are used.

The organic vehicle of the pastes are usually composed of thinner, organic binders, plasticizers, and dispersing agents. Through sintering, conductors include inorganic additives that form voids inside the conductor and generally show higher resistance than the specific resistance of the metal itself. Figure 2.9 shows the resistance values of silver paste with respect to the impurities. Sheet resistance [Ω/\square] is the bulk resistance [$\Omega\cdot\text{cm}$] of the conductive material divided by the nominal thickness (normally $25\ \mu\text{m}$), and it is frequently used as a unit of resistance for thick film conductors [47]. In order to achieve high conductivity it is necessary to have minimal contamination and impurities. Nanoparticle ink also could had been used as being reported in [48-50], as a way to improve the resistance.

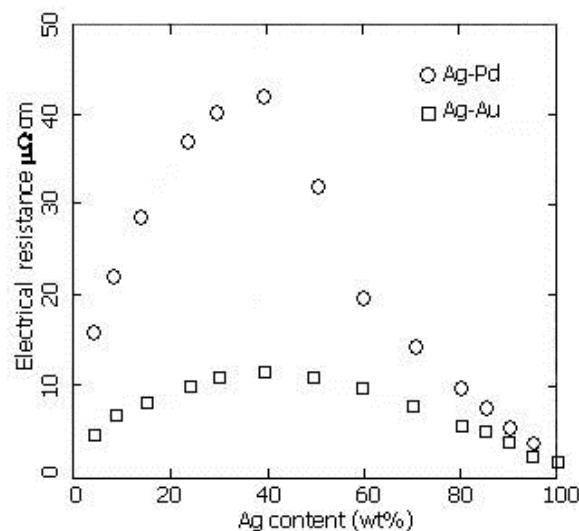


Figure 2.9 The composition dependence of resistance values Ag-based pastes [47].

In our case, this could be done by deposition of silver paste with an extra thickness, more than recommended by the supplier, to compensate for voids and to gain better conducting layer uniformity.

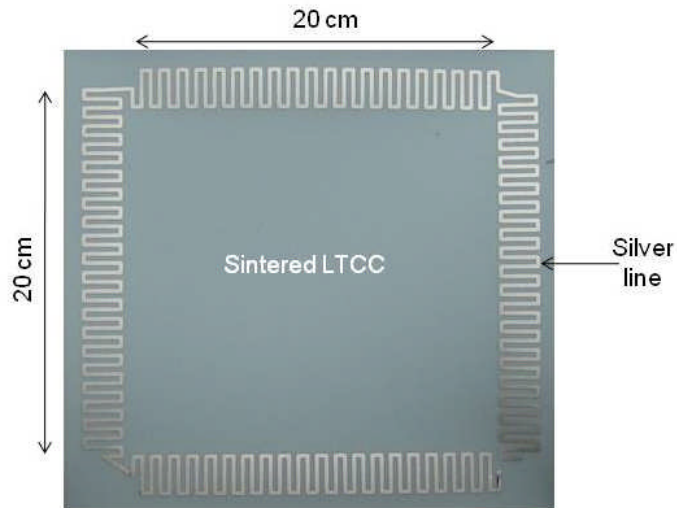


Figure 2.10 Resistance measurement scheme of conductor strip to check the improvement in the conducting layer.

Although the direct current four-probe method is generally used to measure the volume electrical resistivity of conductors [51], the value is measured at DC which is not describing the nature of sheet resistance at higher frequency. In our case we measured the resistance of the sintered conducting paste by preparing samples as shown in Figure 2.10. By measuring the resistance, the resistivity then could be calculated by considering the length of the conductor strip.

2.2.2 Metallisation of vias

Metallisation of vias or via filling is critical in multilayer packaging application and it is directly related to the reliability of the interconnect scheme. The via fillings are done with a conductive paste using a screen printer. The mylar sheet was retained on the LTCC green tape during laser drilling to act as a hard mask in this via metallisation process. The viscosity of the conductive paste is maintained not less than 150 Pa·s at 10 rpm, 25 °C to properly do the filling. For our fabrication, a stainless steel mesh of 325 per inch is used. DuPont LL601 paste is used for via fillings while, LL612 paste is used for conductor line deposition. The LTCC sheet is placed on a vacuum stage to firm hold the sheet as well as to increase penetration of the paste through

the vias. After the screen printing, the mylar is removed and the samples are dried in the oven under the environment of 70 °C for 10 minutes. Figure 2.11 shows the metallisation example of a via array for a cavity filter.

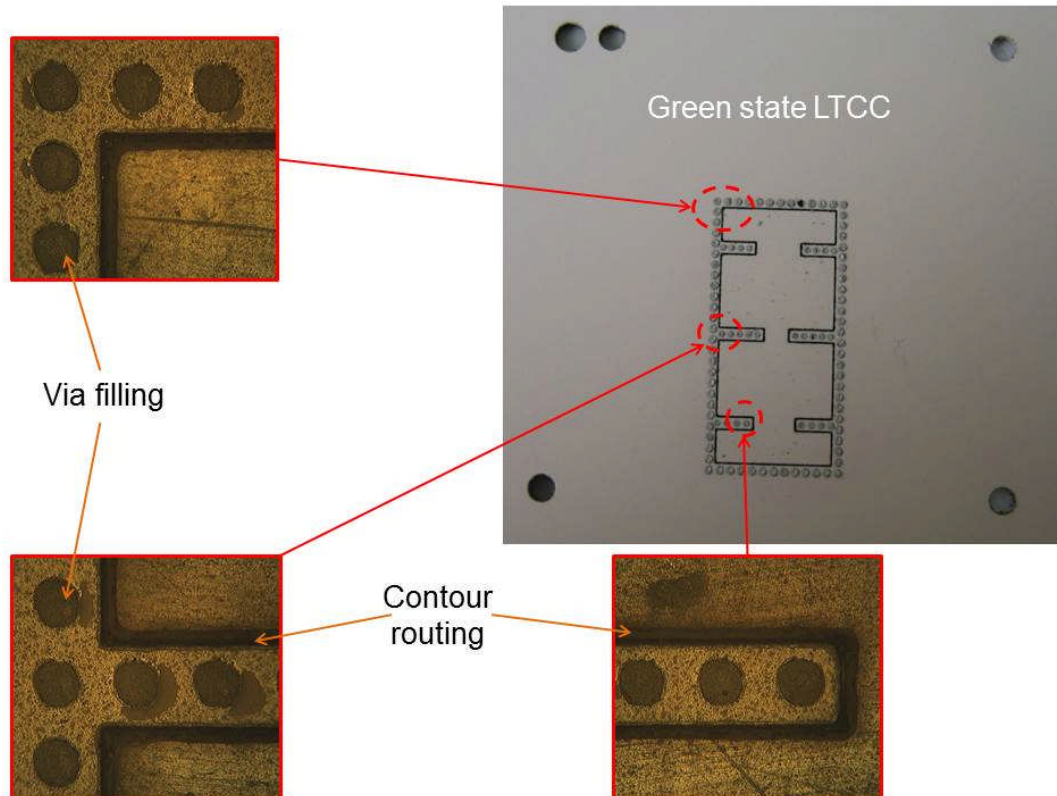


Figure 2.11 Green state LTCC sample is laser drilled and cut before being metallised with conductive paste. In these pictures, the vias are filled with DuPont LL601 silver paste.

In the direct laser etch, it is recommended that the conductor layer is printed and dried before the laser drilling of vias takes place. This is due to the nature of via filling paste with higher content of silver making a proper contact with the conducting layer through the sintering process.

2.3 Alignment and Stacking

After LTCC sheets have been laser machined and printed with Ag conductor, they are then dried in an oven at 70 °C for 10 minutes. These sheets are then aligned and stacked together on register pins with the help of fiducials. LTCC tapes are aligned using a manual alignment jig as shown in Figure 2.12 or a camera assisted translation stage or an automated

alignment may be used. A 180° rotation of the lamination is required after the first 5 minutes to ensure a balanced pressure and temperature applied to the entire tapes.

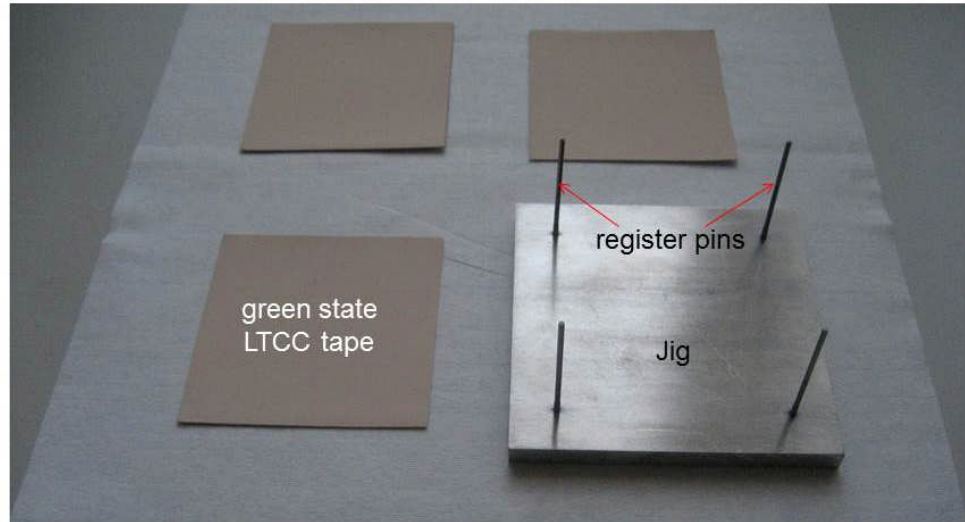


Figure 2.12 Alignment jig.

2.4 Lamination

The quality of 3D structures fabricated in LTCC technology depends strongly on the processing steps used: tape micro-structuring, lamination, and firing. Guidelines supplied in the data sheets for tape processing meet only the requirements for conventional applications but are not suitable for the fabrication of 3D structures such as cavities and channels. The recommended standard isostatic lamination pressure ranging up to 30 MPa is not appropriate for the realisation of unsupported structures. The even pressure applied through the sample results in the structures such as channels and cavities being crushed due to lack of support that could be provided by walls separated in a few hundred μm apart or more.

In fact, a lower pressure lamination techniques needs to be found to overcome this issue. Recently, a lamination performed at 6 MPa or less been reported [52]. As an alternative to the standard lamination technique, a uniaxial lamination such as illustrated in Figure 2.13 offers an effective technique for realising cavities.

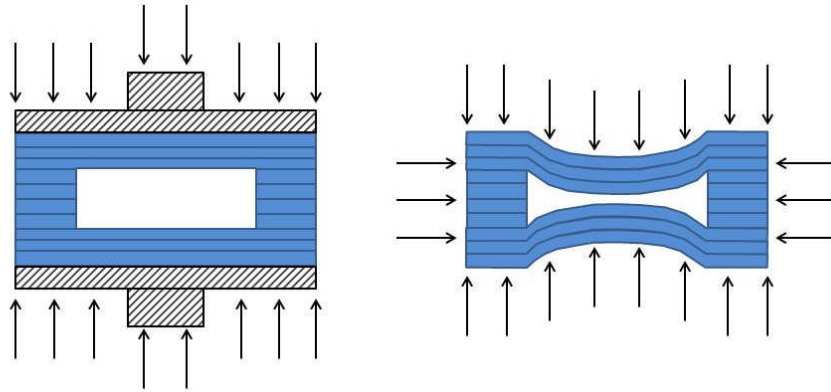


Figure 2.13 Uniaxial and isostatic laminator.

To realise these channels/cavities, a multistage lamination using a uniaxial laminator is discussed in detail in the next Chapter.

2.5 Sintering

Although there are various sintering methods proposed to improve the shrinkage issue in LTCC as shown in Figure 2.14, in reality there are no methods that could eliminate the shrinkage as far as the sintering process is involved. Due to this fact, the unconstrained sintering method has been used to deal with the normal characteristic of LTCC. The other reason is that we want to gain knowhow and experience in integrating passive components such as embedded passive elements (spiral inductors, capacitors) that have been developed in-house by the same sintering method.

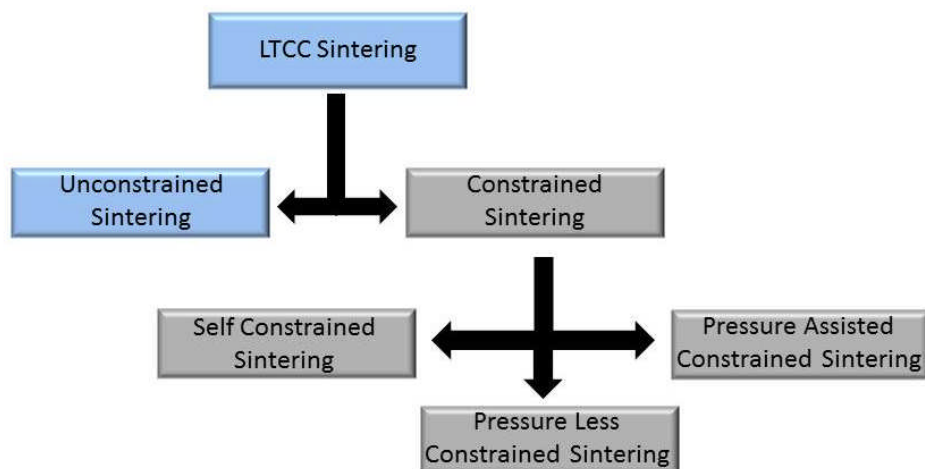


Figure 2.14 LTCC sintering types [47, 53].

To achieve the desired dielectric constant and low loss performance properties with the 9K7 tape system, the material was co-fired for 26.5 hours according to the temperature profile shown in Figure 2.15. The longer sintering time as compared to 943 tape system is to allow ample time for burnout of the organic constituents occurring between the temperatures of 200 °C and 550 °C. Peak temperature of 850 °C for 17-23 minutes applied to make sure densification of the alumina and glass happened before the cooling down.

From the test data provided by DuPont, the dielectric constant of 9K7 is very tightly distributed within expected specification range of 7.1 ± 0.2 . Loss tangent of all lots was found to be less than 0.0012 at the test frequency of 9 GHz.

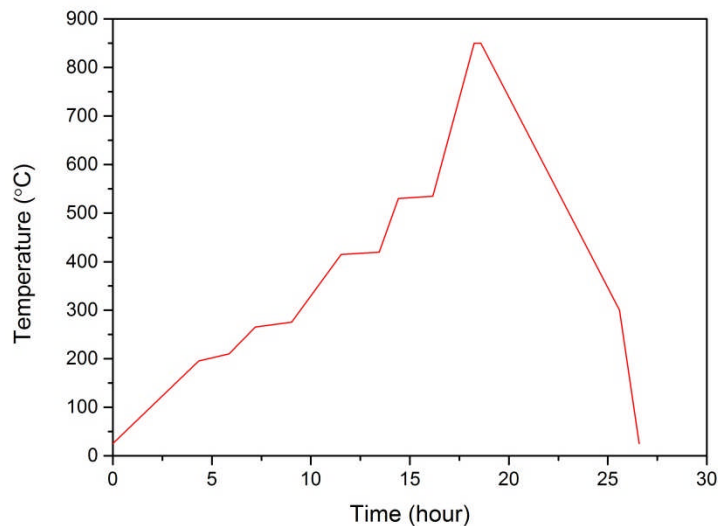


Figure 2.15 To achieve the desired dielectric constant and low loss performance properties the green tape undergoes 26.5 hours co-fire profile control points [51]. Organic burnout phase occurs between 200 °C and 550 °C. The sintering phase of composite ceramics is completed at the peak temperature for 17-23 minutes.

2.6 Surface roughness

Characterisation of the surface roughness is necessary to minimise loss for high frequency applications. The surface of the laser etched LTCC substrate was analysed and the surface roughness was measured using an Alpha-Step IQ surface profiler from KLA-Tencor.

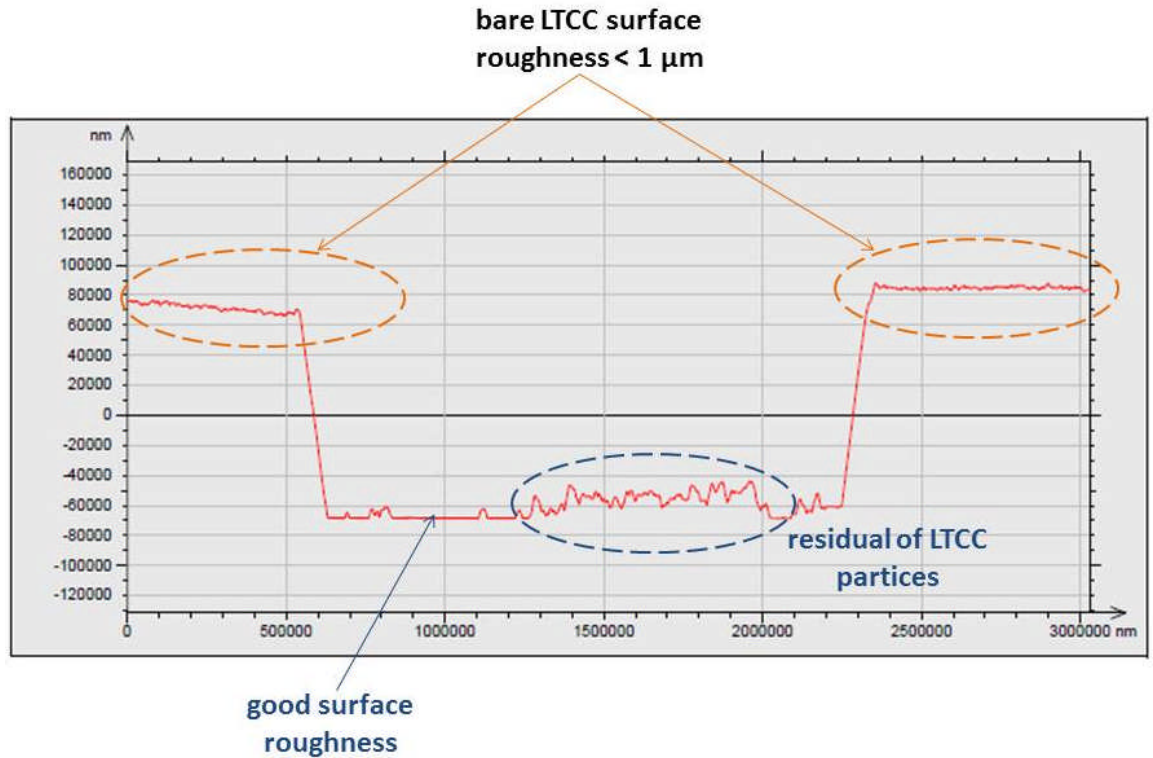


Figure 2.16 The sintered LTCC surface measured by surface profiler. By changing the repetition of laser etching, the etch depth with a sufficient flat surface is achievable as observed on the sintered LTCC.

Figure 2.16 shows the measurement done on etch depth of the sintered LTCC sample. It was observed that R_a of etched samples under pulse frequency: 40 kHz, power: 60% is uniformly distributed below 200 nm, while the R_a of unetched LTCC samples was around 100 nm. This shows that the difference between the two roughness values is almost well below the micron scale. The samples are therefore capable of working at frequencies on the order that the processing material is capable of.

2.7 Laser scribing

Laser scribing involves using the laser to create grooves or lines of holes that are spaced 125 +/- 30 μm centre with a depth of 40% to 50% of the substrate thickness. The scribing allows the ceramic substrates to be processed in an array and finally singulated by snapping apart the individual circuits along the scribe lines. Circuitry should allow at least 250 μm streets for the scribe lines. If the scribe lines are post-machined a higher power of

laser machine is required while at least 100 μm should be allowed from the metallization edges to edges of the scribe to avoid the laser harming the circuitry. The width of the scribe, i.e. diameter of the scribe grooves or holes, will increase with substrate thickness.

2.8 Conclusion

A direct laser etching process that could provide rapid prototyping such as sample patterning and conductor removal, via holes drilling, thinning process has been demonstrated. But, standard LTCC process has issues especially in realising 3D structures such as channels, cavities, and hollow waveguides. These need to be improved by introducing new techniques that will be discussed in detail in the next Chapter.

Chapter 3

Enhanced LTCC Process

To address and/or overcome the issues such as sagging and delamination in LTCC process in the previous chapter, we are focusing our investigation on an enhanced LTCC process. The preparation and the processing parameters of LTCC materials composition to improve shrinkages still undergoes extensible studies.

The following techniques may offer breakthrough in realising 3D structures in LTCC if studied further:

- i. Progressive lamination
- ii. Sacrificial paste or sacrificial volume material (SVM).

In this chapter, the detail on how these methods could be employed to fabricate 3D structures in LTCC is given based on processes achievable in the Leeds LTCC laboratory. This is done by fabricating cavities to replicate RWG in various dimensions.

3.1 Lamination technique

The lamination of multilayer ceramic substrates with embedded structures is a more difficult process to accomplish than the initial patterning of the layers such as conductor deposition. Currently available lamination techniques are summarised in Table 3.1.

Table 3.1 Lamination techniques for fabricating 3D structures [41].

<i>Technique</i>	<i>Advantage</i>	<i>Disadvantage</i>
Lamination with fugitive material	<ul style="list-style-type: none"> · Could realise complex 3D structures and suspended thick film (dimensions of 100 μm to 10 mm) · Could achieve fully enclosed and embedded structures · Could provide support during lamination and sintering 	<ul style="list-style-type: none"> · Poor dimensional stability · Filling and patterning of fugitive materials are difficult
Lamination sacrificial material	<ul style="list-style-type: none"> · Could realise 3D structures and suspended thick film · Could provide support during lamination and sintering 	<ul style="list-style-type: none"> · Removal of sacrificial material through chemical etching required · Fabrication of embedded structures such as cavities is not feasible · Filling and patterning of sacrificial materials are problem
Lamination with adhesive material	<ul style="list-style-type: none"> · Could realise complex 3D structures with dimensions of 100 μm to 10 mm) 	<ul style="list-style-type: none"> · Precise alignment between green tapes is an issue · Delamination could occur between laminates · Required compatible adhesive and ceramics system · Additional lamination steps required · Interconnection between sintered substrates not feasible for using adhesive layer
Gluing method (post-firing process needed)	<ul style="list-style-type: none"> · Relatively large embedded structures (> 10 mm) could be achieved · Cool temperature process at room temperature 	<ul style="list-style-type: none"> · Precise alignment between sintered substrates is an issue · Interconnection between sintered substrates is difficult · Post-processing required

This section describes the techniques to realise 3D structures such as cavities in LTCCs. While LTCC has a simple process and supports multi-layered structures, a few points in the processing steps need to be further investigated. For example, the relation between the pre-densification (prior to sintering) and sintering behaviour of composite-layered material systems is not well understood and is largely developed by trial and error.

3.1.1 Selection and influence of parameters

Though various investigations based on the analysis of variance have been done, no clear answers had been provided on which parameter of the processes gave a major influence to the manufacturing of 3D structures [36, 41]. Table 3.2 shows the parameters that involved in LTCC process. In one study, low pressure thermo-compressive lamination with insert material is employed, while another study used cold low pressure lamination process [54-57]. However, from these papers, we found that the laminating process plays a substantial role and is very sensitive part of the LTCC process especially when the 3D structures are involved. This may provide some clues to realising 3D structures such as channels and cavities that we are interested in.

Table 3.2 List of parameters and operations that can possibly influence the LTCC finishing.

<i>Parameter / Operation</i>	<i>Purposes</i>
Preconditioning	Temperature, duration
Alignment and stacking method	Orientation, numbers of layers
Lamination method	uni-axial / iso-static, pressure, duration, sequence
Sintering method	Temperature profile, position in the furnace, type of the setter
Type and flow of gas	Air, N ₂

In this study, we are focusing our observation on the following process variables:

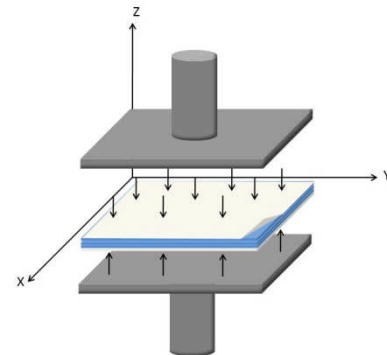
- i. Laminating pressure
- ii. Laminating temperature
- iii. Laminating time, and its sequences
- iv. Number of layers.

In the following part, the influence of these lamination parameters is studied. With the assumption that the lamination pressure and temperature play a non-negligible role on deformation during sintering process. The more pre-densification of the tape during lamination, the less deformation occurred during firing.

Figure 3.1 (a) shows the photo of the hydraulic uniaxial laminator system that was used for the study. Figure 3.1 (b) depicts the mechanism of how the pressure is applied to the LTCC tapes.



(a)



(b)

Figure 3.1 (a) uni-axial laminator with upper and bottom platen controlled by temperature controller system. (b) The mechanism of uni-axial laminator.

It would be interesting to know the effects of lamination, i.e. pressure, temperature and duration on the quality of tapes' interpenetration that translated into sag and crack free structures. Most suppliers recommended a lamination of 30 MPa, 70 °C for 10 min as their standard condition, but

altering this process could add an advantage for mass production. Although choosing the right parameters for processing 3D structures and predicting their final dimensions with good accuracy such as shrinkage is desirable, it is critical to take into account the effects of lamination variations when producing 3D structures.

3.1.2 Experiments on lamination without a sacrificial insert

LTCC tape from DuPont 9K7X has been used for the experiments. We start our investigation on lamination without using sacrificial materials. Considering the mass production, it is more realistic to concentrate the experiment on parameters to produce reliable 3D structures such as cavities. Thus, we are focusing on the impacts of following four parameters to the LTCC multilayer sample:

- i. Laminating pressure
- ii. Laminating temperature
- iii. Laminating time, and its sequences
- iv. Number of layers.

The observations such as the finishing profile and dimension changes on the samples are to be done at three states:

- i. After laser machining (2 layers each)
- ii. After lamination
- iii. After sintering.

To monitor the changes in the samples, the effects due to lamination and sintering processes need to be quantified. The parameters of the experiment were given according to Table 3. 3.

Table 3.3 Experimental parameters by considering achievable precision of our equipment.

Level	Pressure p , [MPa]	Temperature T , [°C]	Duration t , [min]	Layer n , [layer]
1	5	30	5	3
2	10	50	10	5
3	30	70	15	10
Supplier recommendations	30	70	10	≥ 4

Justification of the range of values in the Table 3.3 are:

- i. Pressure, p : This parameter is considered to be the most influential to lamination behaviour and the shrinkage. But, the lowest possible pressure is desired for lamination of top/bottom part.
- ii. Temperature, T : To promote organic binder interpenetration between layers and should not deviate too much from the recommended one.
- iii. Duration, t : DuPont recommends 10 min, but there should be interrelation with applied pressure and temperature. The top/bottom layer is interfaced directly with elevated temperature as compared to the inner layers. The time could be reduced due to this reason.
- iv. Number of layers, n : Circuits with cavities require at least 4 layers (unless using sacrificial pastes) since using fewer layers will contribute to more warpage, sag and shrinkage.

3.1.3 Results and observation

All samples are deformed or sagged except for the sample that laminated at 5 MPa. A sample with temperature that diverts from 70°C tends to have warpage and delaminate. No clear distinction is observed for different number of layers other than that all the samples are shrunk at least 10% as compared to the green state. Results in Appendix A show that pressure and temperature are both played an important role in the lamination.

Considering these results, a technique that could realise a hollow structure with a reduced pressure is needed. This technique is discussed in the next section.

3.1.4 Progressive lamination

The lamination can be the most challenging when embedded cavities or channels are involved. To avoid cavity deformation, the cavity is laminated in stages. This technique is referred to as progressive lamination as illustrated in Figure 3.2.

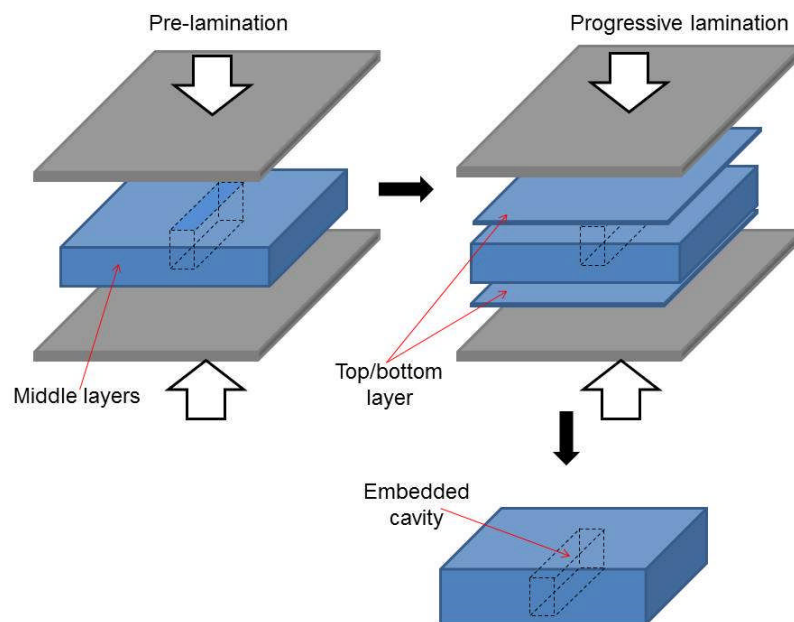
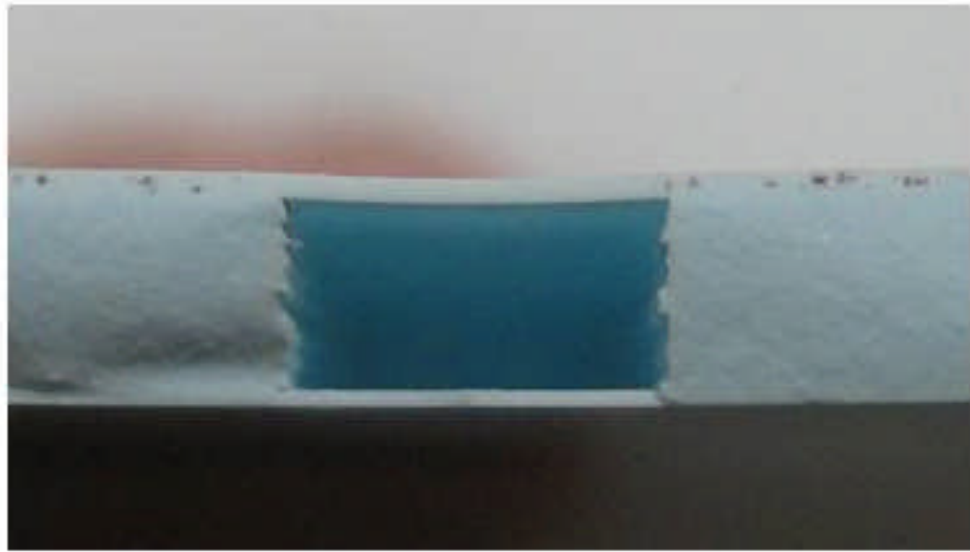


Figure 3.2 Progressive lamination for hollow waveguide.

Prior to the unconstrained sintering, the thermo-compressive lamination is performed at temperature between 30 to 70°C and pressures of 2 to 30MPa hold for 3 to 10 min. These parameters have to be optimised depending on the binder system used. At the contacts of two green tapes, the binders of each tape diffuse into each other through the mass flow movements and the arrangement of particles at the interfacing two adjacent tapes. The interpenetration of the particles from the green state tapes and its organic binders make a defect-free interface between tapes after sintering possible.

This can explain why the density of the laminates is increased by thermo-compression as compared to original green tapes' density [55].



(a)



(b)

Figure 3.3 (a) The cross view of 3D hollow structure produced after green tapes were laminated at 2 MPa and sintered. An excellent bonding between layers and free of crack and deformation. Bottom is with single supporting layer. (b) The hollow structures fabricated in the LTCC substrate with the broadwalls and sidewalls need to be metallised to replicate rectangular waveguide in LTCC.

After sintering, it is found that lamination under condition of pressure as low as 2 MPa, temperature of 70 °C applied for 10 min produced structure as shown in Figure 3.3 (a). 7.11 mm wide channels made from six middle layers and one each for the top/bottom layers progressively laminated at 70 °C for 10 min.

The next approach is carried out to obtain new structuring method by using sacrificial layers. The main ideas are to provide support for overlaying structures during lamination and to maintain the structures during sintering.

3.2 Lamination with sacrificial insert

The quality of the final 3D structure as such cavities or micro-channels is determined by the lamination and co-firing steps. The applied lamination pressures and temperatures during these steps can contribute to deformation of the fabricated cavity structures and prevents realisation of structures with complex geometry inside LTCC. Several methods have been introduced to preserve the desired geometry with the most common technique based on sacrificial volume materials (SVM) [58, 59]. Various types of substances can be used as an SVM, for example wax, graphite, polymers or mineral materials. Among these, graphite-based material is particularly attractive due to the simplicity in their mechanism of sacrificial paste oxidation and degassing during the sintering process.

Table 3.4 shows a chart of sacrificial materials that could be classified based on the functionalities:

- i. Dispose before sintering,
- ii. Burn out during sintering,
- iii. Survive sintering and need for removal afterwards.

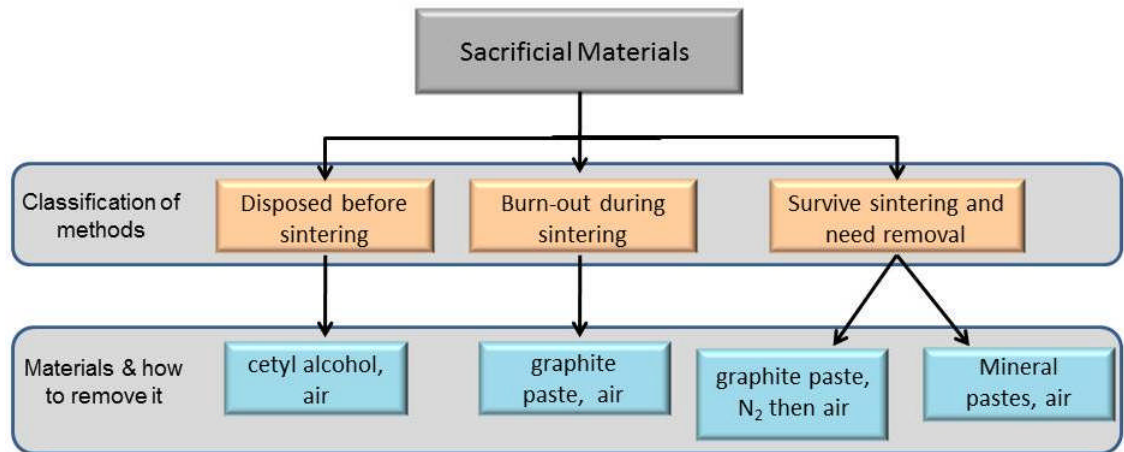


Figure 3.4 Chart of sacrificial volume materials classified by its functionalities [60].

The graphite-based sacrificial material is composed of two main ingredients; graphite powder and additives. The former is the functional element of the sacrificial paste and it supports LTCC laminates up to its full oxidation temperature (~800 °C and 850 °C), which is much higher than that of the organics both in LTCC and in the sacrificial paste (~450 °C and 300 °C) [59]. The additives on the other hand are based on a mixture of binder-solvent-dispersant system, which determines the rheology of the sacrificial paste for screen-printing.

Fabricating cavities in LTCC using sacrificial paste requires determination of the temperature ranges of LTCC open pore elimination and graphite burn out. This is particularly important as the open porosity in LTCC facilitates degassing of the oxidized paste. The LTCC open pore elimination temperature, which was found to be around 790 °C and comparable to the graphite sacrificial paste oxidation temperature [61, 62], suggesting that both of paste oxidation and degassing process could be applied to provide sufficient supports to structures during sintering.

Freestanding structures or cavities in multilayer structures using sacrificial paste are formed by oxidation of the paste as follows:

- i. Transport of oxidant to the graphite layer through direct contact to air or through pores in LTCC.

- ii. Absorption of air onto graphite surface and oxidation reactions
- iii. Transport of reaction product from the graphite surface.

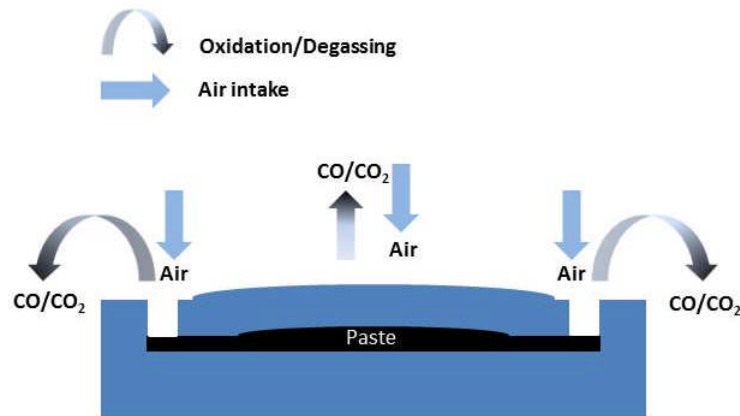


Figure 3.5 Mechanism of air intake and buried paste oxidation. Note that air and/or degassing gas transport through LTCC occurs only at temperatures below the LTCC open porosity elimination temperature [61].

The oxidation mechanism of graphite paste, which is buried in LTCC layers is illustrated in Figure 3.5. Paste oxidation, which can be enhanced by the air intake through the porous LTCC produces oxidized products degassing. Therefore, the balance between the graphite oxidation and the LTCC open porosity elimination process during sintering, play the major role in determining the cavity feature i.e. incomplete paste oxidation when open porosity is ended at densification phase results in deformation. This is an outcome of the increased gas pressure upon oxidation, which exerts force on the nonporous LTCC environment.

The critical materials and processing parameters can be summarised as:

- Particle size and oxidation temperature of the graphite powder
- Composition of the paste: although it does not affect the kinetics of the oxidation process, it determines the rheology and screen-printability of the paste, and thus has an indirect but important influence on the final structure.

- Heating rate influences the oxidation and LTCC densification process simultaneously. Higher heating rates shift both oxidation and LTCC open porosity elimination to higher temperatures [59].

3.2.1 Preparation of the sacrificial pastes

There are three types of pastes with composition designed to cater to three different situations and needs. They can be categorised as:

- i. Organic-based paste
- ii. Water-based paste
- iii. Wax-graphite-based paste

3.2.1.1 Organic-based graphite pastes

Sacrificial paste is prepared in a manner similar to that of commercial thick-film pastes. The graphite powder was mixed with an organic vehicle to obtain appropriate rheology for screen-printing [61]. The composition of mixture is shown in Table 3.4. Constituents were blended at 26:74 ratio by weight of graphite powder to organic additives (binder, solvent and dispersant). Initially, the binder and the solvent were mixed at 15:85 ratio at 87 °C until complete dissolution of the binder. This is followed by gradual introduction of the graphite powder into the mixture simultaneously with the dispersant.

Table 3.4 Organic-based sacrificial paste composition .

Material	Function	Specification	Product
Graphite	Sacrificial	<ul style="list-style-type: none"> • Particle size: 1-20 µm • Burn-out temperature ~780 °C 	Fisher Scientific
Ethyl Cellulose	Binder	<ul style="list-style-type: none"> • Binding particles in the paste • Decomposition temperature ~120 °C 	Fisher Scientific
Terpineol	Solvent	<ul style="list-style-type: none"> • Lower slurry viscosity • Boiling point ~215 °C 	Fisher Scientific
Acetyl Acetone	Dispersant	<ul style="list-style-type: none"> • Dispersing additive • Boiling point ~140 °C 	Fisher Scientific

Commercially available thick film pastes are usually formulated using terpineol as solvents for the organic vehicle, which is aggressive to the LTCC binder of most commercial compositions. In order to overcome this problem, a water-based graphite sacrificial paste is proposed [37].

3.2.1.2 Water-based graphite pastes

To overcome the corrosive character of organic-based paste on green state LTCC tapes, a water-based sacrificial paste is considered. The composition of the paste is given in Table 3.5.

Table 3.5 Water-based sacrificial paste composition.

Material	Function	Specification	Product
Graphite	Sacrificial	<ul style="list-style-type: none">• Particle size: 1-20 μm• Burn-out temperature $\sim 780\text{ }^{\circ}\text{C}$	Sigma-Aldrich
Polyvinylpyrrolidone (PVP)	Binder	<ul style="list-style-type: none">• Binding particles in the paste	Sigma-Aldrich
Propylene Glycol (PG)	Solvent	<ul style="list-style-type: none">• Lower slurry viscosity	Sigma-Aldrich
Glycerol (G)	Plasticiser		Sigma-Aldrich

Both of sacrificial pastes mentioned above are more suitable for small dimensions such as in microfluidics or to realising gap at limited dimension. The main reason is because the complex filler set-up is necessary [52]. A huge volume of paste also not preferred due to longer time of drying in the oven is need which may deteriorate the green state tapes condition.

As an option, a simpler filling using wax-graphite-based paste is propose.

3.2.1.3 Wax-graphite-based pastes

While the organic-based graphite paste and water-based graphite paste have their own advantages as being indicated previously, both of them however are more suitable to application such as MEMS and microfluidics where small spaces and channels are required. For structures such as channels/cavities with large dimensions, different issue such as large volume filling need to be addressed as well. For instance, is the sacrificial paste suitable for large volume filling, offering better support at lamination stage as well as during sintering. The proposed wax-graphite paste may not be suitable for screen printing but it may offer a solution for realising structures like hollow waveguides. The filling process needs to be done at the melting temperature of paraffin (a mineral wax) which is in between 46 to 68 °C.

Table 3.6 Wax-graphite-based sacrificial paste composition.

Material	Function	Specification	Product
Graphite	Sacrificial	<ul style="list-style-type: none">•Particle size: 1-20 µm•Burn-out temperature ~780 °C	Fisher Scientific
Wax (Paraffin)	Binder/Solvent	<ul style="list-style-type: none">•Binding particles in the paste•Lower slurry viscosity•Melting point ~46 to 68 °C•Decomposition temperature >370 °C	Fisher Scientific

To provide better support at the lamination temperature, are higher melting point wax candidate such as montan wax with melting range 82-95 °C could be proposed.

3.2.2 Insertion of sacrificial paste

The sacrificial paste is screen-printed on the LTCC substrate, a process in which a squeegee forces the paste through the screen/stencil as illustrated in Figure 3.6. The printed tape is then dried at 120 °C for 10 mins. The

printed thickness was measured using a surface profiler (KLA Tencor). The thickness varied as a function of screen used for printing, which is designated by the number of wires per inch and emulsion thickness. The resolution is decided by the particle size; the finer the particle size, the better the resolution of deposition. These methods are usually more suitable for microfluidic applications where the sacrificial insert is only needed to obtain gaps or channels on the micron scale.

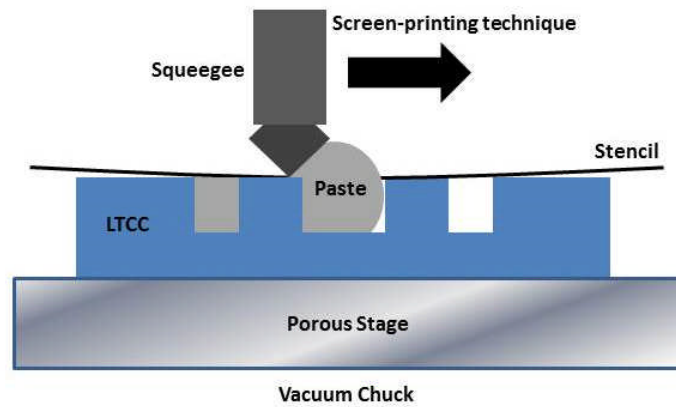


Figure 3.6 Screen-printing of sacrificial paste.

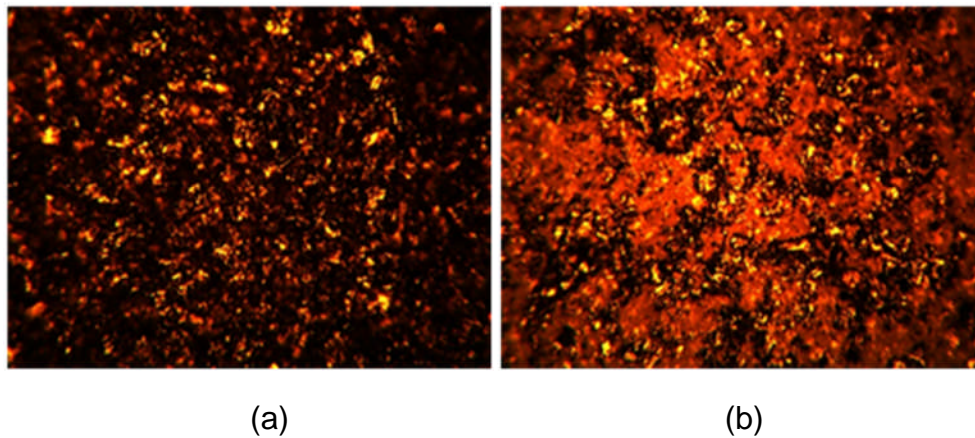


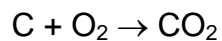
Figure 3.7 (a) Heavy and (b) light screen-printed graphite paste.

Considering the materials in addition to their interactions and effects on the sacrificial paste properties, investigation has to be done to study the influence of parameters on the paste. There are factors such as particle size of graphite, weight percentage of graphite, binder, solvent and dispersant,

heating rate, powder burnout temperature, and the dimensions of the desired structure. The early stages of the membrane fabrication were carried out by using graphite powder from Fisher Scientific with graphite purity of 99.5% in the weight ratio as given in Table 3.6. Figure 3.7 (a), (b) show heavy and light screen-printed graphite paste.

3.2.3 Lamination with sacrificial paste

Lamination with carbon-based sacrificial layers has been reported and the purpose of introducing them are to provide a support during sintering process for free-standing or 3D structures such as bridges and cavities. Carbon that burns out during firing is beneficial for closed cavities by maintaining the shape through the oxidation of carbon at LTCC melting stage such described by [59]:



To observe the effect of the pastes to LTCC, organic and water-based paste has been used as a sacrificial layer for the micromachined bridges/cantilevers. As for wax-based paste, the channel is filled with the paste before top and bottom layers are laminated to replicated embedded cavity. Each sample then laminated using uniaxial laminator before then undergoes sintering process for 26.5 hours.

3.2.4 Results and observation

The observation after lamination and sintering are discussed as the followings:

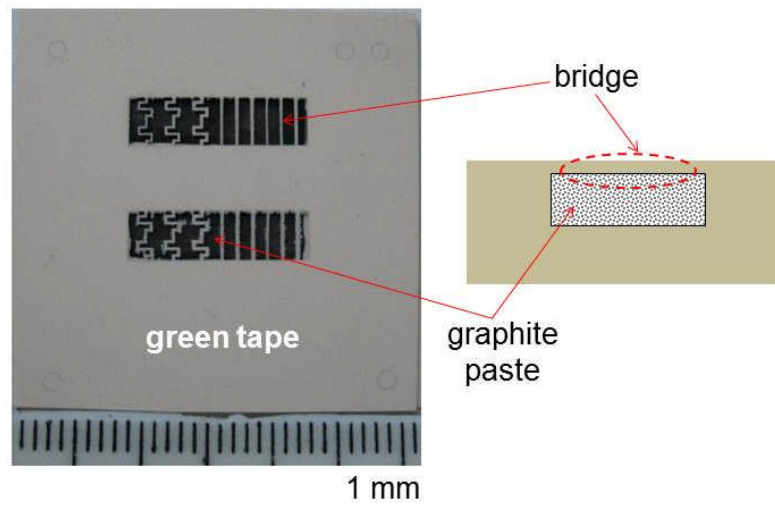
i. Organic-based sacrificial paste

Organic composition in the paste such as acetone is found could dissolve the green state tape during filling process. This can be confirmed where crack is observed in a sample shown in Figure 3.9. A balanced between high drying rate and prevention of bubbling as seen in Figure 3.8 is necessary to stimulate vaporisation of the organic material and maintain the shape of the structure.

ii. Water-based sacrificial paste

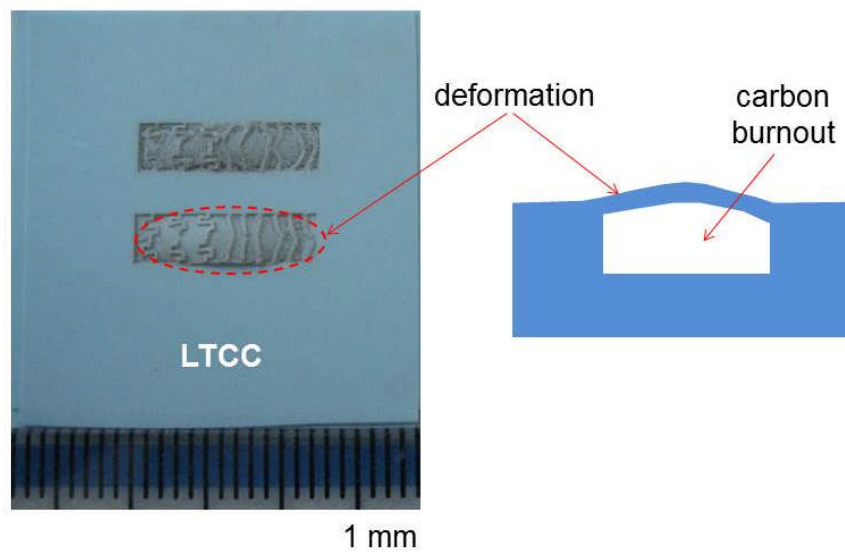
A balanced between high drying rate and prevention of bubbling is necessary. Residuals of paste material compositions were observed in the sintered sample in Figure 3.9.

Before sintering



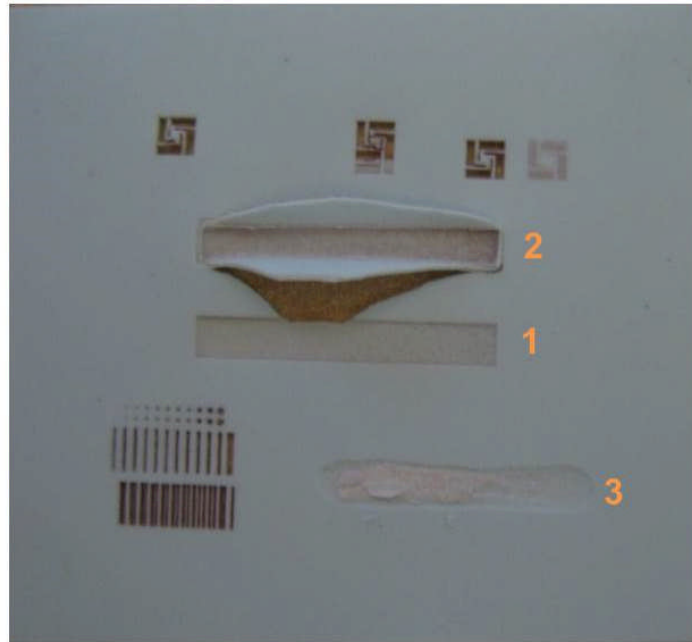
(a)

After sintering



(b)

Figure 3.8 (a) organic-based sacrificial paste inserted underneath the bridge structures. (b) deformation of free-standing structures happened when sacrificial inserts dried in the oven at 70 °C for 30 min. The lower temperature setting for almost an hour is needed to prevent bubbling phenomenon in the paste during the drying.



- 1: Channel without paste
- 2: Channel with organic-based paste
- 3: Channel with water-based paste

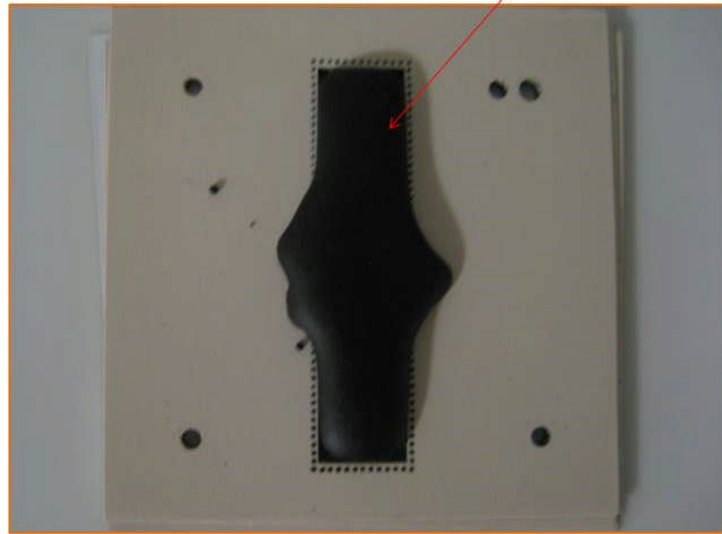
Figure 3.9 Photo of sample with channel without paste, with organic-based paste and water-based paste.

iii. Wax-graphite sacrificial paste

Based on weight ratio of 50:50, the paste insert is done through filling, flattening and laminating steps as shown in Figure 3.10. 3D structure is attained by using the sacrificial insert laminated using uniaxial press. The composition of the paste in term of the ratio of graphite to the wax may need to be studied further to control the stress induce to LTCC especially during sintering.

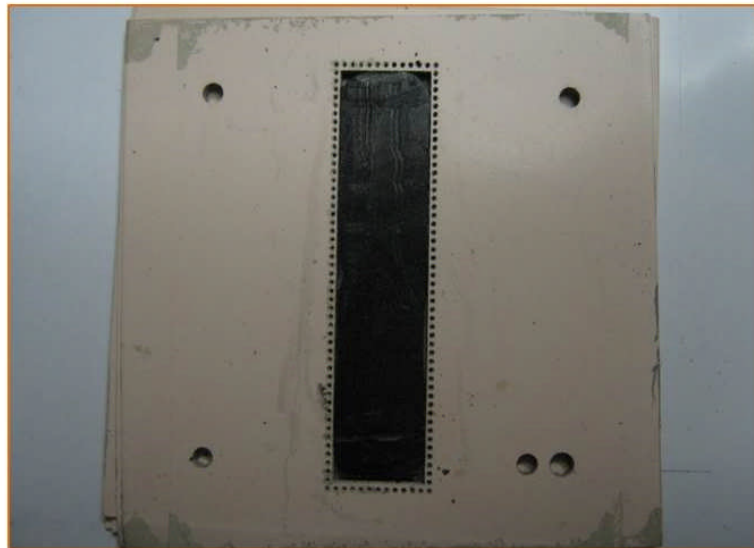
Filling

wax-graphite
paste



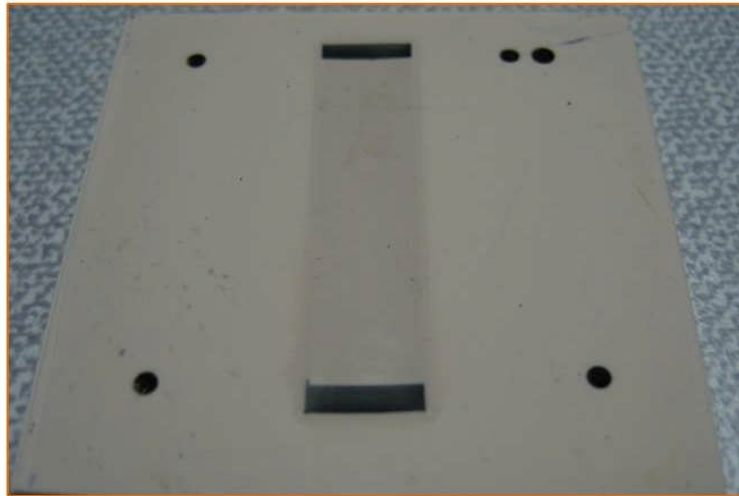
(a)

Flattening



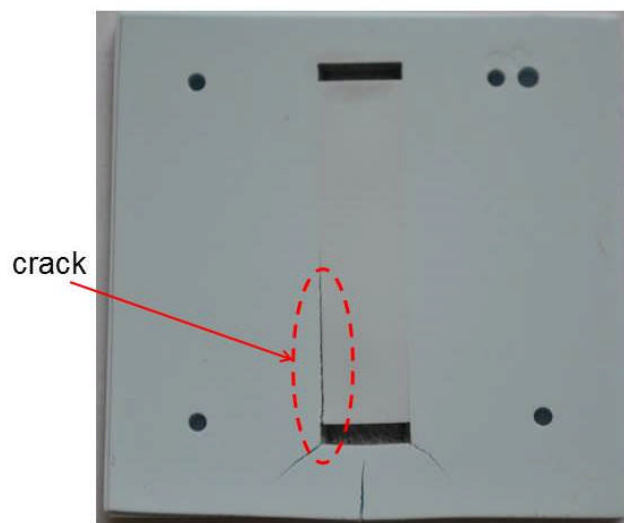
(b)

Laminating



(c)

Inspecting



(d)

Figure 3.10 The flow of large channel: (a) wax-graphite paste filling, (b) flattening, (c) laminating and (d) sintering and inspecting. The crack observed on the sintered sample may be due to excessive pressure induced by sacrificial materials degassing during the oxidation process.

3.3 Conclusion

3D structures have been achieved by the introduction of progressive lamination or by sacrificial volume material. The optimized processing procedures enable the fabrication of channels/cavities with suspended structures may span a channel width of 7 mm. Wax-graphite sacrificial paste is introduced due to its simplicity in the filling process and offer support for 3D structure in larger dimension as compared to organic-based and water-based paste which are more suitable to lower dimension application such as microfluidics. Whatever the actual mechanism of these sacrificial paste is, it need be understood in the future in order to achieve a better control of the 3D structure.

Chapter 4

Hollow Substrate Integrated Waveguides (HSIW) in LTCC

Telecommunication links over long distances, radar, and many other systems at millimetre-wave frequencies require a low-loss transmission medium. The high attenuation and low power handling capability of the conventional planar millimetre-wave waveguides supporting the dominant mode may be prohibitive for many system applications [1]. Thus, a transmission line with lower attenuation, offering an integration with other and possibly supporting higher power requirement needs to be found. In general, a transmission line is characterised by a propagation constant and a characteristic impedance. These quantities are derived by field theory analysis for the various lines and waveguides [63].

The transmission line completely characterises the behaviour of the dominant mode in the waveguide. Mode voltages and currents are introduced as measures of the amplitudes of the transverse electric and magnetic field intensities of each of the modes [64]. These waveguides, often consisting of a conductor that supports transverse electric (TE) and/or transverse magnetic (TM) waves, characterised by the presence of longitudinal magnetic or electric field components.

4.1 Rectangular waveguides (RWGs)

The most important part of the rectangular waveguides (RWGs) is that of rectangular cross section. As in Figure 4.1, an air region with width, a and height, b extends indefinitely in the axial z direction and is closed by conducting boundaries on the four sides. In the ideal guide, both conductor and dielectric are loss-free. There can be no transverse electromagnetic (TEM) wave inside the hollow pipe since, TEM waves have transverse variations like static fields, and no static fields can exist inside a region bounded by a single conductor.

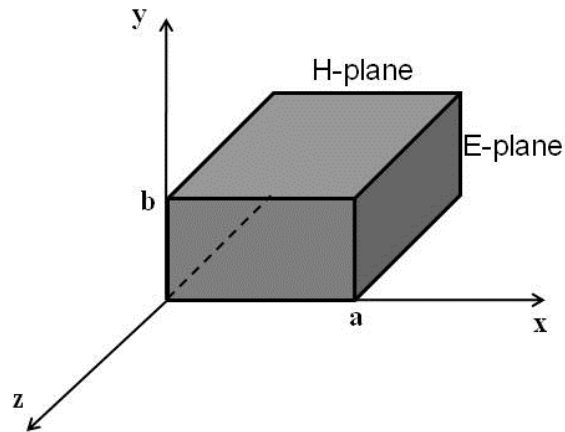


Figure 4.1 Rectangular waveguide.

Though a RWG supports TM and TE modes, the physical dimensions of a waveguide determine the cutoff frequency for each mode. If the frequency of the signal is above the cutoff frequency for a given mode, the electromagnetic energy can be transmitted through the waveguide for that particular mode with minimal attenuation. Otherwise, the electromagnetic energy with frequency below the cutoff for that particular mode will be attenuated to a negligible value in a relatively short distance. The dominant mode in a particular dimension of waveguide is the mode having the lowest cutoff frequency [64]. For RWGs this is the TE_{10} mode. This mode notation signifies that all electrical fields are transverse to the direction of propagation and that no longitudinal electric field is present. However, there is a longitudinal component of magnetic field and for this TE_{mn} mode are also sometimes called H_{mn} modes. Figure 4.2 shows a graphical depiction of the E field variation in a waveguide for the TE_{10} , TE_{20} , and TE_{30} modes. As can be seen, the first index indicates the number of half wave loops across the width, a of the RWG and the second index, the number of loops across the height of the guide which in this case is zero.

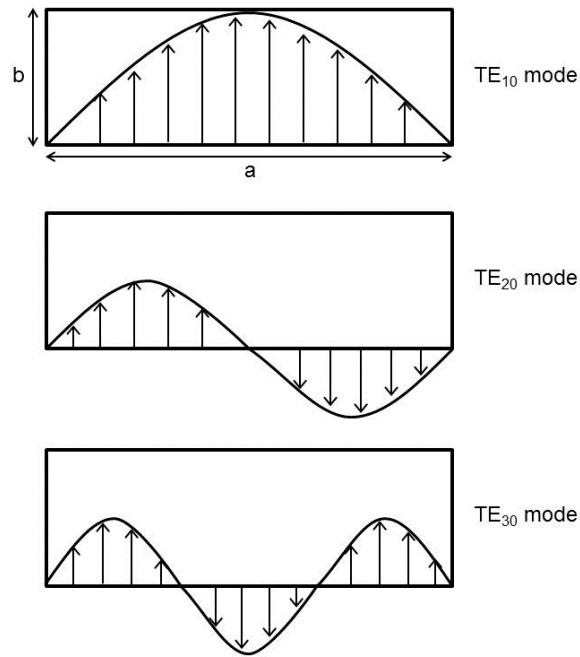


Figure 4.2 TE modes.

Considering the dimensions of the RWG in Figure 4.1, the aspect ratio is b/a which usually has a value of approximately 0.5. This ratio is used to preclude generation of field variations with height and avoid unwanted modes. At a given operating frequency f , only those modes having frequency higher than cutoff frequency f_c will propagate while mode with lower frequency field components will decay exponentially away from the source of excitation. Such modes are referred to as cutoff, or evanescent modes [63].

Though classical RWGs were proved to have an extremely low loss and could work at millimetre-wave region, it is obviously bulky thus not suitable for further miniaturization that required for modern devices. A new way needs to be found to address these hurdles.

4.2 Integrated waveguides/cavities

Waveguides have the best transmission characteristics as compared to other types of transmission lines due to their very low electromagnetic radiation loss. However the proliferation of waveguides in the circuit boards or packages is due to two reasons. The first is because its size is huge as a transmission line to be embedded in circuit board. The second one, vertical

metal walls are very difficult if not impossible to be manufactured considering a standard fabrication technique for microwave circuits board or packages.

Integration of active and passive components made of the rectangular waveguide generally requires transition from planar to non-planar circuits. Various approaches to solving this problem have been proposed that ended with complex transition structures. High precision mechanical adjustment or a subtle tuning mechanism is needed to obtain good performance for mass production. A planar microstrip circuit also often needs to be cut into a specific shape, which is hard to realise in the millimetre-wave range. RWG components are three dimensional structures and very costly to manufacture, which make the planar/non-planar integration bulky and expensive [65].

Recently a new type of waveguide in the form of a dielectric waveguide constructed of two sidewalls of two rows metallic posts are reported by Hirokawa *et al.* and Ke Wu *et al.* [66, 67]. According to this method, the RWG could be fabricated by a traditional technique of making microwave circuit boards. But, a dielectric constant material causes bandwidth narrowing due to long line effects associated with the series fed travelling wave operations. To cope this disadvantage and to utilize the huge bandwidth in millimetre wave, drastic change in series feeder of arrays is necessarily important [68]. Glass could be mixed into LTCC to reduce the dielectric constant up to about 5 but this method will increased the loss instead. In order to reduce the dielectric constant further, a method of introducing the air region into the structure seems promising to attain waveguide uniformly filled with dielectric medium.

The realisation of hollow structures in previous chapter have motivating us to design low loss waveguide which we do called hollow SIW (HSIW). Figure 3.3 (b) in Section 3.1.4 shows a 3D channels/cavity that could possibly can be turned into waveguides if the broadwalls and sidewalls are successfully metallised.

4.3 Hollow Substrate Integrated Waveguides (HSIW)

To meet the demand for low cost transceivers, particularly for high data rate wireless communications and automotive radar sensors, both silicon and compound semiconductor integrated circuit (IC) technologies are immensely important. There is a need for system-in-package or system-on-substrate technology that can integrate ICs with low loss passive components such as resonators, filters, power combiners and antennas. Among the various transmission lines, RWG still offer an excellent solution at these frequencies due to their lower loss [6]. Substrate integrate waveguide (SIW), a dielectric-filled waveguide formed in a substrate, is particularly interesting as it can be fabricated using PCB or LTCC technology, and can dramatically reduce the cost of millimetre-wave systems [65, 69]. LTCC is especially interesting because resistors, capacitors and inductors can be embedded, instead of using additional surface-mount technology (SMT) components, potentially leading to very small transceiver modules.

The conventional SIW is normally based on a solid dielectric substrate with two parallel rows of metallic posts (vias) used to replace the side walls of a traditional RWG. For lower loss, and in antenna applications, it is desirable to integrate an air-filled waveguide into the substrate [70]. However, this presents substantial fabrication challenges, such as the requirement to metallise the walls.

The proposed LTCC hollow SIW (HSIW), as shown in Figure 4.5 retains the use of via-hole sidewalls, but has a hollow cavity inside with the upper and lower broadwall metallization placed on the adjacent dielectric layers. The broadwall metallization can be either on the inside of the cavity – as shown in Figure 4.3 (a) - in which case the lowest possible loss is expected, but the HSIW is more difficult to connect to other circuitry – or on the outside the cavity, as shown in (b), which makes it easy to connect to the other circuitry but has the drawback that there is a thin layer of dielectric inside the main air cavity that might increase the loss.

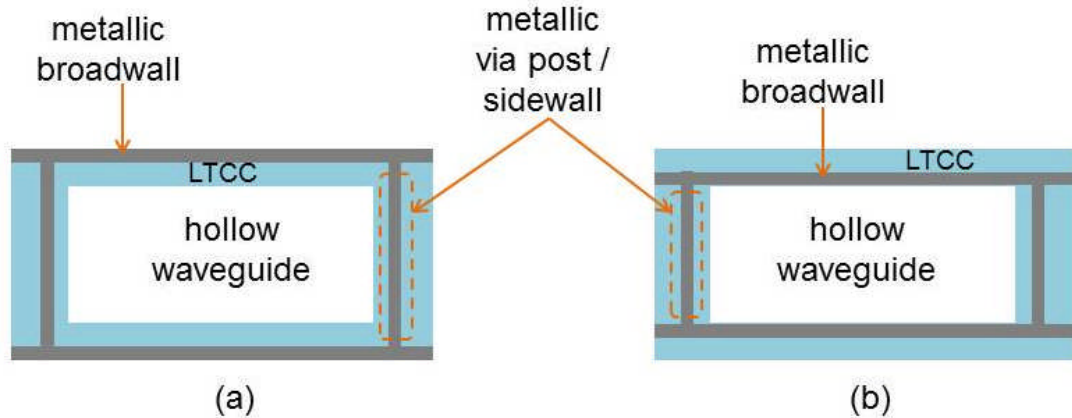


Figure 4.3 Cross-section of two example HSIW configurations: (a) with metallization outside: (b) with metallization inside the cavity.

By incorporating this hollow cavity, the following advantages are expected:

- i. Lower loss due to the removal of the most of the lossy dielectric material.
- ii. The HSIW can be realised with high permittivity substrates and at higher frequencies, where the size of SIW otherwise tends to be too small to accommodate the vias.
- iii. The HSIW can be potentially directly connected with normal RWGs, whereas the SIW requires more complicated transitions with potentially more loss.
- iv. The low ϵ_r is advantageous for the design of many antennas.

Although HSIWs have significant advantages, there are major LTCC process challenges that need to be addressed to realize them. In particular, hollow cavities are seriously deformed in the lamination and co-firing stages of the standard LTCC process recommended by the green tape suppliers. A sacrificial layer may be used to support the upper and bottom layers of the channels/cavities during these stages. However, they still undergo large deformation and it is very difficult to overcome the residual deformation of

the channels/cavities, even if the lamination conditions are carefully optimized [41].

In this chapter we present a technique for realising HSIWs by applied a novel multi-stage lamination process. The aim is to establish a technology that could realised the advantages of HSIWs mentioned above while employing as many LTCC standard process steps as possible. This is achievable by employing top and bottom broadwalls on dielectric layers suspended above and below the cavity, as will be shown in Figure 4.4. From fabrication point of view this is a technically challenging task due to the fact that the suspended conducting layer in LTCC is usually too weak to obtain a stable surface profile during lamination and sintering process.

4.3.1 HSIW structure and design

For a partially-filled RWG which is represented as a two-dielectric symmetrically loaded RWG, the characteristic equations can be derived from the Maxwell's Equations constrained by boundary conditions [6]. As a result, the lowest cut-off frequency is from the TE₁₀ mode. The cut-off frequency of the TE modes is decided by the speed of light, c and divided by $2a$ which is dependant of the width, a but independent of the height, b [63]. Therefore, it is expected that TE₁₀ mode will be the dominant mode below a certain point, which proves to be when the ration $b/a \leq 1$. The cut-off wave number of the TE₁₀ mode thus derived and given as:

$$\frac{\sqrt{\varepsilon_r} k_0 a_1}{2} = \tan^{-1} \left(\frac{\sqrt{\varepsilon_r}}{\tan \left(\frac{k_0 a_2}{2} \right)} \right) + m' \pi, \quad m' = 0, 1, 2, \dots \quad (4-1)$$

where, ε_r is the permittivity of the filling dielectric (the other dielectric is assumed to be air), k_0 is the free space wavenumber at the cut-off frequency. Solve this equation to find k_0 and k_c , and hence, the corresponding wavelength and frequency are the cut-off wavelength λ_c . It should be noted that m' has nothing to do with m in [63]. In other words, when $m'=1$, it does not means that the guided mode is TE₁₀. In fact, when m' takes one single value, it corresponds to a series of continuous guided

modes depending on the number of curve intersections represented by the two sides of (4-1).

For a desired cut-off frequency, the width, a , of the partially-filled RWG can be obtained from (4-1) and then according to the SIW analysis in [71], the width can be adjusted using the following:

$$a_e = a - \frac{d^2}{0.817 \cdot s} \quad (4-2)$$

where, a_e is the final width of the equivalent HSIW.

From (4-2), the Ka-band HSIW dimensions were found and modeling was then performed using HFSS™. Table 4.1 shows the parameters of the WR28-like HSIW, where a_1 and a_h are the width of the filling dielectric and the HSIW, respectively. The HSIW has the same cutoff frequency as the standard WR28 (21.10 GHz).

Figure 4.4 shows the illustration of the hollow substrate integrated waveguide (HSIW). The electric field should be continuous on the boundaries in the x direction while the electric displacement should be continuous on the boundaries in the y direction. Most of the electrical energy is concentrated in the centre, and energy density in dielectric part of the waveguide is weak in the y direction.

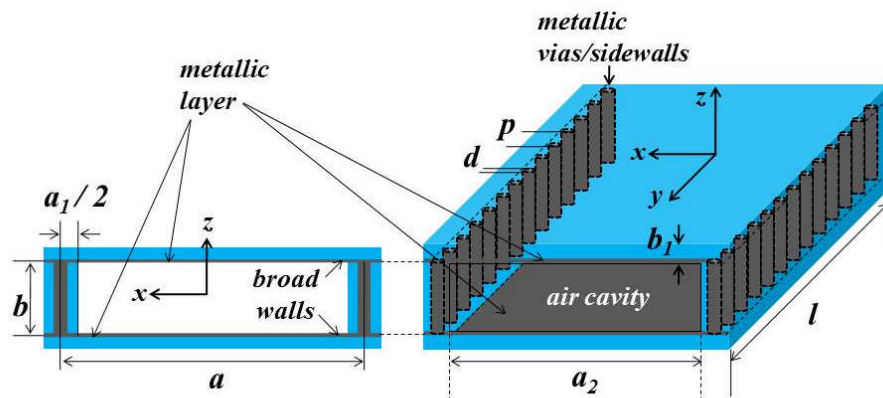


Figure 4.4 HSIW configurations: (a) cross section with metallization inside, (b) 3D view with metallization inside the cavity.

Table 4.1 The parameters of WR28-like HSIW (unit in mm).

HSIW	ϵ_r	d	ρ	a_1	a_e	b
WR28-like	7.1	0.30	0.60	0.70	7.26	1.0

The feed into the HSIW was realised with a slot cut in the bottom supporting layer/broadwall to match with a standard WR28 waveguide flange; a set of three transition pairs with different waveguide lengths was fabricated as will be shown in Figure 4.9.

4.3.2 Fabrication of HSIW structure

The 9K7 tape system of DuPont was chosen as it is suitable for frequencies up to 100 GHz and beyond [51] with dielectric constant, ϵ_r , of 7.1, loss tangent of 0.001 measured by cavity resonance technique at 10 GHz and specified DC conductivity of 3.7×10^7 S/m for silver conductor. The broadwalls/supporting layers of the waveguides were via punched and cut using a Nd:YAG laser machine (the ProtoLaser 200 from LPKF™). A series of via holes with a diameter of 300 μm , hole pitch of 600 μm were produced as shown in Figure 4.5. Then, LL601 Ag-Pd paste was used for via filling. The intermediate part which represents the channel part was then stacked and laminated at 20 MPa, 70 °C for 10 min, to provide sufficient material pre-densification for minimising the shrinkage. Another type of Ag-Pd paste, LL612 was deposited with an Aurel VS1520A screen printer for top and bottom broadwalls' conductor layer. The top and bottom layers were pressed separately with the same conditions before via holes were laser machined to ensure the dimensions of the via holes were maintained. All layers were then aligned using a jig and laminated using a uni-axial laminator.

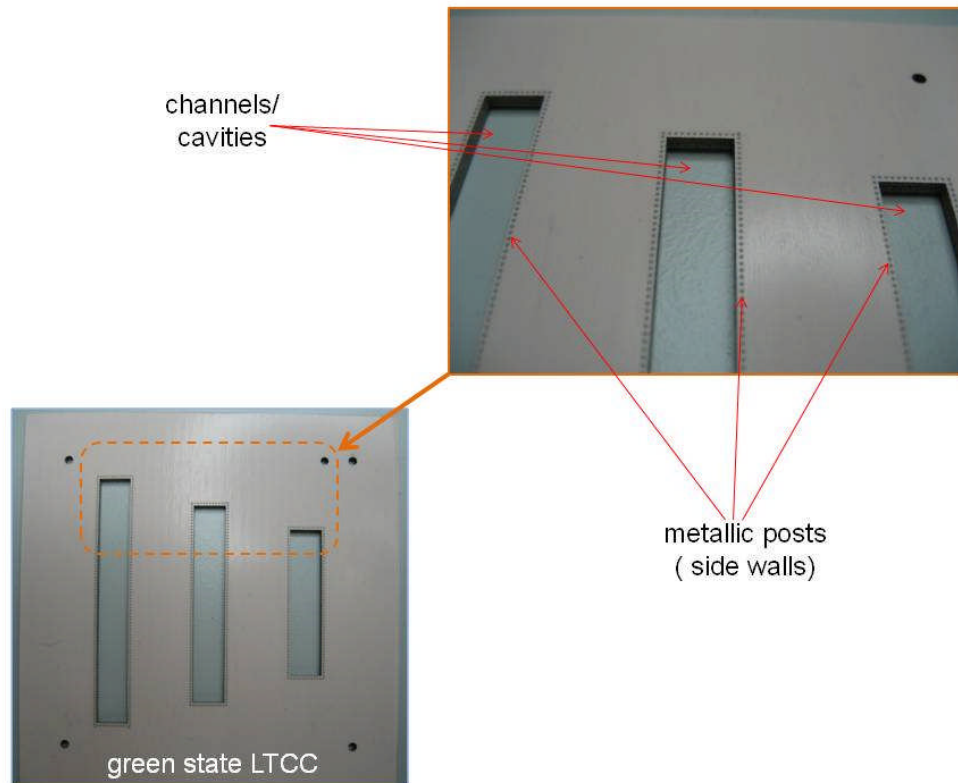


Figure 4.5 Preparation of HSIW's middle part in the green state, where the metallic posts act as sidewalls.

- **Fabrication issues**

There were a few fabrication issues that arise when the HSIW samples were prepared. They are related to:

- i. Via filling
- ii. Sheet resistance of the conducting layer

respectively. For the via filling case, it is originated from the contraction of Ag paste when the organic vehicle that composing the paste evaporated. The contraction in the dimension of via posts were also expected to occur during sintering due to the nature of the particles in the paste itself which are not pure Ag but, rather a Ag rich mixture with organic vehicle. It is for this reason, a paste of LL601 with 94-95% solid at 750 °C was used for via filling. To improve this, a treatment through compensation of Ag paste was done as shown in Figure 4.6.

For the case of conducting layer, the conductivity could be improved by applying additional thickness considering the nature of the LL612 paste which is 80-83% solid at 750 °C. The additional thickness of conducting paste will works to fill the voids among Ag particles at their melting point.

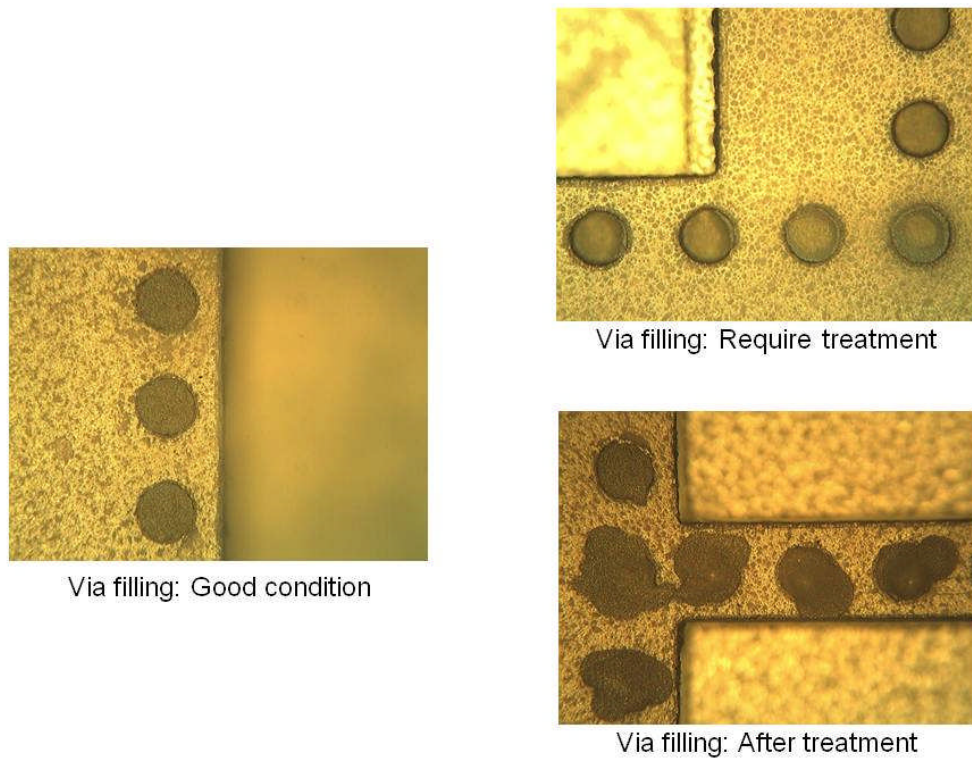
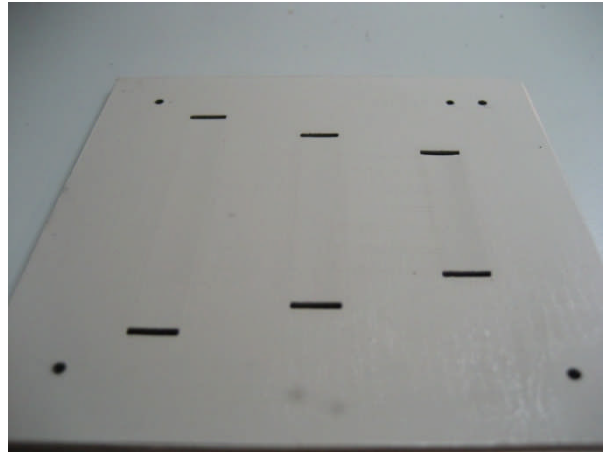


Figure 4.6 The metallization of vias using conductor paste.

Figure 4.7 shows the sample with three different lengths of HSIWs after lamination. A flat broadwalls with no sagging around the windows can be confirmed from the two photos. Considering the feeding from the sample to waveguide flanges, fixing holes are laser drilled surrounding the back-to-back waveguide windows.



(a)



(b)

Figure 4.7 (a) Flat broadwalls observed after lamination of top and bottom layers, (b) holes for fixing the sample to waveguide flanges laser drilled around the back-to-back waveguides.

The stacked green tapes were then co-fired by using a programmable furnace according to a temperature profile, for 26.5 hours. A separate sample was prepared with the same condition for the purpose to confirm the cross section of x-y direction of the waveguide as shown in Figure 4.8. The cutting was performed by a laser scribing technique where a shallow indent was prepared with the laser before the sintering process. The substrate was then cut by concentrating force to the indent, the same way how glass is often cut. The cut edge was then polished using a 400 grit coarse and 1000 grit fine master class whetstone to confirm the interconnection of metallic post between LTCC layers.

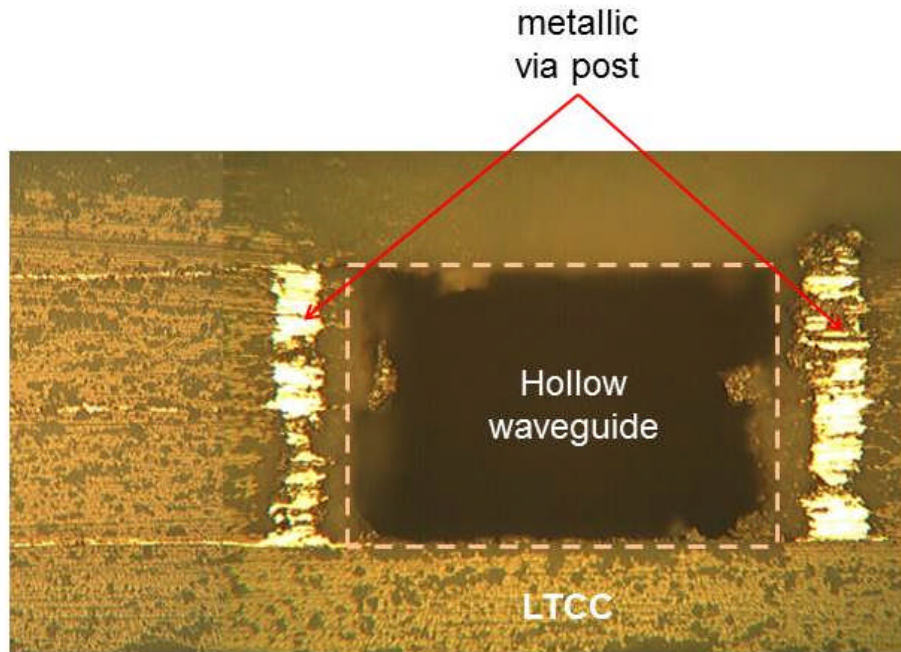


Figure 4.8 Cross-section of HSIW after being cut and polish using a whetstone. The sample was fired under unconstrained sintering. Metallic posts are clearly connected between layers to perform as a sidewalls to the waveguide.

Though a more sophisticated method could have been use to verify the interconnect such as ultrasonic imaging, the photos shows that the metallic posts somehow have been successfully constructed and it is feasible to demonstrate as sidewalls as well as the proposed HSIW.

4.3.3 Multimode calibration method

As shown in , only TE_{m0} modes can be propagated within an SIW, since the discrete posts will cut off the longitudinal currents of all other modes. A few methods have been applied to analyse the propagation characteristics of this newly-emerged structure.

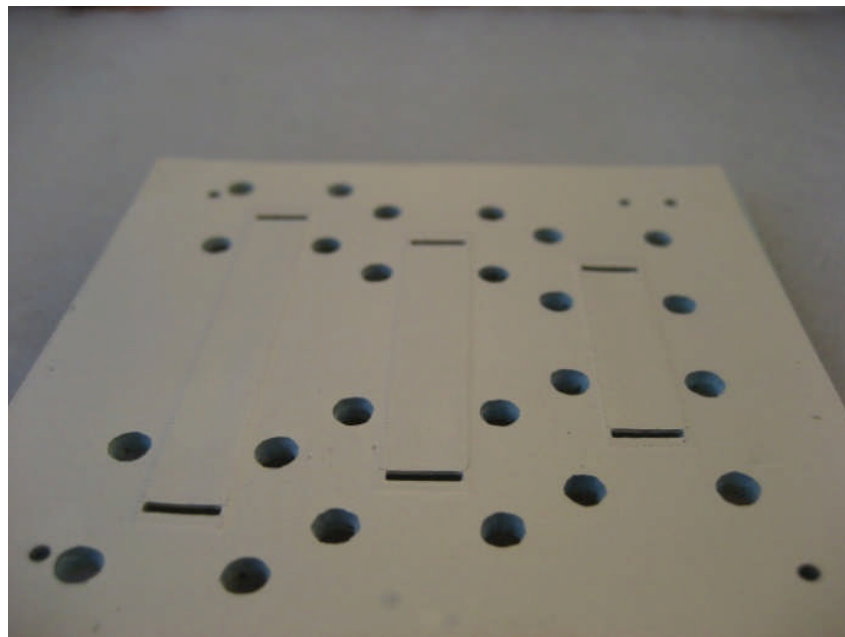
By assuming a uniform longitudinal electric current on the post surface, J. Hirokawa *et al.* used dyadic Green's function for the electric field produced by a unit electric current in the analysis of this dielectric filled waveguide or later known as SIW. The work later extended by applying BI-RME method, the FDTD method, and a multimode calibrated FEM method to find an

approximation in terms of numerical formula that help to determine the equivalent dimension of the waveguide [71].

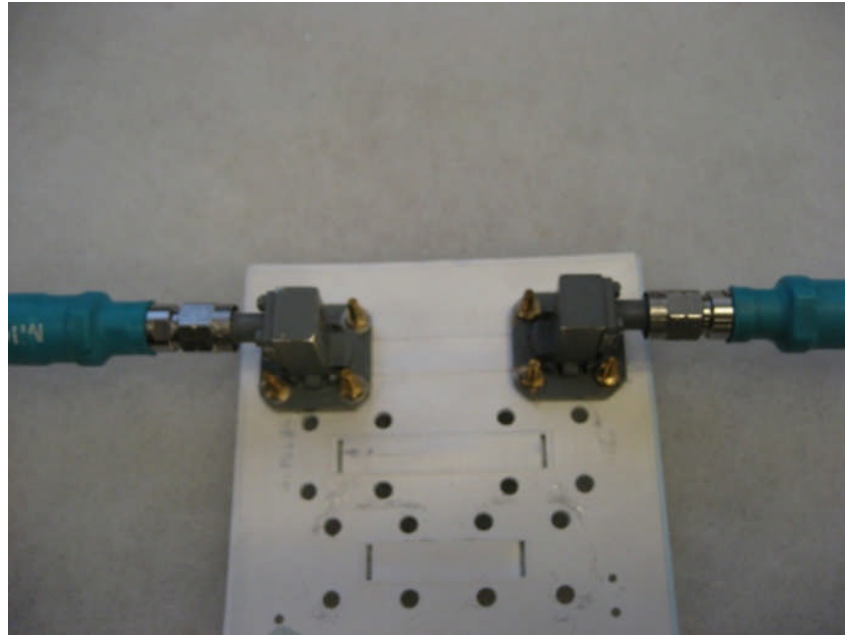
The multimode calibrated FEM method is needed to perform the 3D modeling such as the HSIW. The two lowest-order modes will be calculated by the FEM method using HFSSTM. The multimode calibration method replicates a multiline method, where the basic principle is to determine the propagation constant through uncalibrated S-parameter measurements of at least two transmission lines [72, 73].

4.3.4 Measurements and results

The WR28-like HSIW samples were fabricated and measured to verify the design, as shown in Figure 4.9 (a), and (b). HSIWs with lengths of 30, 40 and 50 mm were fabricated on the same substrate. A pair of transversal slots is employed to couple the energy in and out.



(a)



(b)

Figure 4.9 (a) Photograph of sintered substrate incorporating three WR28-like HSIWs with lengths of 30, 40 and 50 mm respectively, (b) a back-to-back transversal slot-pair is used to couple the energy in and out. The WR28-like HSIW measured by 67 GHz PNA using 2.4 mm coax-to-WR28 adapter that is mounted and screwed to the HSIW.

To verify this feeding scheme, the measured and simulated S -parameters of the 30 mm HSIW are shown in Figure 4.10. It can be seen that they agree well though the HSIW measurements though tend to diverge from the simulation towards the edges of the operating band. A multimode calibration method is used to extract the propagation constant from the three transmission lines with different lengths [54, 73]. For comparison of the simulated and extracted propagation constant of this WR28-like HSIW is plotted in Figure 4.11, showing that the measured phase constant, β , stays very close to the simulated one, including around the cut-off frequency. The extracted propagation loss constant, α , in Figure 4.11 shows some ripple and the loss is higher than the simulated one, as would be expected in the sample with lossy characteristics. The possible reasons are surface roughness issues and formation of voids in the sintered Ag paste which contribute to the loss performance of HSIW at higher frequency.

Nevertheless, the average α below 10 dB/m represent a significant achievement for a transmission line that is in-house manufacturable in LTCC technology.

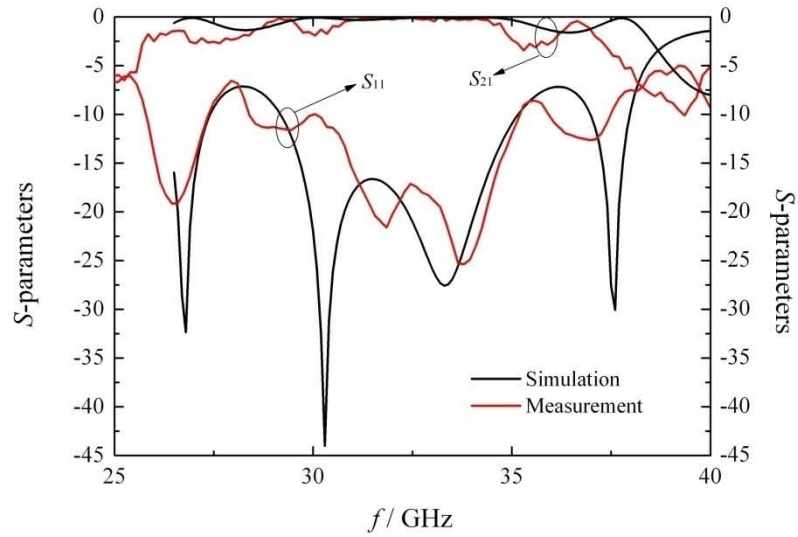


Figure 4.10 The modelling and measurement of HSIW with length of 30 mm.

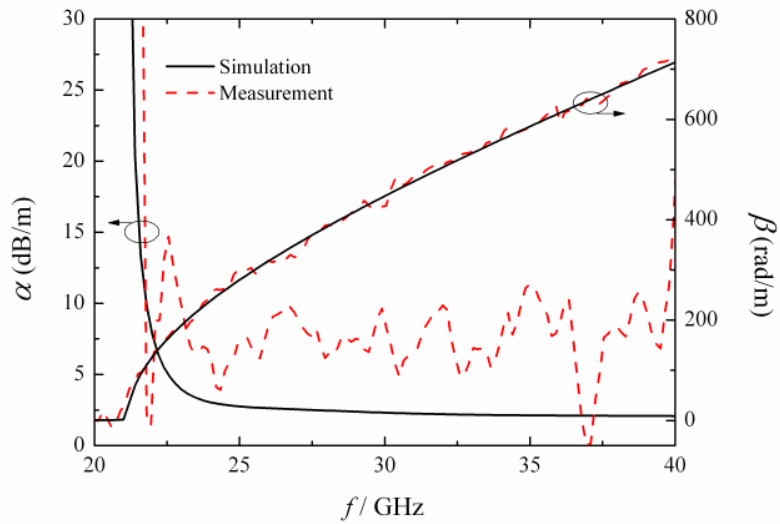


Figure 4.11 Extracted attenuation constant and phase constant of the WR28-like HSIW.

Figure 4.12 shows the attenuation of WR28-like HSIW was improved significantly compared to SIW and it exhibits very low loss, at a level

comparable to RWG. For comparison wise, the attenuation of SIW also plotted with respect to frequency normalised to cutoff frequency of 1.

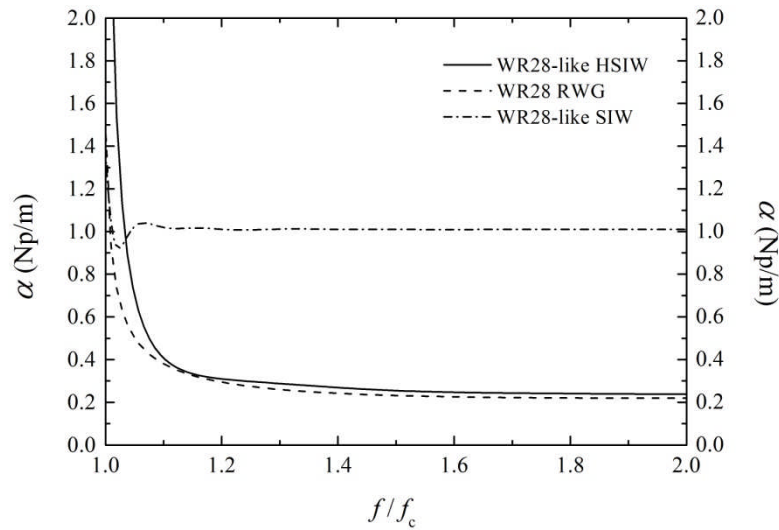


Figure 4.12 The attenuation of HSIW with respect to WR28 RWG and WR28-like SIW.

4.5 Conclusion

It has been shown that a novel transmission line, hollow substrate integrated waveguide (HSIW), can be fabricated and embedded into LTCC modules by using a multi-stage lamination technique. This is simpler and more straight forward than employing sacrificial volume materials, although this technique may also be used. The HSIW has been successfully demonstrated working in the millimetre-wave region with measurements performed on 26.5 to 40 GHz test samples. With further optimization of the process parameters, it is anticipated that hollow waveguides could be further improved and possibly work at much higher frequencies. HSIW will provide a means of integrating high performance passive components along with ICs and other components to form lower cost systems. To demonstrate the possibilities of HSIW, millimetre-wave components such as waveguide antennas and cavity filters will be discussed in the next Chapter.

Chapter 5

Hollow waveguide components in LTCC technology

The development of device systems that work at millimetre-wave frequencies such as automotive collision avoidance system is rapidly advancing. Currently, these devices are mounted on circuit boards or in packages before being connected to antennas. By integrating the circuit board or package with an antenna, a compact and high-performance device system could be realised as being mentioned by M. Henry *et al.* and Aftanasar, M. S. *et al.* [74, 75]. While microstrip lines are popular as the simplest structure for feeding lines, they suffer from the electromagnetic radiation loss at discontinuous parts such as bends and branches [76]. In case of coplanar waveguides, the signal lines and grounds are fabricated on the same plane which causes radiation in the similar way as microstrip lines.

Considering miniaturisation and signal integrity, it is highly desirable to feed the microwave circuits from underneath the antennas. Therefore, the feeding line needs to be embedded in the substrate and needs to have low insertion loss. Waveguides for instance exhibit very low loss as compared to other transmission lines due to their ability to suppress the electromagnetic radiation at a minimum level. Thus, realising RWG or RWG-like structures in the substrate offer advantages as mentioned in Chapter 4.

To fully extract the potential of millimetre-wave frequencies, waveguide structures and components that are based on 3D fabrication (i.e. cavity waveguide for antennas and filters) should be demonstrated. Another interesting thing about 3D fabrication is that the integrated passive elements such as integrated waveguide slot antenna and cavity filter could minimize parasitic capacitance and inductance that are usually fabricated separately.

To demonstrate the advantages of the embedded waveguide particularly HSIW, integrated passive elements such as antennas and filters will be studied. For the antenna, we are focusing on a slot antenna that exhibits linear polarization and low sidelobes. For the filter, a direct-coupled cavity

waveguide filter is chosen for the advantage of small size, directivity and high performance.

5.1 Antenna

Fabrication and integration of microwave and millimetre-wave components are essential in systems design. Generally, microstrip antennas or patch antennas are popular and preferred due to their compatibility with planar systems. But, the drawbacks of these antennas such as poor polarisation purity, spurious radiation from feeding networks and losses to substrate modes are well known. Different structures of antennas with lower loss which could work more efficiently in the millimetre-wave region need to be found. Rectangular waveguides (RWGs), for example, have been used for decades due to their advantages such as high gain, high efficiency, linear polarisation, low sidelobes and high power handling [77]. However, in reality the RWG antennas such as horn and slot antennas encounter difficulties in manufacturing and integration stages when it comes to planar circuitry that works at millimetre-wave frequencies.

Recent developments in microwave integrated circuit fabrication offer an opportunity for the integration of RWGs. For instance, LTCC technology has potential due to its flexibility from the fabrication point of view and its ability to form 3D structures such as dielectric-filled waveguides i.e. the emerging substrate integrated waveguides (SIW) [66, 69]. For lower loss, and for antenna applications, it is desirable to integrate an air-filled waveguide into the substrate as mentioned in previous chapter. Although studies of metallised channel and enclosed structures, using methods such as electroless copper plating or chemical vapour deposition and sputtering are available, these techniques will introduce extra process steps that deviate from the standard LTCC process [78, 79].

5.1.1 Waveguide slot antennas

The slot is a commonly used radiator in antenna systems. The most attractive feature of the slot is that it could be easily integrated into feed systems such as a waveguide without requiring a complex matching

network. It is important to understand the modal field within a waveguide in order to place slots at position where it is properly excited. The basic principle of the slot waveguide is when a slot cut into the waveguide wall interrupts the flow of currents which forcing the current to go around the slot where the power is coupled from the waveguide modal field through the opening (slot) to free space [80]. To have a good control of the excitation of slots, it is recommended that the waveguide only operates in a single mode, which is the fundamental mode. For RWG this is the TE_{10} mode as shown in Figure 5.1.

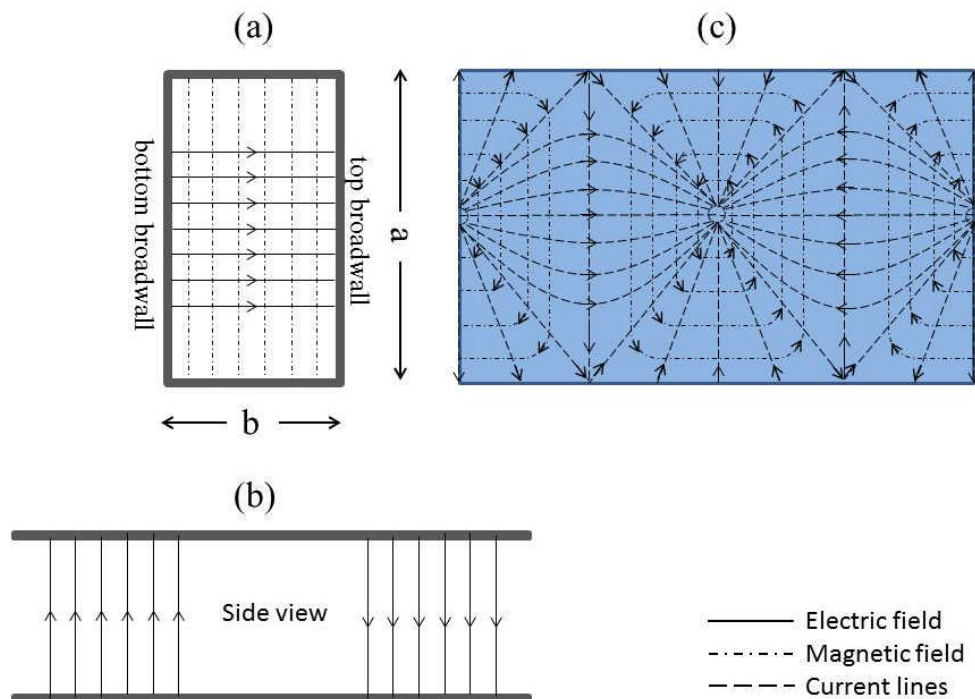


Figure 5.1 Surface current distribution for rectangular waveguide TE_{10} mode: (a) Cross-section view shows E - and H -fields. (b) Side view shows polarity of E -field along the waveguide. (c) Surface view shows broadwall and sidewall currents and H -field.

It is well known that the effective shunt conductance of the slot in RWG could be expressed by [81]:

$$g(x) = g_0 \sin^2\left(\frac{\pi x}{a}\right) \quad (5-1)$$

where g_0 is a normalised conductance, which is dependent to the slot dimensions waveguide b/a ratio, and x is the displacement of the slot from the centre of the waveguide. In a normal design, slots are usually positioned on the opposite side of the waveguide at intervals of half a guided wavelength. The required value of conductance of each slot is set by displacement x . For a dielectric-filled waveguide with dielectric constant of ϵ_r , the slot length can be simplified to:

$$L_{SIW} = \frac{\lambda_0}{\sqrt{2(\epsilon_r + 1)}} \quad (5-2)$$

For a HSIW, since it is an air-filled waveguide where $\epsilon_r = 1$, the slot length could be approximated as:

$$L_{HSIW} = \frac{\lambda_0}{2} \quad (5-3)$$

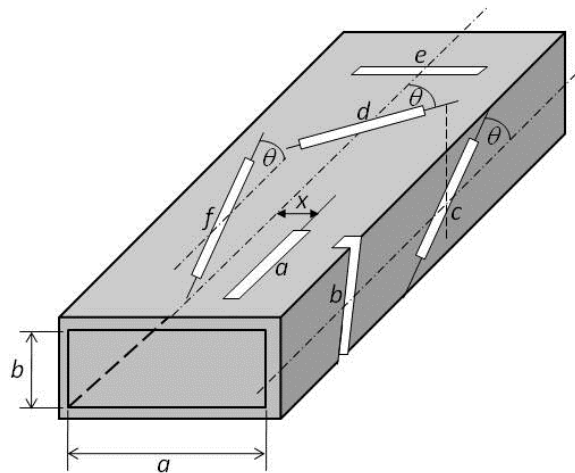


Figure 5.2 Radiating slots cut in the walls of a RWG [80].

Rotating the slot with the respect to the peak current direction can control the power coupled to the slot [77]. Slot e in Figure 5.2 exhibits maximum

power, while the power is proportional to $\sin^2\theta$ for slot c , d and f . by offsetting longitudinal slots such as slot a from the centre of the waveguide, the power coupled to the slots can be adjusted. The ability to control the radiation degree from the slots are important to acquire a designed arrays with tapered sidelobes. Depending on how the array is fed, the coupling of the waveguide to the slots need to be adjusted progressively according to the length of the waveguide where if the first slots are not to radiate all the power, the remaining power will be channelled to the remaining slots.

The power coupled to a slot could be controlled by rotating the slot respect to a peak current direction. Coupled power also could be controlled by take an advantage of the field intensities within the waveguide by arranging the slot position appropriately. For example, the current is zero at the centre of the surface broadwall and varies sinusodially as approach the sidewall. The ability to control the excitation of slots in a linear waveguide is important in order to design arrays with tapered sidelobes. Depending on how the array is fed, the coupling of the waveguide to the slots must vary progressively down the length of the waveguide if the first elements are not to radiate all the power, the remaining power is channelled to the remaining elements. However complicated slot designs should be avoided since it is more costly to manufacture.

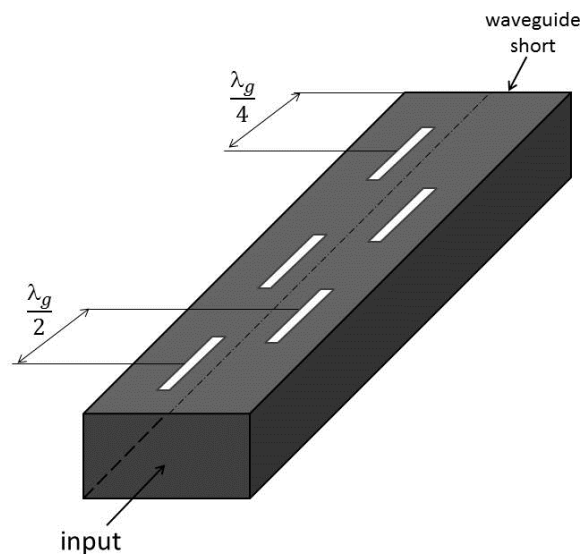


Figure 5.3 Standing-wave arrays with longitudinal slot elements is fed from the waveguide end.

Most slot array designs such in Figure 5.3 are for fixed beam or mechanically and/or electronically scanned applications. It is a big advantage to have waveguides to feed the arrays due to its very low loss characteristic. The ability to couple energy to other waveguides precisely is the other advantage. This waveguide-based antenna array will be studied briefly in the following section.

5.1.2 HSIW Antenna (Slotted waveguide antenna)

Utilising 3D fabrication in realising the hollow waveguides, a slotted waveguide antennas has been design and fabricated. The fabrication flow is attached in Appendix B. The dimensional parameters of the antennas have been extracted from HFSS modeling as shown in Figure 5.4.

Figure 5.5 shows the analysis results of the radiation pattern of the HSIW slot antenna array with centre frequency of 35 GHz. The simulation shows

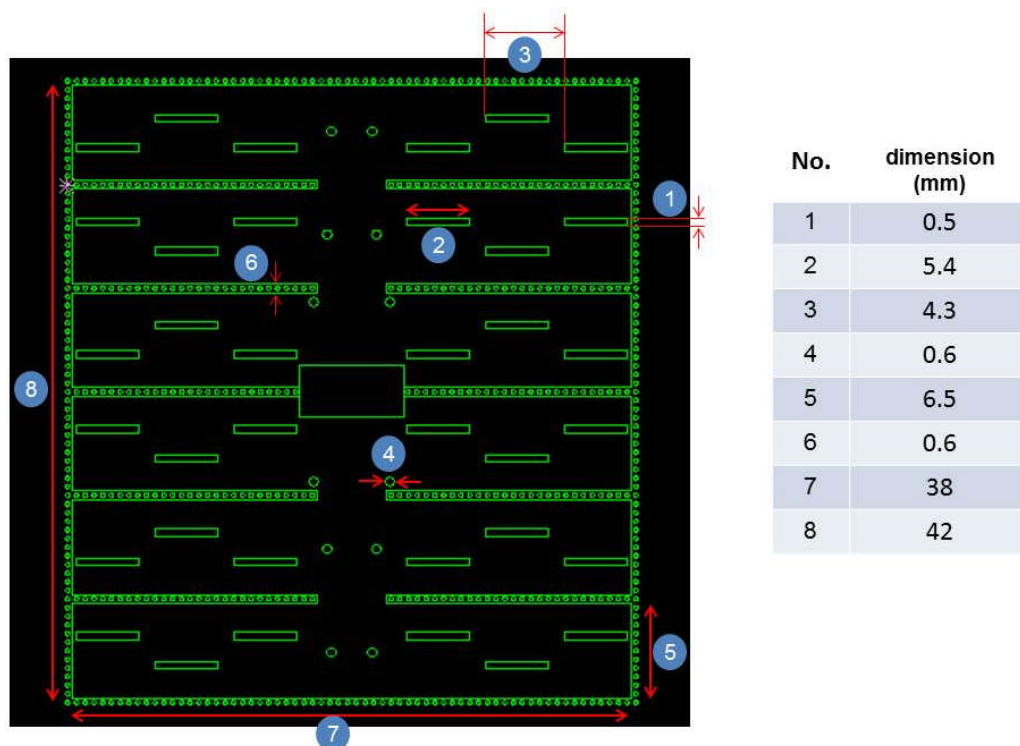


Figure 5.4 Dimensional parameters of HSIW-based antenna arrays extracted from HFSS modeling.

that the coupling energy between waveguides occur in a good manner which is made possible due to low loss feeding to the slot elements.

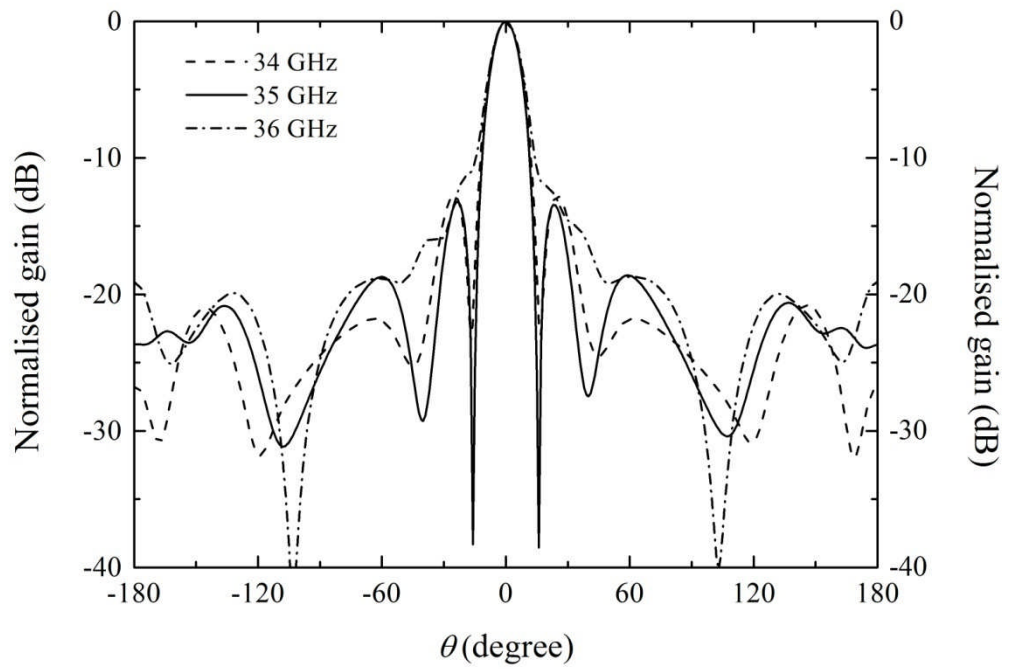


Figure 5.5 Simulated H -plane of slotted antenna arrays.

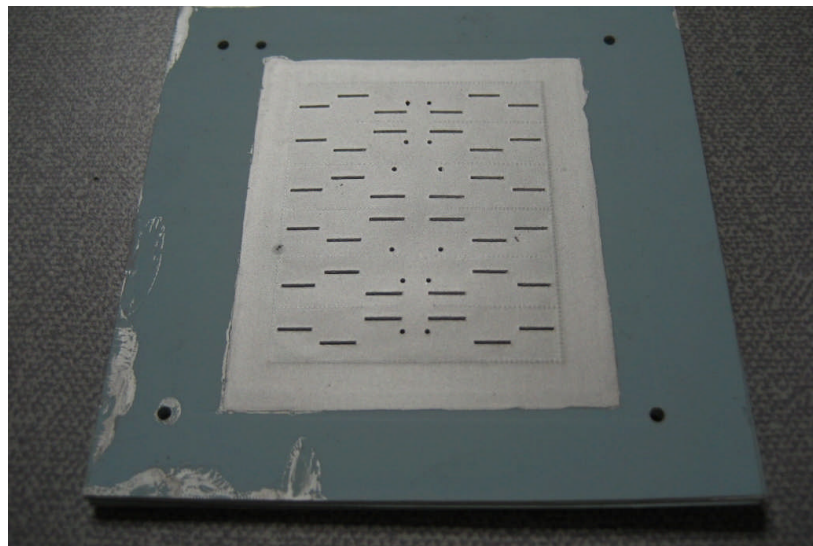


Figure 5.6 The 'In-house' fabricated HSIW-based slot antenna arrays.

Through our in-house fabrication, six slots are structured on each one of waveguide for all six of HSIWs as shown in Figure 5.6. The purpose is to increase coupling between slots in order to increase gain and directivity.

5.2 Filter

There are various type of filters available but, waveguide filters are particularly interesting due to their high Q factor and narrow bandwidth. The fabrication of 3D millimetre-wave components such as filters using HSIW is now explored.

5.2.1 Waveguide filters

Although planar filters such as the parallel coupled-line filter are available, they are more suitable to be fabricated on the planar surface plane of the LTCC substrate and may not efficiently occupy the volume of the entire substrate. To maximize the potential of LTCC technology, 3D fabrication such as waveguide-based filters needs to be explored. Here, the cavity waveguide filter, particularly the direct-coupled cavity waveguide filter, is chosen for its benefits of small size and high performance.

The other advantage of introducing waveguide with an air cavity inside is to maintain high Q for filter applications, where dielectric-filled waveguides tend to have a higher loss. The definition of the quality factor, Q in general is given by the following [82]:

$$Q = 2\pi \frac{\text{Maximun energy stored in a cycle}}{\text{Energy dissipated per cycle}} \quad (5-4)$$

Nonetheless, filters in the form of waveguides have much higher Q factor as compared to planar type filters such parallel coupled-line filter due amongst other things to the significant loss in the form of unwanted electromagnetic wave radiation.

5.2.2 Cavity waveguide filter design

These filters are particularly interesting since they used cavity resonators to replace the transmission-line stubs in coupled-line filters. Direct-coupled

cavity filters have the advantage that the physical structure is more compact than quarter-wave-coupled cavity filters. The theoretical derivation can be found in reference [77, 83, 84].

Based on S. B. Cohn [77], the waveguide cavity and its equivalent circuit may be represented by the π network shunted with inductive susceptances at each end, as shown in Figure 5.7. The two shunt susceptances \bar{B} could be neglected as compared to \bar{B}_k which is the dominant element. The electrical length, θ_k , on the other hand is nearly equal to π . The series reactance, \bar{X} is used as the series resonant circuit in the prototype filter.

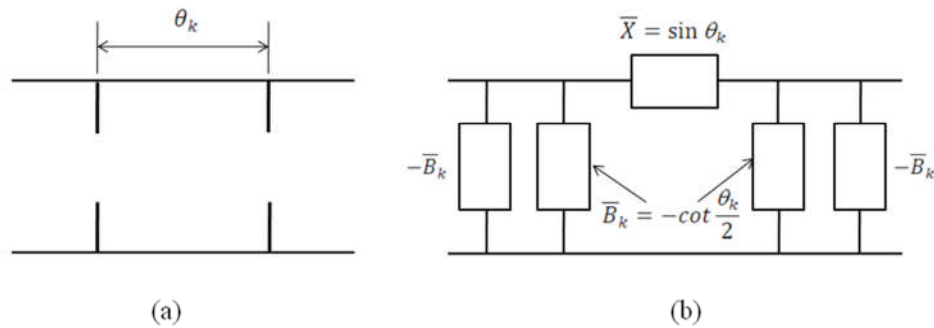


Figure 5.7 A waveguide cavity and its equivalent circuit [77].

Impedance inverters could be realized as the shunt inductive reactance and two equivalent transmission lines as shown in Figure 5.8. The impedance inverting properties are obtained when:

$$\theta_{1k} = -\frac{1}{2} \tan^{-1} \frac{2}{\bar{B}_k} \quad (5-5)$$

$$\bar{B}_k = \frac{1 - K^2}{K} \quad (5-6)$$

where, K is the characteristic impedance of the quarter-wave impedance inverter. In general, the direct-coupled waveguide cavity filter can be illustrated schematically as in Figure 5.9.

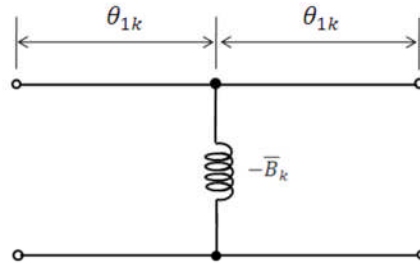


Figure 5.8 The impedance inverter.

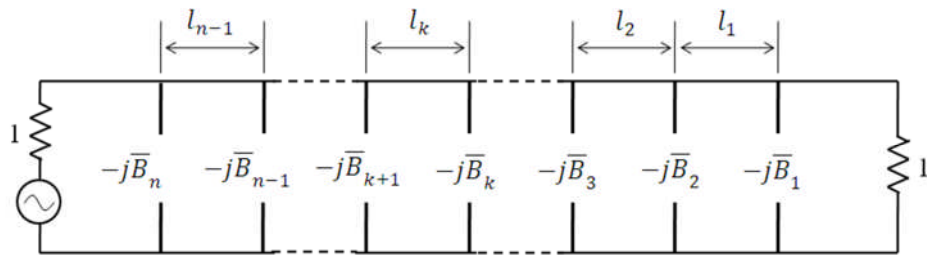


Figure 5.9 General illustration of direct-coupled waveguide cavity filter [77].

Before that, the bandpass filter configuration needs to be initially determined. As the Impedance inverters are absorbed as part of the cavity length, the physical length of the k -th cavity becomes (5-7).

$$l_k = \frac{\lambda_{g0}}{2} + \frac{\lambda_{g0}}{2\pi} (\theta_{1k} + \theta_{1k+1}) \quad (5-7)$$

Thus, the length of the k -th cavity at $\beta = \beta_0$ given by (5-8):

$$l_k = \frac{\lambda_{g0}}{2} + \frac{\lambda_{g0}}{4\pi} \left(\tan^{-1} \frac{2}{\overline{B}_{k+1}} + \tan^{-1} \frac{2}{\overline{B}_k} \right) \quad (5-8)$$

Using (5-8) to calculate the resonator length and HFSS to model the length of the irises, parameters as shown in Table 5.1 were extracted. For the two

order filter, the length of the upper iris and lower iris were set the same length.

Table 5.1 Dimensional parameters of two order direct-coupled cavity filter.

	upper iris length, g_u [mm]	bottom iris length, g_b [mm]	resonator length, l_k [mm]
1 st	1.95	1.95	4.85
2 nd	2.54	2.54	4.94
3 rd	2.00	2.00	-

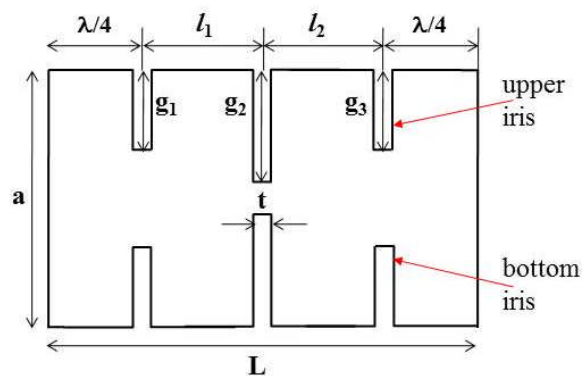


Figure 5.10 The dimensional parameters of two order cavity filters.

The layout of the second order cavity filter is shown in Figure 5.10 that represents a compact cavity-based bandpass filter. The HFSS simulation result of the cavity filter is shown in Figure 5.11.

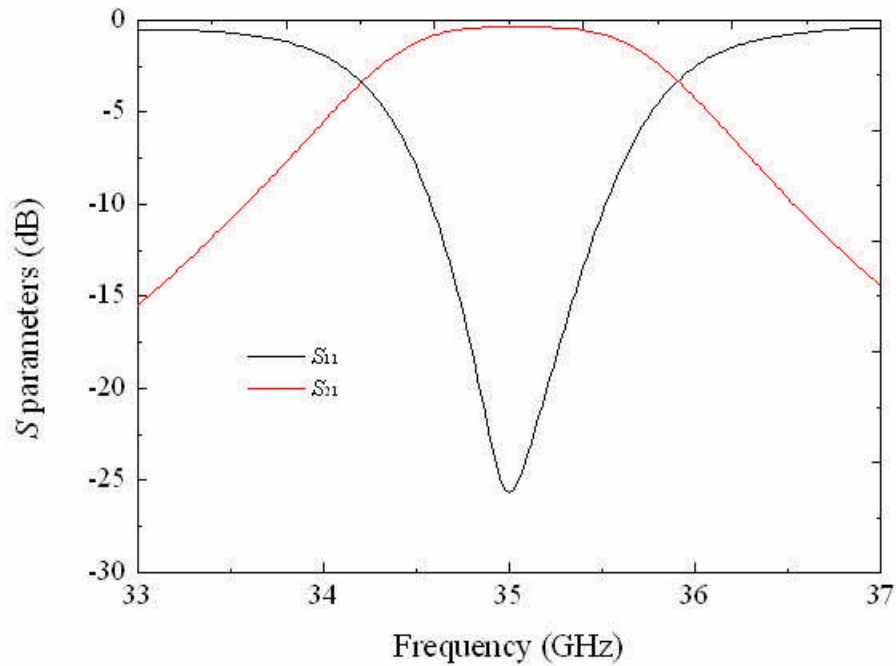


Figure 5.11 The simulation result of second order direct-coupled cavity filter.

From the analysis of the antenna and the filter, it is very interesting to move towards implementing the integration of both through fabrication of a compact three dimensional waveguide antenna and filter. This will be discuss in the next section.

5.3 Integrated waveguide antenna and filter

The Integration of the antenna with filter could further miniaturise a front-end module. It also offers a solution to suppress the spurious harmonic resonance of an antenna [85, 86]. The HSIW offers a platform to realise these through improvement in the compactness by easily integrating the antennas and filters. A single slot antenna that exhibit linear polarization and low sidelobes is modelled to fit the dimension of the cavity filter, using the method of A. Farrall and P. Young to model the slot antenna [81, 87]. Figure 5.12 is an illustration of the slot antenna integrated with the waveguide cavity filter and a photograph of it is shown in Figure 5.13 (b).

The position of the slot as referred to e in Figure 5.2 is expected to produce the maximum radiation as compared to longitudinal one. The dimension of a

three pairs of iris separated by spacing l_k is illustrated in Figure 5.12. Figure 5.13 (a) shows a photograph of the iris filters sample, part way through the fabrication process so that the internal detail is visible. Figure 5.13 (b) shows the actual photo of the integrated waveguide antenna and filter.

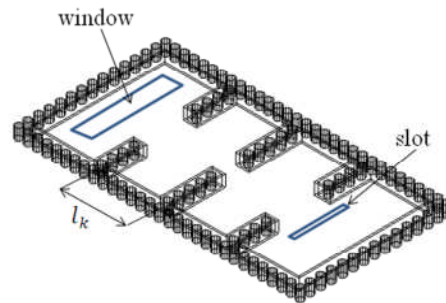
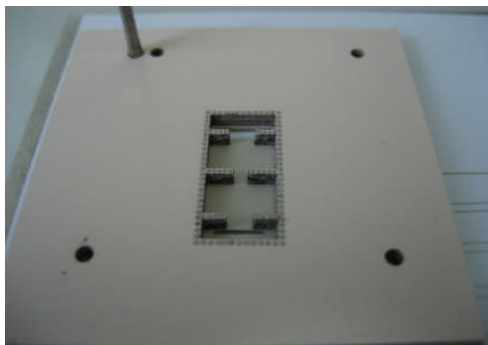
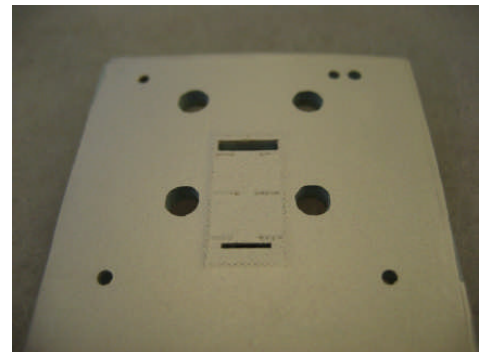


Figure 5.12 Illustration of cavity filter with a slot antenna fabricated using the same technique as HSIW.



(a)



(b)

Figure 5.13 (a) photograph of the waveguide cavity filter showing the three irises of the cavity filter before the top broadwall is laminated, and (b) complete integrated slot antenna and waveguide filter after firing.

The feed into the HSIW is realised with a window cut at the bottom supporting layer to match with the dimension of the standard coax-to-WR28 adapter to feed the electromagnetic signal through the filter before being radiated from the other slot that acts as the slot antenna to the performance of the bandpass filter.

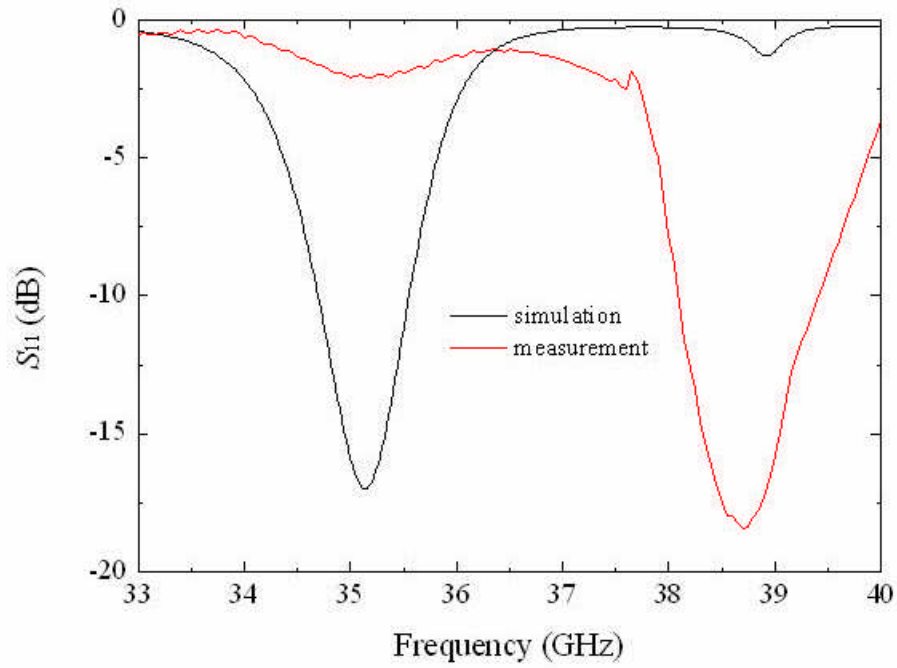


Figure 5.14 Measured return loss of the integrated waveguide slot antenna and cavity filter. The measurement has hugely shifted from the simulated one due to shrinkage in the filter.

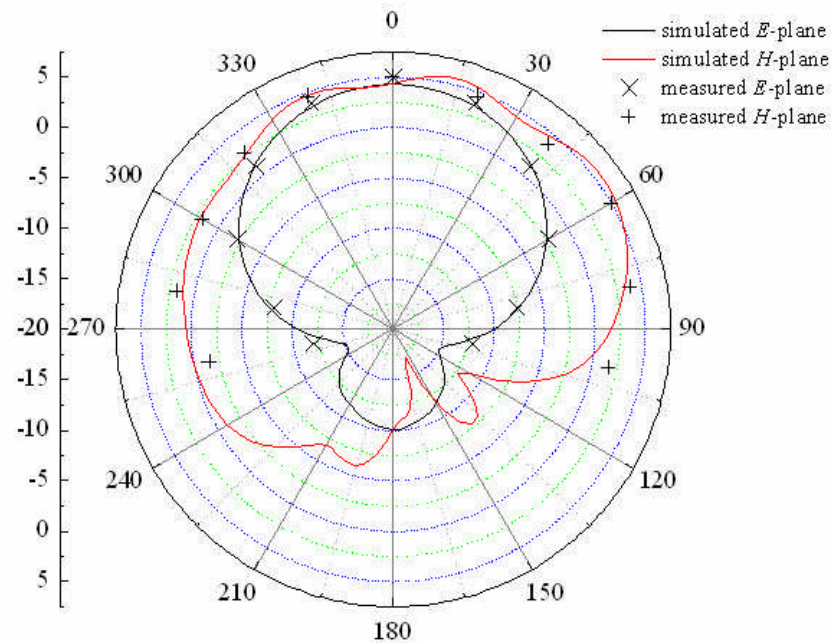


Figure 5.15 Simulated and measured radiation pattern of the integrated antenna with filter. Linear polarization was observed with both E - and H -plane matching well.

The measurement of the cavity filter, and the radiation pattern of the waveguide slot antenna and cavity filter was performed using 67 GHz PNA and a standard gain horn antenna placed inside an anechoic box. Figure 5.14 indicates shrinkage in the dimension of filter especially in the irises is critical to the performance of the filter. The measured radiation pattern is shown in Figure 5.15. The plot shows both the *E*- and *H*-plane patterns, with a close fit with the modelled performance.

5.4 Conclusion

Antennas with linear polarisation and low sidelobes have been design and measured. The radiation patterns agree well with the simulated one. Filters working at millimetre-wave region possibly could be demonstrated if further research is done to figure out shrinkage relationship to filter performance. The integrated waveguide antenna with cavity filter has been fabricated and demonstrated. Further research is necessary to establish a more robust integrated antennas and filters.

Chapter 6

Conclusions and Suggestions for Future Works

6.1 Conclusions

LTCC is one of the most promising integration technologies for passive components, such as resistors, inductors, capacitors and filters. It is also attractive for its unique set of combined characteristics; dielectric material characteristics and high conductivity metals, as well as the simplicity and flexibility of its processes. All of these features invite us to discover other applications of LTCC through fabrication of Hollow Substrate Integrated Waveguide (HSIW) that could be operational in the microwave and millimetre-wave region. The 'In-house' fabrication method which leads to lower cost, simple process and rapid prototyping solution is considered.

Rapid prototyping through infra-red laser machining is adopted. The process does not involve chemicals and a single plain screen is sufficient for printing and via filling of any number of layers. The process does not require any special mask and is performed in the ordinary laboratory environment. Optimisation of laser power, pulse rate, and scanning speed produces high repeatability and selective thinning, cutting and drilling of complex structure and number of layers made possible with optical camera assisted alignment. The laser ablated 9K7 green state tape produces surface roughness acceptable for microwave fabrication requirements.

Our aim is to establish techniques that could realise rectangular waveguides embedded in LTCC substrates. The standard LTCC process has been considered to deliver this concept but, It was found unable to produce channels/cavities. The hurdle was mainly at the lamination stage which is a crucial processing step not only to integrate the multi-layered structure in LTCC but also to attain fine channels/cavities.

For the solution, we adopted an enhanced technique to realise the 3D structures by using a novel multi-stage/progressive lamination technique.

With this technique, crack- and sag-free 3D hollow structures laminated at pressure as low as 2 MPa have been realised. Three types of sacrificial inserts have also been prepared and examined to enhance the process variation. The usage is based on purposes and requirements. While organic-based and water-based sacrificial pastes are more suitable for preparing trenches and channels in the micrometres scale, wax-graphite based sacrificial insert is suitable for large channels and cavities applications. The ratio of carbon to wax could be adjusted to tailor the influence of supporting mechanism of freestanding or cavity structure during the lamination and sintering stages.

While SIW is a very attractive transmission medium for signal propagation as compared to other transmission lines at higher frequency, further reduced loss through the introduction of novel low loss hollow substrate integrated waveguide (HSIW) will improve the attenuation of the transmission line. A WR28-like HSIW is fabricated and measured using WR28 waveguide flanges. A multimode calibration technique is used to determine the complex propagation constant. The HSIW has been successfully demonstrated working in the millimetre-wave region with measurements on 26.5 to 40 GHz test samples.

An attempt to apply this novel transmission line to integrated components such as cavity-based antenna and filter has been made that shows its potential. The measurement of the radiation pattern of the waveguide antenna and cavity filter is performed using a 67 GHz PNA and a standard gain horn antenna placed inside an anechoic box. The measured radiation pattern shows both *E*- and *H*-plane pattern closely fit with the modelled performance.

With further optimization of the process parameters it is anticipated that a more compact HSIW with higher integration and multifunctionality at much higher frequencies can be realized and this will provide a means of integrating high performance passive components along with ICs and other components to form low cost systems.

6.2 Issues with research in LTCC

Issues of LTCC sintering are discuss next.

- i. For shrinkage glass filled ceramics such as LTCC have found wide use in microelectronic industry for high integrated multilayer circuits. To meet the quality standards for such devices, an accurate control of raw materials and processing as well as detailed knowledge about sintering and shrinkage/densification are essential.
- ii. For LTCC applications manufactured with UCS (Unconstrained Sintering), the main hurdle is the shrinkage during sintering: in X-Y axis, it ranges up to 0.5 % for near “zero-shrinkage” tapes technology, and up to 15 % for “standard” tapes technology. However, the effects of deviating from the standard parameters at lamination process are not formally known since the LTCC tape suppliers provide not enough information. For instance, a different shrinkage than the values provided in datasheets is often found, in spite of carefully following the manufacturing guidelines.
- iii. UCS method or free sintering is the mostly used sintering methods for producing LTCC substrates. The disadvantage of this method is that the shrinkage of substrates in all directions. Module warping caused by TCE mismatch of conductor inks leads to problems at assembly. The relative high lamination pressure however often generates deformation of cavities and via holes. By contrast, constrained sintering essentially almost overcome the X and Y direction shrinkage, but not in the Z direction shrinkage. The main disadvantages of the constrained sintering in realisation of microfluidics or cavities are the non-existence of realistic method to produce free standing or hollow structures. As for hollow structure are completely crushed for this sintering method.

6.3 Potential improvements

Further improvement could be achieved by employing material and process technology development to achieve higher frequency modules with higher

integration levels. Technological development of LTCC for the future should address material and process development as follows:

6.3.1 Material development

i. Conductive material

To reduce conductor loss at high frequency, it is necessary to take an approach that reduces conductor resistance to the minimum level. It is important to keep voids in the conductive materials to a minimum level in order to achieve resistance close to that of the bulk material. It is effective to reduce the surface roughness of the conductor in order to reduced conductor loss. For this reason it can be considered necessary to develop a process to print the conductor after flattening the cast green sheet by applying pressure, or processes to apply pressure to the conductor after printing to make the conductor surface more flat.

ii. Dielectric material

To provide a single module with a variety of high frequency functions, materials with low dielectric loss and varying dielectric constants are necessary. The ability to integrate the high-performance passive components into the package in a low-cost way is the compelling attribute of this approach.

6.3.2 Process development

i. Conductor deposition development

With the current thick film printing processes, line widths of 80 μm are the limit. The development of a new processes is desirable for achieving finer interconnects. The reason for the difficulties in achieving miniaturization lies in the principle of the screen printing technique itself in which ink is presses through the stencil, although the surface roughness of the substrate also has a significant impact. For example, conductor is screen printed on plastic film with a smooth surface. Then, the printed surface is applied to the green sheet and a method of transfer is applied, so that the finer line widths could be achieved.

ii. Dielectric development

To develop modules using materials adaptable to various functions, high level process technologies to incorporate ceramics with different characteristics such as dielectric constant are necessary. There are a few issues when combining dissimilar materials to make composite material such LTCC, but the main issue is the firing shrinkage behaviour between different materials. To solve this issue, the 'zero-shrinkage process' where the shrinkage in the x and y axis is suppressed, allowing shrinkage only in the z axis [88].

6.4 Suggestions for Future Work

For passive components like capacitors and filters, it is desirable to use a ceramic that has optimal dielectric characteristics for the function required. Compared to other materials, the high frequency loss of LTCC is small and they are adaptable to different platforms which, make them the most suitable candidate as a material for component used in communication and sensing.

The research on LTCC could be extended to the following areas:

6.4.1 LTCC-based RF MEMS

In the future, system integration will become more sophisticated and involve more functions of the package, such as sensors, actuators, MEMS, or power supply components. Currently, filtering and switching are among the electrical functions which cannot effectively be integrated onto active silicon. Moreover, tunable capabilities are strongly expected to offer more flexible radio front-ends for future software-defined-radio. MEMS devices have shown promise for realizing tuning functions. Incorporating RF MEMS components such as switches, variable capacitors and tunable filters in RF module platforms will drastically increase the functionality and will be the next challenging development. Figure 6.1 shows some cantilevers and bridges produced through laser thinning and cutting. These structures currently studied for the application to MEMS switches.

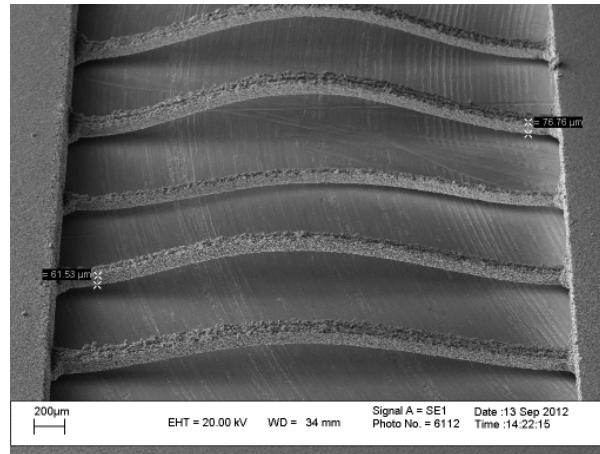


Figure 6.1 Suspended bridges made from LTCC has been successfully realised in the Leeds LTCC fabrication laboratory.

6.4.2 Waveguide at sub-millimetre-wave region

A package integration concept where film components embedded in packages , SiP modules, SoC devices, battery and user interface, leads to multi-functional systems in the short term and ultimately multi-function systems in the future [19].

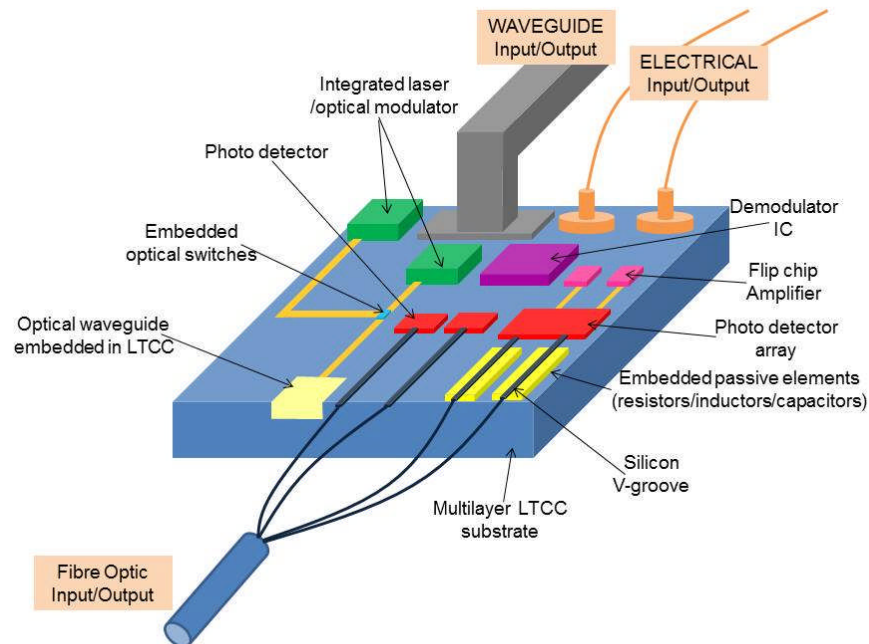


Figure 6.2 System-in-Package vision.

6.4.3 Other 3D fabrication techniques

Selected sintering ceramics by using laser for 3D structuring. Currently, this technique is more towards producing three dimensional ceramic components for medical purposes.

Other process and fabrication that interesting to be explore are:

- Metallization using an aerosol technique [89]
- Vertically stacked filter [90]

6.5 Publications

The work presented in this thesis has been presented in conference as well under review for publication. Among the publications produced throughout this research are:

Conference posters and proceedings

Jin, Lukui; **Lee, R. M.**; Robertson Ian D., "Design and Performance of log-periodic substrate integrated waveguide Slot Antenna", *IEEE International Microwave Symposium Digest*, 2012

Jin, Lukui; **Lee, R. M.**; Robertson I. D., "Modelling of a double-sided dielectric resonator antenna array fed from dielectric insulator image guide", *Loughborough Antennas and Propagation Conference*, Nov. 2012

R. M. A. Lee, A. Sunday, N. Kapur, N. Somjit, P. Steenson, I. D. Robertson, M. D'Auria, S. Lucyszyn, D. N. Rathnayake-Arachchige, Hutt, P. P. Conway, "3D Microwave and Millimeter-wave system-on-substrate using sacrificial layers for printed RF MEMS Components", *R2i2 Electronics Conference: Connecting Research to Industry, Joint IMAPS-UK, ESP-KTN & IeMRC Event*, Holywell Park Conference Centre, Loughborough, July 2013, **(Best Paper Award)**

Dilshani Rathnayake-Arachchige; David A. Hutt; Paul P. Conway; Mario D'Auria; Stepan Lucyszyn; **Razak M. Lee**; Ian D. Robertson, "Excimer Laser Machining of Fired LTCC for Selectively Metalized Open Micro-channel Structures", *IMAPS 2013*.

Dilshani Rathnayake- Arachchige; David A. Hutt; Paul P.Conway; Mario D'Auria; Stepan Lucyszyn; **Razak M. Lee**; Ian D. Robertson, "Patterning of Electroless Copper Deposition on Low Temperature Co-fired Ceramic", *15th Electronics Packaging Technology Conference*, Singapore, Dec 2013.

Publication

Jin, Lukui; **Lee, Razak M.**; Robertson, I. D., "Analysis and design of a novel low loss hollow substrate integrated waveguide", *IEEE Transactions of Microwaves Theory and Techniques* (submitted)

List of References

- [1] N. A. Sherwani, Q. Yu, and S. Babida, *Introduction to multichip modules*. New York; Chichester: Wiley, 1995.
- [2] W. Brown, *Advanced Electronic Packaging: With Emphasis on Multichip Modules*: Wiley-IEEE Press, 2006.
- [3] H. Jantunen, T. Kangasvieri, J. Vähäkangas, and S. Leppävuori, "Design aspects of microwave components with LTCC technique," *Journal of the European Ceramic Society*, vol. 23, pp. 2541-2548, 2003.
- [4] T. Vaha-Heikkila and M. Lahti, "LTCC 3D integration platform for microwave and millimeter wave modules," in *2012 IEEE International Symposium on Radio-Frequency Integration Technology (RFIT 2012)*, 21-23 Nov. 2012, Piscataway, NJ, USA, 2012, pp. 95-7.
- [5] M. T. Sebastian and H. Jantunen, "Low loss dielectric materials for LTCC applications: A review," *International Materials Reviews*, vol. 53, pp. 57-90, 2008.
- [6] R. R. Tummala, "Ceramic and Glass-Ceramic Packaging in the 1990s," *Journal of the American Ceramic Society*, vol. 74, pp. 895-908, 1991.
- [7] J. Muller, H. Thust, and K. H. Drue, "RF-design considerations for passive elements in LTCC material systems," *International Journal of Microcircuits and Electronic Packaging*, vol. 18, pp. 200-6, / 1995.
- [8] B. Schwartz, "Review of multilayer ceramics for microelectronic packaging," *Journal of Physics and Chemistry of Solids*, vol. 45, pp. 1051-1068, 1984.
- [9] R. C. Buchanan, *Ceramic materials for electronics*, 3rd ed., rev. and expanded. ed. New York,, 2004.
- [10] A. J. Moulson and J. M. Herbert, *Electroceramics : materials, properties, applications*. Chichester: J. Wiley, 2003.
- [11] H. Ohsato, "Research and development of microwave dielectric ceramics for wireless communications," *Journal of the Ceramic Society of Japan*, vol. 113, pp. 703-11, 2005.
- [12] O. Dernovsek, A. Naeini, G. Preu, W. Wersing, M. Eberstein, and W. A. Schiller, "LTCC glass-ceramic composites for microwave application," *Journal of the European Ceramic Society*, vol. 21, pp. 1693-1697, 2001.
- [13] E. Koga, Y. Yamagishi, H. Moriwake, K. Kakimoto, and H. Ohsato, "Order-disorder transition and its effect on microwave quality factor Q in Ba(Zn_{1/3}Nb_{2/3})O₃ system," *Journal of Electroceramics*, vol. 17, pp. 375-9, 12/ 2006.
- [14] M. Valant, "New LTCC materials: From fundamental to applied research," in *2012 1st International Symposium on Physics and Technology of Sensors (ISPTS)*, 7-10 March 2012, Piscataway, NJ, USA, 2012, p. 1 pp.
- [15] A. A. Shapiro, M. L. Mecartney, and H. P. Lee, "A comparison of microstrip models to low temperature co-fired ceramic - silver microstrip measurements," *Microelectronics Journal*, vol. 33, pp. 443-447, 2002.

- [16] M. R. Gongora-Rubio, P. Espinoza-Vallejos, L. Sola-Laguna, and J. J. Santiago-Aviles, "Overview of low temperature co-fired ceramics tape technology for meso-system technology (MsST)," *Sensors and Actuators, A: Physical*, vol. 89, pp. 222-241, 2001.
- [17] M. Richtarsic and J. Thornton, "Characterization and optimization of LTCC for high density large area MCM's," in *Proceedings. 1998 International Conference on Multichip Modules and High Density Packaging*, 1998, pp. 92-97.
- [18] W. Simon, R. Kulke, A. Wien, I. Wolff, S. Baker, R. Powell, *et al.*, "Design of passive components for K-band communication modules in LTCC environment," in *1999 International Symposium on Microelectronics*, USA, 1999, pp. 183-8.
- [19] I. Szendiuch, "Development in electronic packaging - Moving to 3D System Configuration," 2011.
- [20] R. L. Li, G. DeJean, M. Maeng, K. Lim, S. Pinel, M. M. Tentzeris, *et al.*, "Design of compact stacked-patch antennas in LTCC multilayer packaging modules for wireless applications," *IEEE Transactions on Advanced Packaging*, vol. 27, pp. 581-589, 2004.
- [21] H. Yong and W. Ke-Li, "A broadband integrated LTCC laminated waveguide to metallic waveguide transition," Piscataway, NJ, USA, 2003, pp. 2237-40.
- [22] T. Baras and A. F. Jacob, "Manufacturing reliability of LTCC millimeter-wave passive components," *IEEE Transactions on Microwave Theory and Techniques*, vol. 56, pp. 2574-2581, 2008.
- [23] A. Pietrikova, "Potentiality of LTCC for sensor applications," Piscataway, NJ, USA, 2001, pp. 112-16.
- [24] G. Radosavljevic, W. Smetana, A. Maric, L. Zivanov, M. Unger, and G. Stojanovic, "Micro force sensor fabricated in the LTCC technology," Piscataway, NJ, USA, pp. 221-4.
- [25] M. Gongora-Rubio, L. M. Sola-Laguna, P. J. Moffett, and J. J. Santiago-Aviles, "The utilization of low temperature co-fired ceramics (LTCC-ML) technology for meso-scale EMS, a simple thermistor based flow sensor," *Sensors and Actuators A (Physical)*, vol. A73, pp. 215-21, 1999.
- [26] H. Klumbies, U. Partsch, A. Goldberg, S. Gebhardt, U. Keitel, and H. Neubert, "Actuators to be integrated in low temperature cofired ceramics (LTCC) microfluidic systems," Brno, Czech republic, 2009.
- [27] F. Barlow, J. Wood, A. Elshabini, E. F. Stephens, R. Feeler, G. Kemner, *et al.*, "Fabrication of precise fluidic structures in LTCC," *International Journal of Applied Ceramic Technology*, vol. 6, pp. 18-23, 2009.
- [28] M. Schirmer, J. Uhlemann, L. Rebenklau, T. Bauer, and K. J. Wolter, "3D-microfluidic reactor in LTCC," in *Electronics Technology, 2008. ISSE '08. 31st International Spring Seminar on*, 2008, pp. 484-489.
- [29] R. N. Dean and A. Luque, "Applications of Microelectromechanical Systems in Industrial Processes and Services," *Industrial Electronics, IEEE Transactions on*, vol. 56, pp. 913-925, 2009.
- [30] R. Allan, "MEMS Designs Gear Up For Greater Commercialization," *Electronic Design*, June 12, 2000 2000.

- [31] V. Heikkinen, J. Aikio, T. Alajoki, J. Hiltunen, A. J. Matilla, J. Ollila, *et al.*, "MEMS packaging using precision machined LTCC substrates," Piscataway, NJ, USA, 2003, pp. 81-2.
- [32] B. Yong-Seung, K. Jung-Mu, K. Jong-Man, K. Yong-Kweon, and J. Yun-Ho, "LTCC-based vertical via interconnects for RF MEMS packaging," *Microwave and Optical Technology Letters*, vol. 52, pp. 252-7.
- [33] H. Kopola, J. Lenkkeri, K. Kautio, A. Torkkeli, O. Rusanen, and T. Jaakola, "MEMS sensor packaging using LTCC substrate technology," USA, 2001, pp. 148-58.
- [34] C. Zhang, D. Liu, S. A. Mathews, J. Graves, T. M. Schaefer, B. K. Gilbert, *et al.*, "Laser direct-write and its application in low temperature Co-fired ceramic (LTCC) technology," *Microelectronic Engineering*, vol. 70, pp. 41-49, 2003.
- [35] J. Liu, Y. Cao, X. Wang, J. Duan, and X. Zeng, "A homogeneous electrically conductive silver paste," *IEEE Transactions on Advanced Packaging*, vol. 33, pp. 899-903.
- [36] Z. W. Zhong, P. Arulvanan, and C. K. Goh, "Effects of four key process variables on size shrinkages of low temperature co-fired ceramic substrates," *Materials and Manufacturing Processes*, vol. 23, pp. 21-28, 2008.
- [37] K. Malecha, T. Maeder, and C. Jacq, "Fabrication of membranes and microchannels in low-temperature co-fired ceramic (LTCC) substrate using novel water-based sacrificial carbon pastes," *Journal of the European Ceramic Society*, vol. 32, pp. 3277-3286, 2012.
- [38] R. Bauer, M. Luniak, L. Rebenklau, K. J. Wolter, and W. Sauer, "Realization of LTCC-multilayer with special cavity applications," Reston, VA, USA, 1997, pp. 659-64.
- [39] C.-H. Fan and J. P. Longtin, "Modeling optical breakdown in dielectrics during ultrafast laser processing," *Applied Optics*, vol. 40, pp. 3124-3131, 2001.
- [40] M. F. Shafique, K. Saeed, D. P. Steenson, and I. D. Robertson, "Laser prototyping of microwave circuits in LTCC technology," *IEEE Transactions on Microwave Theory and Techniques*, vol. 57, pp. 3254-3261, 2009.
- [41] L. E. Khoong, Y. M. Tan, and Y. C. Lam, "Overview on fabrication of three-dimensional structures in multi-layer ceramic substrate," *Journal of the European Ceramic Society*, vol. 30, pp. 1973-1987, 2010.
- [42] K. M. Nowak, H. J. Baker, and D. R. Hall, "Cold processing of green state LTCC with a CO₂ laser," *Applied Physics A: Materials Science & Processing*, vol. 84, pp. 267-270, 2006.
- [43] R. Rozman, B. Kmetec, B. Podobnik, D. Kovacic, and E. Govekar, "Optimisation of direct laser structuring of printed circuit boards," *Applied Surface Science*, vol. 254, pp. 5524-5529, 2008.
- [44] J. Vanek, I. Szendiuch, W. Smetana, and M. Unger, "Performance of laser machined and metallized via holes in LTCC tape materials," in *2008 31st International Spring Seminar on Electronics Technology (ISSE 2008)*, 7-11 May 2008, Piscataway, NJ, USA, 2008, pp. 540-4.
- [45] J. Kita, A. Dziedzic, L. J. Golonka, and T. Zawada, "Laser treatment of LTCC for 3D structures and elements fabrication," *Microelectronics International*, vol. 19, pp. 14-18, 2002.

- [46] K. M. Nowak, H. J. Baker, and D. R. Hall, "A model for "cold" laser ablation of green state ceramic materials," *Applied Physics A: Materials Science & Processing*, vol. A91, pp. 341-8, 2008.
- [47] Y. Imanaka, "Multilayered Low Temperature Cofired Ceramic Technology," *Springer*, 2005.
- [48] K. Sasaki and N. Mizumura, "Development of low temperature sintered nano silver pastes using MO technology and resin reinforcing technology," in *2013 IEEE 63rd Electronic Components and Technology Conference, ECTC 2013, May 28, 2013 - May 31, 2013*, Las Vegas, NV, United states, 2013, pp. 1066-1070.
- [49] K. Park, D. Seo, and J. Lee, "Conductivity of silver paste prepared from nanoparticles," *Colloids and Surfaces A: Physicochemical and Engineering Aspects*, vol. 313–314, pp. 351-354, 2/1/ 2008.
- [50] M. Hosokawa, K. Nogi, M. Naito, and T. Yokoyama, *Nanoparticle Technology Handbook*: Elsevier, 2008.
- [51] DuPont, "Green Tape Design Layout Guidelines."
- [52] W. Smetana, B. Balluch, G. Stangl, S. Luftl, and S. Seidler, "Processing procedures for the realization of fine structured channel arrays and bridging elements by LTCC-technology," *Microelectronics Reliability*, vol. 49, pp. 592-9, 2009.
- [53] M. Hintz, R. Perrone, H. Thust, and M. Hein, "Electrical properties of low temperature cofired ceramics with integrated bulk metals," in *ISSE 2006 - 29th International Spring Seminar on Electronics Technology: Nano Technologies for Electronics Packaging, May 10, 2006 - May 14, 2006*, St. Marienthal, Germany, 2006, pp. 103-108.
- [54] A. Roosen, "New lamination technique to join ceramic green tapes for the manufacturing of multilayer devices," *Journal of the European Ceramic Society*, vol. 21, pp. 1993-1996, 2001.
- [55] K. Schindler and A. Roosen, "Manufacture of 3D structures by cold low pressure lamination of ceramic green tapes," *Journal of the European Ceramic Society*, vol. 29, pp. 899-904, 2009.
- [56] D. Jurkow, H. Roguszczak, and L. Golonka, "Cold chemical lamination of ceramic green tapes," *Journal of the European Ceramic Society*, vol. 29, pp. 703-9, 2009.
- [57] D. Jurków and L. Golonka, "Low-pressure, thermo-compressive lamination," *Journal of the European Ceramic Society*, vol. 32, pp. 2431-2441, 2012.
- [58] K. Malecha, D. Jurkow, and L. J. Golonka, "Comparison of solvent and sacrificial volume-material-based lamination processes of low-temperature co-fired ceramics tapes," *Journal of Micromechanics and Microengineering*, vol. 19, p. 065022, 2009.
- [59] H. Birol, T. Maeder, C. Jacq, S. Straessler, and P. Ryser, "Fabrication of Low-Temperature Co-Fired Ceramics Micro-Fluidic Devices Using Sacrificial Carbon Layers," *International Journal of Applied Ceramic Technology*, vol. 2, pp. 364-373, 2005.
- [60] T. Maeder, C. Jacq, Y. Fournier, W. Hraiz, and P. Ryser, "Structuration of thin bridge and cantilever structures in thick-film technology using mineral sacrificial materials," ed, 2009.
- [61] H. Birol, T. Maeder, and P. Ryser, "Processing of graphite-based sacrificial layer for microfabrication of low temperature co-fired

- ceramics (LTCC)," *Sensors and Actuators, A: Physical*, vol. 130-131, pp. 560-567, 2006.
- [62] Y. M. Tan, L. E. Khoong, Y. C. Lam, S. C. Tan, and R. Paramasivam, "Process development for realization of embedded structures in multi-layer ceramics platform using carbon fugitive material," in *2008 10th Electronics Packaging Technology Conference (EPTC 2008)*, 9-12 Dec. 2008, Piscataway, NJ, USA, 2008, pp. 982-7.
- [63] D. M. Pozar, "Microwave Engineering," *John Wiley & Sons*, vol. 3rd Edition, 2005.
- [64] N. Marcuvitz, *Waveguide Handbook [electronic resource]*. Stevenage: IET, 1986.
- [65] D. Deslandes and K. Wu, "Single-substrate integration technique of planar circuits and waveguide filters," *IEEE Transactions on Microwave Theory and Techniques*, vol. 51, pp. 593-6, 2003.
- [66] D. Deslandes and K. Wu, "Integrated microstrip and rectangular waveguide in planar form," *IEEE Microwave and Wireless Components Letters*, vol. 11, pp. 68-70, 2001.
- [67] J. Hirokawa and M. Ando, "Single-layer feed waveguide consisting of posts for plane TEM wave excitation in parallel plates," *IEEE Transactions on Antennas and Propagation*, vol. 46, pp. 625-30, 1998.
- [68] S. Park, Y. Tsunemitsu, J. Hirokawa, and M. Ando, "Center feed single layer slotted waveguide array," *IEEE Transactions on Antennas and Propagation*, vol. 54, pp. 1474-1480, 2006.
- [69] M. Ando, J. Hirokawa, T. Yamamoto, A. Akiyama, Y. Kimura, and N. Goto, "Novel single-layer waveguides for high-efficiency millimeter-wave arrays," USA, 1998, pp. 792-9.
- [70] S. Yuanfeng, R. Fujino, J. Hirokawa, M. Ando, D. Hanatani, and M. Fujimoto, "Loss reduction and bandwidth enhancement by air-region insertion to LTCC rectangular-waveguide slot arrays in the millimeter-wave band," in *Antennas and Propagation Society International Symposium (APSURSI)*, 2012 IEEE, 2012, pp. 1-2.
- [71] X. Feng and K. Wu, "Guided-wave and leakage characteristics of substrate integrated waveguide," *IEEE Transactions on Microwave Theory and Techniques*, vol. 53, pp. 66-73, 2005.
- [72] R. B. Marks, "A multiline method of network analyzer calibration," *IEEE Transactions on Microwave Theory and Techniques*, vol. 39, pp. 1205-1215, 1991.
- [73] M. D. Janezic and J. A. Jargon, "Complex permittivity determination from propagation constant measurements," *IEEE Microwave and Guided Wave Letters*, vol. 9, pp. 76-78, 1999.
- [74] M. Henry, N. Osman, T. Tick, and C. Free, "Integrated air-filled waveguide antennas in LTCC for G-band operation," Piscataway, NJ, USA, 2009, p. 4.
- [75] M. S. Aftanasar, P. R. Young, I. D. Robertson, and S. Lucyszyn, "Fabrication of dielectric-filled rectangular waveguide using thick-film processing," Cardiff, United kingdom, 2001, pp. 82-87.
- [76] L. Lewin, "Radiation from discontinuities in strip-line," *Proceedings of the IEE - Part C: Monographs*, vol. 107, pp. 163-170, 1960.
- [77] S. B. Cohn, "Direct-coupled-resonator filters," *Proceedings of the Institute of Radio Engineers*, vol. 45, pp. 187-196, 1957.

- [78] K. Kordas, A. E. Pap, J. Saavalainen, H. Jantunen, P. Moilanen, E. Haapaniemi, *et al.*, "Laser-induced surface activation of LTCC materials for chemical metallization," *IEEE Transactions on Advanced Packaging*, vol. 28, pp. 259-63, 05/ 2005.
- [79] P. W. Gian, X. Shan, Y. N. Liang, B. K. Lok, C. W. Lu, and B. L. Ooi, "High aspect pattern formation by integration of micro inkjetting and electroless plating," in *DTIP of MEMS and MOEMS - Symposium on Design, Test, Integration and Packaging of MEMS/MOEMS, April 9, 2008 - April 11, 2008*, Nice, France, 2008, pp. 162-167.
- [80] R. C. Johnson, "Antenna Engineering Handbook," *McGraw-Hill*, 1993.
- [81] A. J. Farrall and P. R. Young, "Integrated waveguide slot antennas," *Electronics Letters*, vol. 40, pp. 974-5, 2004.
- [82] D. K. Cheng, *Field and wave electromagnetics*. Reading, Mass.: Addison-Wesley Pub. Co., 1989.
- [83] R. E. Collin, "Foundations for microwave engineering," *IEEE Press*, 2001.
- [84] I. Hunter, *Theory and design of microwave filters*. London, UK: IEE, 2001.
- [85] M. Moradian and M. Tayarani, "Spurious-response suppression in microstrip parallel-coupled bandpass filters by grooved substrates," *Ieee Transactions on Microwave Theory and Techniques*, vol. 56, pp. 1707-1713, 2008.
- [86] C. Saeidi and D. van der Weide, "Periodic substrate structure suppresses spurious response in coupled line filters," *Microwave and Optical Technology Letters*, vol. 54, pp. 2175-8, 2012.
- [87] S. Silver. (1984). *Microwave Antenna Theory and Design*. Available: <http://digital-library.theiet.org/content/books/ew/pbew019e>
- [88] J. U. Knickerbocker and S. H. Knickerbocker, "Low-Temperature Co-Fired Ceramic Chip Carriers," in *Handbook of Advanced Materials*, ed: John Wiley & Sons, Inc., 2004, pp. 129-148.
- [89] Y. Imanaka, N. Hayashi, M. Takenouchi, and J. Akedo, "Aerosol deposition for post-LTCC," *Journal of the European Ceramic Society*, vol. 27, pp. 2789-95, / 2007.
- [90] S. Tze-Min, C. Chi-Feng, H. Ting-Yi, and W. Ruey-Beei, "Design of vertically stacked waveguide filters in LTCC," *IEEE Transactions on Microwave Theory and Techniques*, vol. 55, pp. 1771-9, 2007.

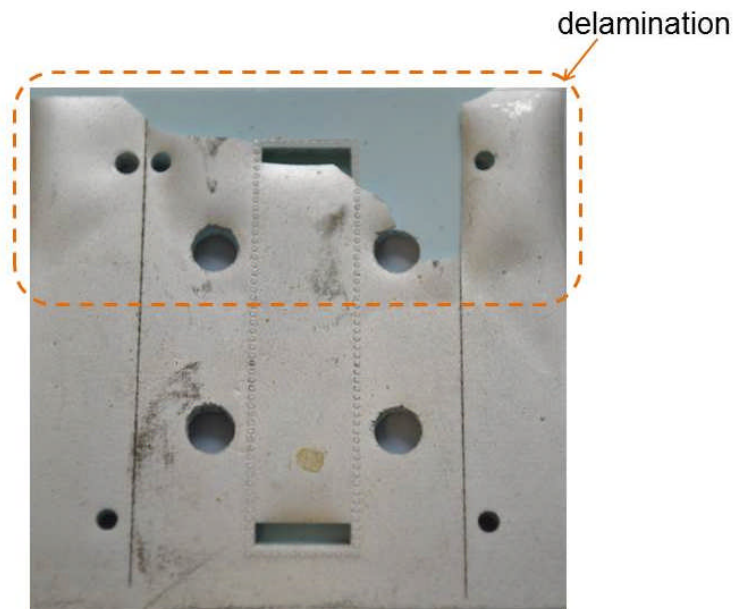
List of Abbreviations

BI-RME	Boundary Integral-Resonant Mode Expansion
CNC	Computer Numerical Control
DC	Direct Current
EMI	Electromagnetic Interference
FDTD	Finite-Difference Time-Domain
FEM	Finite Element Method
GPS	Global Positioning System
HFSS	High Frequency Structural Simulator
HSIW	Hollow Substrate Integrated Waveguide
HTCC	High Temperature Co-fired ceramic
IC	Integrated Circuit
I/O	Input/Output
LTCC	Low Temperature Co-fired Ceramic
MCM	Multi-chip Module
MCM-D	Multi-chip Module-Deposition
MCM-L	Multi-chip Module-Laminate
MCM-C	Multi-chip Module-Ceramic
MEMS	Microelectromechanical System
MMIC	Monolithic Microwave Integrated Circuit
Nd:YAG	Neodymium-doped Yttrium Aluminium Garnet
Nd:YVO4	Neodymium-doped Yttrium Orthovanadate
PCB	Printed Circuit Board
PNA	Power Network Analyser
RF MEMS	RF Microelectromechanical System
RWG	Rectangular Waveguide
SiP	System-In-Package
SIW	Substrate Integrated Waveguide
SVM	Sacrificial Volume Material
SMT	Surface Mount Technology
SoC	System-On-Chip
SEM	Scanning Electron Microscope

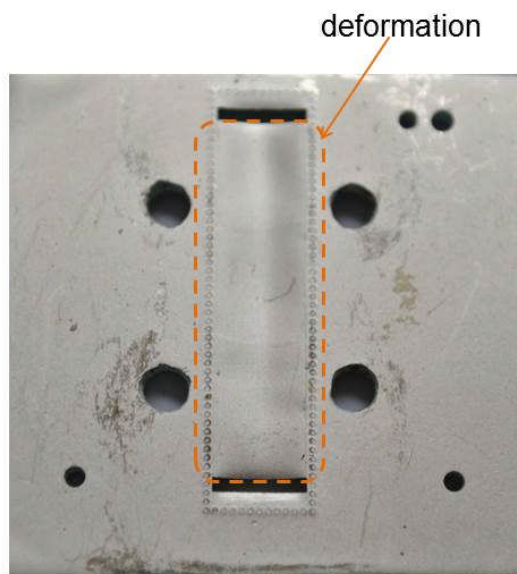
TCE	Thermal Coefficient of Expansion
TE	Transverse Electric
TEM	Transverse Electromagnetic
TM	Transverse Magnetic
2D	Two Dimension
3D	Three Dimension
VLSI	Very Large Scale Integrated
WSI	Wafer Scale Integration

Appendix A

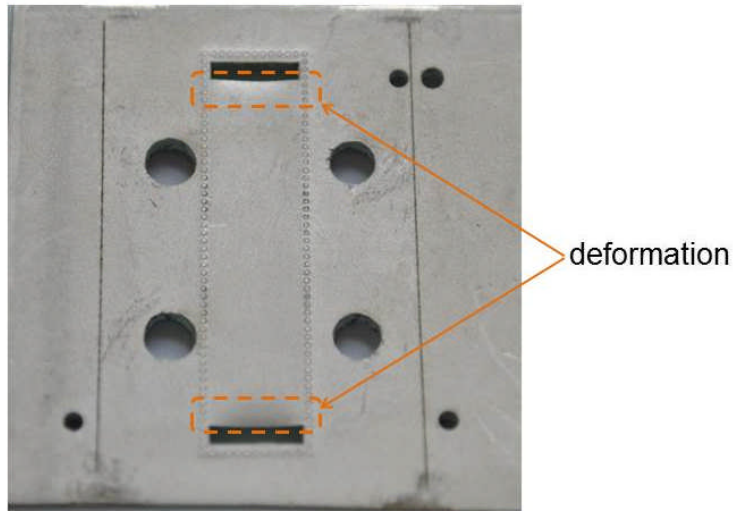
Lamination results



Lamination: 5 MPa, 50 °C, 5 min



Lamination: 10 MPa, 70 °C, 5 min



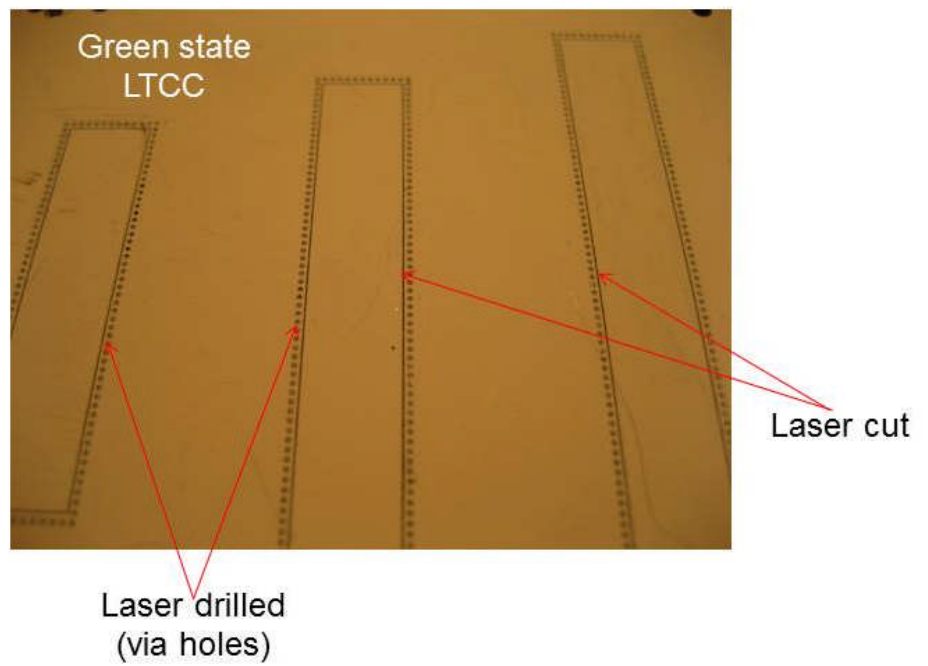
Lamination: 5 MPa, 70 °C, 10 min

Appendix B

HSIW fabrication flow

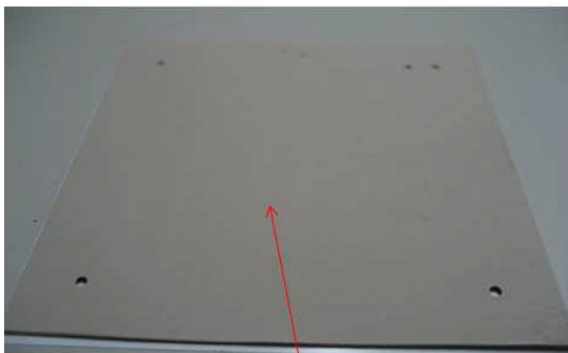
Laser Machining: Via machining/drilling

- LPKF Protolaser 200 (Nd:YAG 1064nm)
- Power/frequency/speed: 6.2 W / 40 kHz / 500 mm/s

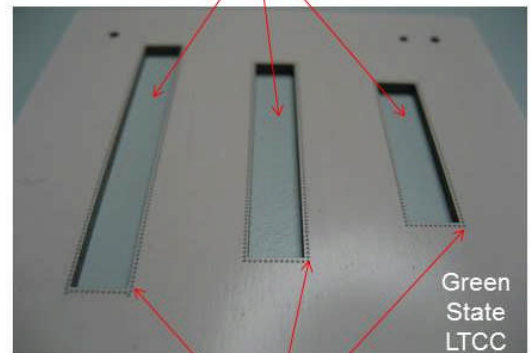


Screen Printing: Conductor Printing/Via Filling

- Standard 280 screen mesh is set-up
- Conductor printing: Ag-Pd Paste LL612
- Via filling: Ag paste LL601 (via filling)
- Drying 80°C for 10 minutes



conducting
layer (LL612)



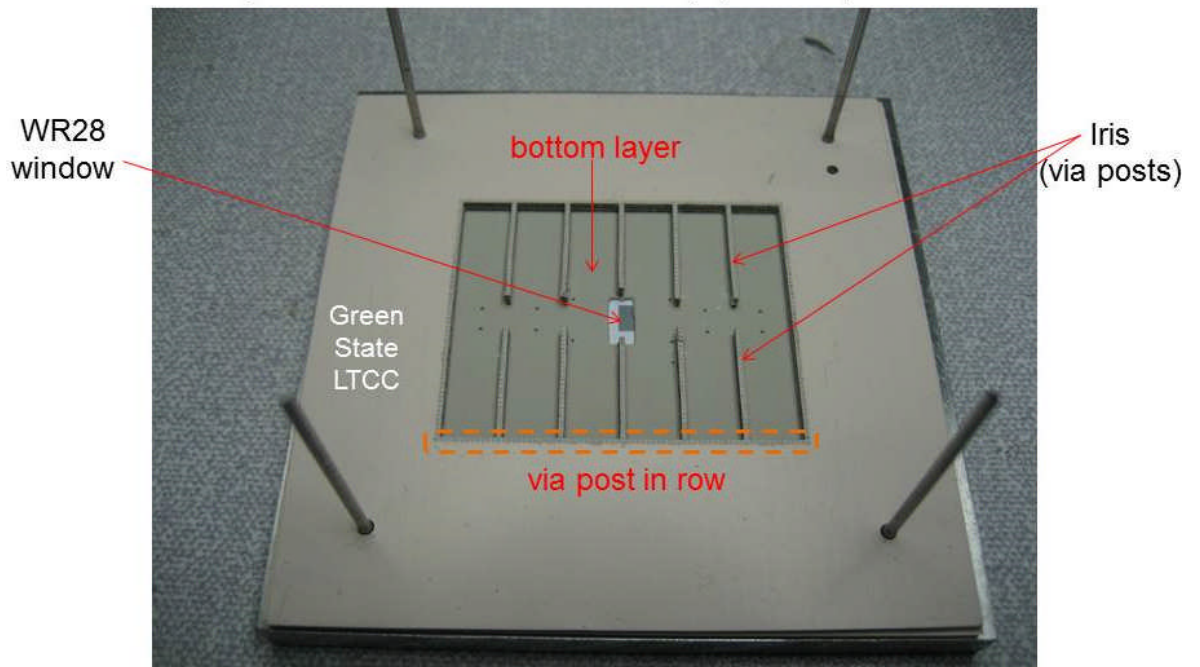
channels/
cavities

via posts
(LL601)

Green
State
LTCC

Lamination: Uniaxial lamination

- Progressive lamination
- Pressure/Temp./Duration: 30 MPa/70 °C/10 min (main)
- Pressure/Temp./Duration: 2 MPa/70 °C/5 min (top/bottom)



Laser Machining: Via machining/drilling

UCS sintering using Carbolite Type 301 temperature controller

